UNIVERSITY OF NAPOLI FEDERICO II

DEPARTMENT OF STRUCTURES

FOR ENGINEERING AND ARCHITECTURE (DI.ST.)

PhD Programme in Materials Engineering and Structures (XXVII cycle)

Coordinator Prof. Giuseppe Mensitieri

Ciro Del Vecchio

PhD Thesis

SEISMIC BEHAVIOR OF POORLY DETAILED BEAM-COLUMN JOINTS RETROFITTED WITH FRP SYSTEMS: EXPERIMENTAL INVESTIGATION AND ANALYTICAL MODELING

TUTOR: PROF. ANDREA PROTA

CO-TUTOR: ING. MARCO DI LUDOVICO

YEAR 2015

Dedication, devotion,
turning all the night time into the day

Dire Straits, Walk Of Life (1986)

Table of Contents

List of Figures

List of Tables

CHAPTER 1
INTRODUCTION

The investigation on the seismic behavior of existing structural systems is nowadays a critical issue in the protection of modern societies in seismic-prone areas. Recent earthquakes demonstrated the high vulnerability of reinforced concrete (RC) structures and, in particular, those designed not conforming to current seismic codes. The great effort of the research community in developing and promoting new design strategies and structural detailing strongly reduced the seismic vulnerability of new structural systems. Concerning the structural safety, the main scope of the code development has been to provide different prescriptions to guarantee specific levels of performances associated with a well-defined probability of exceedance. This process resulted in substantial improvements in modern seismic codes.

However, the seismic code development and the adoption in national standards has taken several years with a substantial gap in each country. In many cases, devastating earthquakes such as Messina 1908, El Centro 1940, San Fernando 1971, Loma Prieta 1989, Northridge 1994, Kobe 1995, L'Aquila 2009, promoted the development and adoption of new design codes. These

earthquakes contributed to the engineering understanding of earthquakes and structural response by pointing out several problems in the quantification of seismic action and severe structural deficiencies (Calvi, 2010). In particular, the Messina earthquake resulted in the inclusion of some basic prescriptions for seismic resistant structures, seismic input estimation and performance levels in the Italian Technical standards. New targets for the seismic design accelerations were later defined based on the observations of two strong earthquakes (Long Beach, 1933 and El Centro 1940). Using the first recorded earthquakes, refined values of the peak ground acceleration and the concept of response spectra were introduced. The San Fernando, 1971, and Friuli, 1976, earthquakes, resulted in a new focus on concept of ductility and the ability of the structural members to maintain the bearing load capacity when subjected to large displacements. Three events in quick succession (Loma Prieta, 1989, Northridge, 1994 and Kobe, 1995) made other issues with the code provisions clear. The analysis of the earthquake signals and the structural damage on different buildings promoted important scientific studies which resulted in the development of the more recent design approaches based on the probabilistic method and the performance-based design. In regards to beam-column connections, the earthquakes in the 80's (El Asnam, 1980, Mexico 1985, Loma Prieta 1989) resulted in a focus on these structural members. Before these events the joint shear reinforcements were almost never provided. This is because of the lack of widely accepted theories and formulations on the joint capacity which resulted in a complete overlook in the design and construction practice (Paulay and Priestley 1992). Considering that in many countries the largest development of civil infrastructures took place in the 70-80's and the first seismic codes were adopted in the design practice at the end of the 80's, it is notable that many structural systems are vulnerable to seismic events because of the obsolete design strategies, underestimation of seismic input and lack of proper structural details. Indeed, a large number of existing structural systems in seismic prone areas have been designed with code provisions not adequate to current seismic codes. This is particularly true in the Italian context, where modern seismic codes were adopted at the end of

the last century. In particular, internal transverse reinforcements in the joint panel were introduced in the Italian design practice in the 1997 (D.M. 1996 and Circolare M.LL.PP. 1997). Indeed, most existing structures have poorly detailed beam-column joints.

Recent events have demonstrated the high vulnerability of existing structures. Field inspections in the aftermath of major earthquakes (Priestley et al., 1996; Reluis, 2009; Leon et al., 2014; Dolce and Goretti, 2015) reported significant structural damages to RC structures designed for gravity load and having small amounts of transverse reinforcements (see Figure 1.1).

(a) (b)

Figure 1.1 Joint panel damages in the aftermath of L'Aquila earthquake 2009 (Reluis, 2009): diagonal tension failure (a) and bar buckling (b).

In many cases the structural deficiencies are related to insufficient amounts of transverse reinforcement in the members. This led to shear failures, commonly associated to a reduced seismic capacity and structural collapse. This is also confirmed by recent numerical studies (Kwon and Kim, 2010; Frascadore et al., 2014). Furthermore, the brittle failures are dangerous for the structural stability because of a reduced ductility exhibited under imposed horizontal loads. The lack of proper confinement pressure and shear reinforcement results in the structure not being able to carry the

seismic ductility demands. Shear critical members, such as squat column, shear walls and partially confined beam-column joints are most susceptible to these failures. Consolidated assessment procedures and field-inspections demonstrated that the shear failure of beam-column joints is often detrimental to the seismic capacity of existing structural systems (Paulay and Priestley, 1992; Pampanin et al., 2007; Reluis, 2009; Frascadore et al., 2014; Leon et al., 2014).

1.1 MOTIVATION

Particular emphasis has been given to the seismic behavior of existing structural systems. The interest of the scientific community in the seismic capacity assessment and in the development of reliable strengthening techniques recently increased. This is because of the notable number of existing structures and the number of countries involved on such aspects. In fact, the structural systems designed before the introduction of adequate seismic codes in the mid 1970's, commonly shows structural deficiencies related to inadequate amounts of transverse reinforcement and non-seismic details. This is particularly true of beam-column joints. Over the last century, little attention has been given to these elements in design codes and construction practices. This has led to a large number of structural systems that are vulnerable to seismic events because of poorly detailed beam-column joints.

In the recent years, several techniques have been proposed to improve the seismic capacity of beam-column joints. Current research efforts have focused on developing sound and cost-effective retrofit strategies and techniques. In particular, Fiber Reinforce Polymer (FRP) systems have gained popularity as a strengthening solution because they are light weight, durable and easy to install (Bakis et al., 2002). A large number of experimental tests were carried out to investigate the seismic performance of beam-column joints strengthened with FRP systems. They pointed out the effectiveness of FRP systems to improve the strength and deformation

capacity of beam-column subassemblies. More recent tests (Figure 1.2a) and analytical studies on typical existing RC buildings demonstrated that the adoption of FRP materials as a local strengthening solution is a cost effective solution to improve the global seismic capacity (Pampanin et al., 2007; Di Ludovico et al., 2008; Frascadore et al., 2014; Prota et al., 2014).

(a) (b)

Figure 1.2 FRP retrofit of beam-column joints: experimental test on a existing building (Di Ludovico et al., 2008) (a) and field application in L'Aquila (Balsamo et al., 2012) (b).

This background has promoted the installation of composite materials in the aftermath of major recent earthquakes (see Figure 1.2b). Although the effectiveness of FRP systems for the strengthening of beam-column joints has been investigated, few studies have specifically addressed capacity models to reliably predict their benefits. Several models have been proposed (Antonopoulos and Triantafillou, 2002; Tsonos, 2008; Akguzel and Pampanin, 2010; Bousselham, 2010), but a simple and generalized formulation suitable for practical applications of different joint types and FRP strengthening layouts, is still lacking. Difficulties arise in the model definition once the main parameters affecting the mechanical behavior of the strengthening system are selected. The FRP effectiveness strongly depends on a large number of parameters whose influence should be properly quantified.

1.2 RESEARCH OBJECTIVE

This research work aims at clarifying the seismic behavior of partially confined beam-column joints for existing structural systems and to quantify the benefits provided by FRP strengthening. To support the research activities, a wide experimental program on full-scale beam-column subassemblies has been conducted. The test program involves poorly detailed corner joints, which represents the most vulnerable members of existing RC structural systems. The purpose of the experiments is to investigate the principles of the mechanical behavior and the main parameters that play a key role in the resisting mechanisms. In order to provide further information to be used in the problem theorization, the joint panel strength and deformation capacity will be closely monitored, including the FRP mechanical behavior.

In spite of the demonstrated effectiveness of FRP systems increasing the seismic capacity of existing structural systems, the mechanical behavior of unconfined RC beam-column joints externally bonded with FRP systems remains a critical issue. The large number of parameters involved makes the calibration of simple and reliable formulations difficult. Several models have been proposed in recent years but, in spite of their effectiveness, they implement complex solution procedures or can be applied only to specific joint types or FRP layouts. Therefore, the international guidelines and codes on the design of FRP retrofit systems currently do not provide specific formulations to account for the FRP contribution to the shear strength of beam-column joints.

Based on experimental observations, this research work aims at developing a new capacity model to compute the FRP contribution to the shear strength of poorly detailed beam-column corner joints.

1.3 ORGANIZATION

The present research work focuses on the seismic behavior of beam-column joints of existing structural systems and the strengthening with FRP systems. The main scope of this work is to clarify the behavior of beam-column joints typical of existing buildings in the Mediterranean area and develop a simple theoretical model suitable to design the FRP strengthening. The work is organized as follows.

In the first chapter the seismic vulnerability of existing buildings and the role of the beam-column joints is introduced.

The second chapter deals with the seismic behavior of as-built beam-column joints; the strength and deformation capacity are investigated and the available capacity models are evaluated. The same discussion is carried out for beam-column joints retrofitted with FRP system.

The third chapter reports the design of the experimental program with the specimen details and the test setup. The design of the FRP strengthening schemes are discussed in detail. Furthermore, the test results and experimental observations are described.

In the fourth chapter the tests results are discussed with respect to the accuracy of available capacity models for as-built joints and the effectiveness of the FRP strengthening. Furthermore, the main parameters influencing the joint panel and FRP strengthening mechanical behavior are discussed.

The fifth chapter reports the model formulation. In particular, the mechanical models already developed for as-built joints and a large database of experimental results on FRP strengthened joints have been used to develop and validate a new strength capacity model suitable for practical applications.

The sixth chapter illustrate a new numerical model suitable to reproduce the hysteretic behavior of as-built joint subassemblies with the non-linear Finite Element Method (FEM) software VecTor2. The theories adopted to reproduce the nonlinear shear behavior are briefly introduced and the capabilities of this software to predict the hysteretic behavior, marked by a

strong strength and stiffness degradation, are reported. Furthermore, the comparisons in terms of crack patterns and joint panel shear stress-strain behavior are presented.

In the conclusion final remarks and possible future research actives are discussed.

CHAPTER 2
SEISMIC BEHAVIOR OF BEAM-COLUMN JOINTS

The seismic behavior of beam-column joints represents a challenging task for the research community. Strong effort has been put to investigate the joint cyclic behavior and found reliable solutions to improve their seismic capacity. Experimental programs and theoretical studies have been carried out in order to point out the main parameters affecting the cyclic response. As result of these studies, reliable design formulations have been developed to proper design the amount of transverse reinforcement and allow the joint panel to transfer the actions to adjacent members. Further studies focused on the joint panel deformability provided reliable analytical models to account for the effects of joint shear distortions on the global displacement demand.

Even though the seismic design of beam-column joint is nowadays widely established, difficulties assessing the seismic behavior of poorly detailed beam-column joints still persist. This because of the strong nonlinear behavior related to the joint premature cracking in absence of adequate internal reinforcements.

In order to provide a background on the seismic behavior of beam-column joints, a literature review has been carried out. The mechanical behavior of joint panel with internal reinforcements and the main differences with poorly detailed beam-column joints are reported. The available capacity models and code prescriptions relevant for this research work, are described. Furthermore, recent experimental tests and available capacity models concerning the joint strengthening with FRP systems are deeply analyzed.

2.1 JOINT CLASSIFICATION

The beam-column joints has a key role in the seismic performances of RC moment resisting frames. Seismic events provide reverse cyclic actions on the beam-column joints transmitted by the adjacent members. In particular, the joint panel is subjected to shear forces many times higher than in the adjacent members. The structural response of the joint panel is governed by a large number of parameters. In particular, the position in the RC frame is relevant for the structural response and divides the joints in different categories (see Figure 2.1). The joint can be classified in:

- Two-dimensional 2D (Figure 2.1a,b,c), joints typical of existing buildings with one way frame or bridge bents;
- Three-dimensional joints 3D (Figure 2.1d,e,f) occur in space frames;
- Partially-confined joints (Figure 2.1a,b,c,d,e), with not all the faces confined by framing beams;
- Fully-confined joints (Figure 2.1f), joint of interior frames with all the faces confined by framing beams;

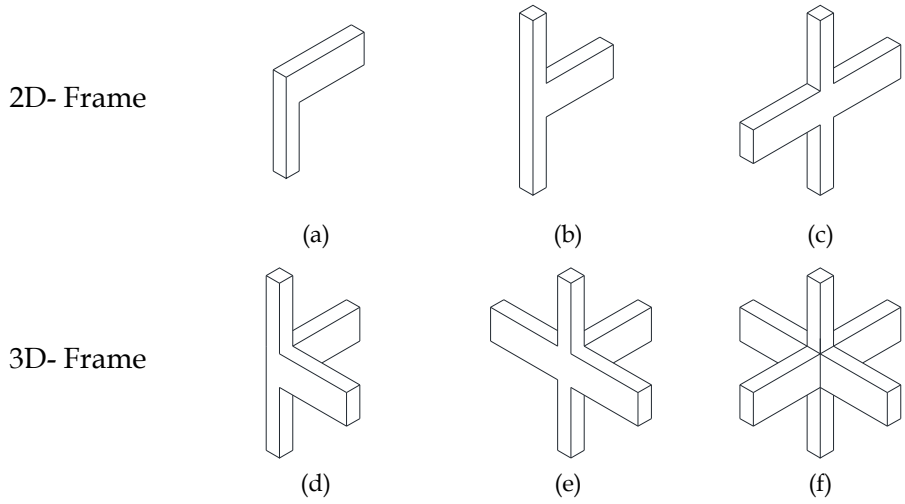

Figure 2.1 Beam-column joints in a RC frame: knee joint (a); T-joint (b); X-joint (c)(e); corner joint (d); fully-confined joint (f).

The structural response strongly depends on the numbers of framing beams and the anchorages type. In particular, the partially confined beam-column joints resulted the most vulnerable to seismic actions. Although the concept of joint confinement has been adopted to distinguish the different joint type, the structural response is mainly related to the external forces transmitted by framing members. Thus, among the partially confined beam-column joints, a further classification is needed in order to make a distinction between 2D-joints with one or more framing beams in the load plane. In particular, the joints with only one beam (Figure 2.1a,b,d) are named exterior joints; the joints with beams framing in the joint panel on both faces (Figure 2.1c,e) are commonly named interior joints. Indeed, in this research work, the terms interior and exterior joints will be adopted hereafter.

In order to investigate the joint mechanical behavior, the shear forces acting in the joint panel should be introduced.

2.2 ACTIONS AT THE JOINT

During a seismic event, large shear forces may be introduced in the joint panel. To establish the origin and the magnitude of acting forces, the equilibrium of a typical 2D subassembly (see Figure 2.2) is analyzed. The subassembly reported in Figure 2.2 is an interior joint with column extending between two points of contraflexure, at approximately half-storey heights.

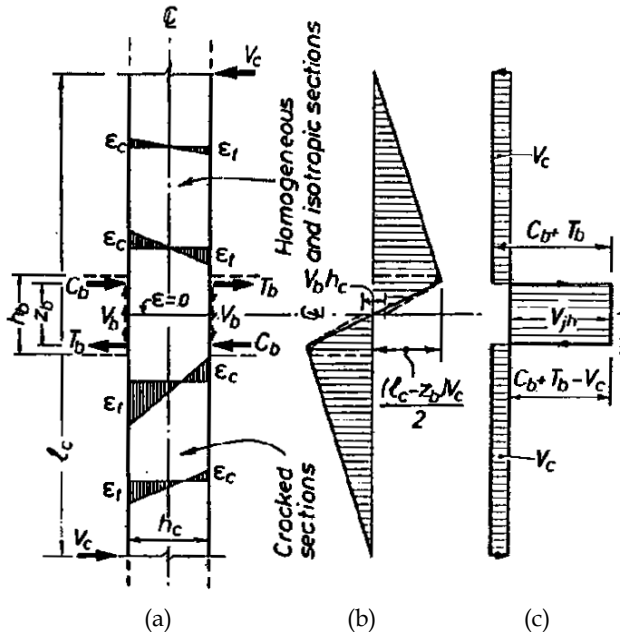

Figure 2.2 Equilibrium of a typical exterior joint subassembly (Paulay and Priestley, 1992): external forces (a); bending moment (b); shear forces (c).

External actions are introduced in the joint panel by beams and columns. In particular, during a seismic event, the joint panel is subjected to bending moment M_b and shear force V_b transmitted by the beams and M_c and V_c plus the axial loads N_c transmitted by the columns. These actions generate a

complex stress field that can be simplified in joint shear and axial force. The beam bending moments can be schematized with internal horizontal tension T_b and compression C_b forces (see Figure 2.2a). The horizontal joint shear force V_{jh} (see Figure 2.2c) can be computed with the expression :

$$V_{jh} = T_b + C_b - V_c \tag{2.1}$$

Assuming that internal forces are equal C_b = T_b and using the notation reported in Figure 2.3 to identify the tension forces transmitted by the two beams, expression (2.1) can be written:

$$V_{jh} = T + T' - V_c \tag{2.2}$$

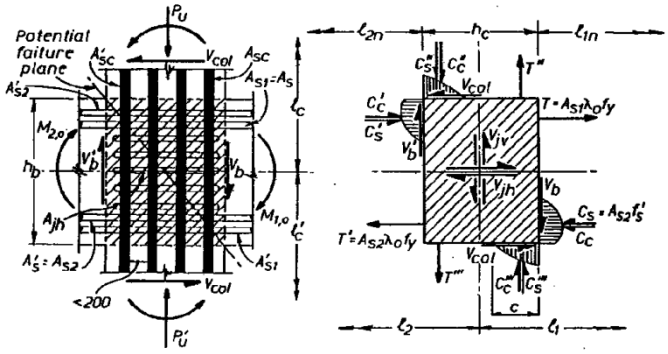

Figure 2.3 External actions on the joint panel (Paulay and Priestley, 1992).

As reported in Figure 2.3, the flexural reinforcement areas can be named A_{s1} and A_{s2} for the beam top and the bottom side, respectively. The tensile steel is assumed to develop the maximum stress $\lambda_o f_y$ where λ_o is the over-strength factor. Fixing the ratio between longitudinal reinforcements β=A_{s2}/A_{s1}, the joint shear becomes:

$$V_{jh} = \left(A_{s1} + A_{s2}\right)\lambda_o f_y - V_c = \left(1+\beta\right)\lambda_o f_y A_{s1} - V_c \tag{2.3}$$

The vertical joint shear V_{jv} can be derived by equilibrium of vertical forces as done for Eq. (2.3) or estimated with sufficiently accuracy as :

$$V_{jv} = \left(h_b + h_c\right) V_{jh} \tag{2.4}$$

which implies, to satisfy the rotation equilibrium of the joint panel, that the vertical joint shear must be proportional to the horizontal shear approximately in proportion by the member heights, h_b/h_c.

2.3 JOINT DIMENSIONS

In order to make consideration on the joint capacity, it could be convenient to express the joint actions in terms of shear stresses. The horizontal shear stresses can be computed dividing the horizontal joint shear V_{jh} for the effective joint area $b_j \cdot h_j$. However, the joint dimensions are not uniquely defined but depend on the dimensions of framing members (see Figure 2.4).

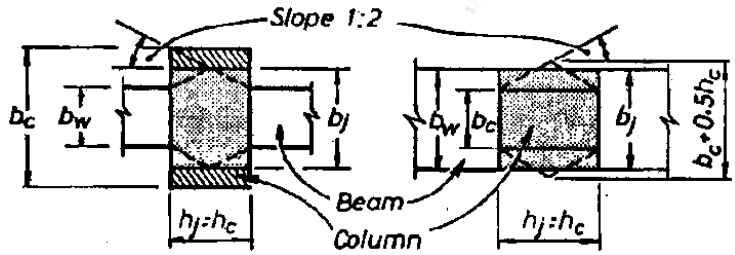

Figure 2.4 Effective joint dimensions (Paulay and Priestley, 1992): $b_c \geq b_w$ (a); $b_w \geq b_c$ (b).

The effective length of the joint core, h_j, can be taken as the overall depth of the column, h_c. The effective width of a joint, b_j depends on the framing member width (b_w in Figure 2.4). In particular, it should account for the stress distribution in concrete surrounding the longitudinal reinforcements (assumed at 45°). It resulted in:

$$\begin{cases} b_j = \min\left(b_c \ ; \ b_w + 0.5h_c\right) & \text{if } b_c \geq b_w \\ b_j = \min\left(b_w \ ; \ b_c + 0.5h_c\right) & \text{if } b_c \leq b_w \end{cases} \quad (2.5)$$

2.4 JOINT WITH INTERNAL REINFORCEMENTS

As a consequence of seismic moments in beams and columns, the joint subassemblies are subjected to large shear force that should be properly resisted to avoid the joint panel brittle failure. In the previous paragraph, general formulations have been suggested to evaluate the magnitude of joint shear. It is now necessary to introduce the joint resisting mechanisms to quantify the joint shear strength. At this stage, due to significant differences in the mechanical behavior, different mechanical models have been developed for interior and exterior joints.

2.4.1 Interior joints

The joint panel resists the shear and axial forces transmitted by adjacent members by means of basic mechanisms of RC member subjected to shear. These mechanisms involve the concrete alone, by means of a resisting diagonal strut (Figure 2.5a) and, where available, the transverse reinforcements in a truss resisting mechanism (Figure 2.5b).

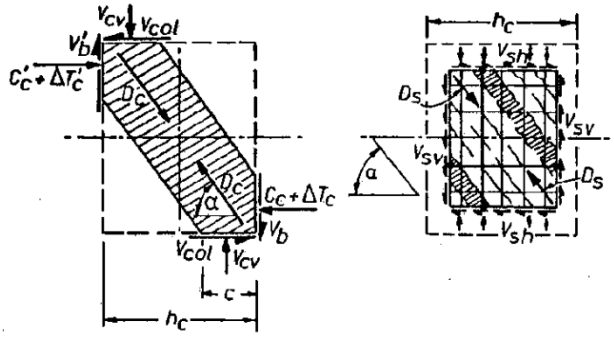

(a) (b)

Figure 2.5 External actions and internal stress in the joint panel (Paulay and Priestley, 1992): diagonal strut (a); truss mechanism (b).

It is reasonable to assume that the shear forces are introduced to the joint in the flexural compressive zones. Furthermore, the main portion of beam internal forces, $T+C'_s$, is introduced by means of bond. Only a fraction of this force, $\Delta T'_c$, will be transmitted to the diagonal strut. Indeed, it can be assumed that the total resisting shear is:

$$V_{jh} = V_{ch} + V_{sh} \tag{2.6}$$

where V_{ch} is the concrete strut contribution and V_{sh} the truss contribution related to transverse reinforcements. Considering the force distribution reported in Figure 2.5, the total force that goes in the concrete strut can be assumed:

$$V_{ch} = C'_c + \Delta T'_c - V_c \tag{2.7}$$

The rest of the external forces $V_{sh}=V_{jh}$ -V_{ch} goes in the truss. In order to proper quantify the two contributions, the bond strength should be closely examined. In particular, a realistic estimation of C'_c and $\Delta T'_c$ magnitudes related to the steel stress and bond force distributions is needed. A realistic distribution is suggested in Figure 2.6. which accounts for steel hardening and bond deterioration. Furthermore, it is assumed that no bond is developed in the concrete cover over a thickness of $0.1h_c$. Closely observing the bond distribution in Figure 2.6b, it can be assumed, over the flexural compression zone of the column, an uniform distribution of the bond force of about 1.25 times the average unit bond force u_o. Moreover, assuming that the bond force is introduced to the diagonal strut over an effective depth of $0.8c$, $\Delta T'_c$ can be evaluated as:

$$\Delta T'_c = 1.25u_o \cdot 0.8c = u_o \cdot c = \left(C'_s + T\right)\frac{c}{h_c} \tag{2.8}$$

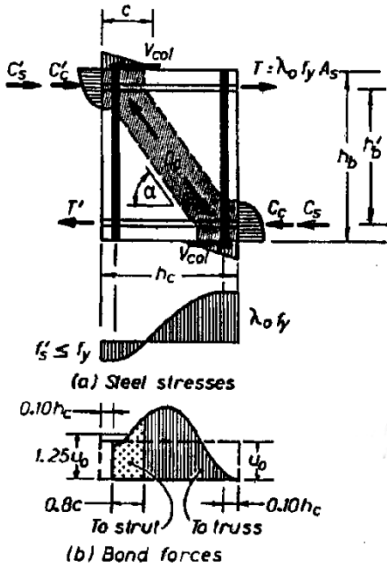

Figure 2.6 Steel stresses and bond forces distribution in a typical joint panel (Paulay and Priestley, 1992).

Because of the bond deterioration along beam bars, the steel compression force is limited to the yield strength f_y. Thus:

$$C'_s = \gamma f_y A_s = \frac{\gamma}{\lambda_o} T \tag{2.9}$$

where γ is the efficiency factor of beam bars in compression. The ratio γ/λ_o can be assumed equal to 0.55. It results that Eq. (2.8) can be written:

$$\Delta T'_c = \left(\frac{\gamma}{\lambda_o} + 1 \right) T \frac{c}{h_c} = 1.55 \frac{c}{h_c} T \tag{2.10}$$

and the compression force in the concrete:

$$C'_c = T - C'_s = \beta T - 0.55T \tag{2.11}$$

Therefore the contribution of the strut mechanism is:

$$V_{ch} = C_c' + \Delta T_c' - V_c = (\beta - 0.55)T + 1.55\frac{c}{h_c}T - V_c \Rightarrow$$
$$V_{ch} = \left(\beta - 0.55 + 1.55\frac{c}{h_c}\right)T - V_c \tag{2.12}$$

The joint shear force resisted by the truss mechanism can be now obtained by Eqs. (2.3), (2.6) and (2.12):

$$V_{sh} = V_{jh} - V_{ch} = \left[(1+\beta)\lambda_o f_y A_{s1} - V\right]_c - \left[\left(\beta - 0.55 + 1.55\frac{c}{h_c}\right)T - V_c\right] \Rightarrow$$
$$V_{sh} = 1.55\left(1 - \frac{c}{h_c}\right)T \tag{2.13}$$

Approximating the depth of the flexural compression zone with:

$$\frac{c}{h_c} = \left(0.25 + 0.85\frac{P}{f_c' A_g}\right) \tag{2.14}$$

where P is the minimum compression force acting on the column,the final expression of the joint shear of the truss mechanism is:

$$V_{sh} = \left(1.15 - 1.3\frac{P}{f_c' A_g}\right)T \tag{2.15}$$

Using the relation $A_{jh}=V_{sh}/f_{yh}$ the amount of horizontal shear reinforcements can be easily computed.

Analyzing the ratio V_{sh}/V_{jh}, the magnitude of the different contributions can be derived.

$$\frac{V_{sh}}{V_{jh}} = \frac{1.15 - 1.3\left(P / f_c' A_g\right)}{0.85(1+\beta)} \tag{2.16}$$

For typical value of the axial load $P=0.1f'_cA_g$ and for $1 \geq \beta \geq 0.5$, the truss mechanism have to resist 60 to 80% of the total horizontal joint shear force with the concrete in compression. The concrete crushing may be a severe limitation for the joint performances and should be carefully checked accounting for the reduction of concrete compressive strength for tensions in joint shear reinforcements and cyclic diagonal cracks. A design limitation to the joint shear stress v_{jh} is suggested by (Paulay and Priestley, 1992):

$$v_{jh} = \frac{V_{jh}}{b_j \cdot h_j} \leq 0.25 f'_c \leq 9.0\text{MPa} \tag{2.17}$$

The same approach can be used to derive the required amount of vertical reinforcements, however the axial load should be accounted for. According to the equilibrium conditions, assuming the contribution of the horizontal shear reinforcements and an inclination of the truss about h_b/h_c, the required amount of vertical reinforcements is:

$$A_{jv} = \frac{1}{f_y}\left[0.5\left(V_{jv} + V_b\right) - P\right] \tag{2.18}$$

Obviously, when Eq. (2.18) becomes negative no vertical joint shear reinforcement is required. Commonly, the effects of axial load, or the amount of column longitudinal intermediate reinforcement (which can be considered as vertical joint shear reinforcement), limit the use of joint vertical reinforcements. In absence of column intermediate reinforcements or in the case of weak columns, as commonly found in existing buildings, joint vertical reinforcement may be required.

2.4.2 Exterior joints

Because at the exterior joints only one beam frames into the column, different formulations are needed to represent their mechanical behavior. The same approach of interior joints can be adopted considering the

differences in external forces. Assuming that external actions are those reported in Figure 2.7, the horizontal shear force is:

$$V_{jh} = T - V_c \tag{2.19}$$

The resisting mechanisms are the same of interior joints. However it is necessary that the longitudinal beam reinforcements are bent in the joint core to allow the concrete strut to develop. In fact, the beam bent reaction is required to contrast the diagonal compression force.

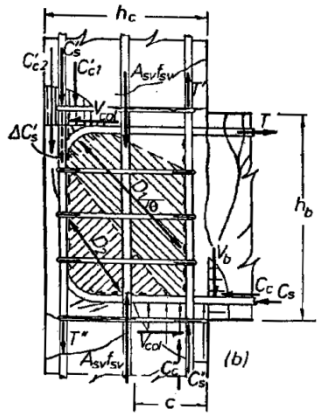

Figure 2.7 External actions on an exterior joint (Paulay and Priestley, 1992).

However, this reaction cannot be easily evaluated, thus the external force acting in the bottom-right corner (see Figure 2.7) will be used for calculations. As assumed for the interior joints, in a RC beam subjected to bending moment the tension and compression force should be equal $T = C = C_c + C_s$. As explained for interior joints, the horizontal component of the strut mechanism is:

$$V_{ch} = C_c + \Delta T_c - V_c \tag{2.20}$$

where ΔT_c is the fraction of the steel compression force C_s of the bottom beam reinforced introduced to the strut by bond. Based on experimental

tests, it can be assumed that the bond deterioration limits the steel compression force to the yield strength:

$$C_s = f_y A'_s = \frac{\beta}{\lambda_o} T \tag{2.21}$$

and it can be derived that $C_c=T-C_s=(1-\beta/\lambda_o)T$, where $\beta = A'_s/A_s$.
A different bond distribution is assumed with respect to interior joints. Over the flexural compression zone of the column, a uniform distribution of the bond force of about 2 times the average unit bond force u_o can be assumed. Assuming that the bond force is introduced to the diagonal strut over an effective depth of $0.7c$, $\Delta T'_c$ can be evaluated as:

$$\Delta T'_c = u_o \cdot c = \frac{1.4 C_s \cdot c}{h_c} = \frac{1.4 \cdot c \cdot \beta \cdot T}{\lambda_o \cdot h_c} \tag{2.22}$$

By assuming again that the effective bond transferred to the diagonal strut occurs over 0.8_c, the magnitude of V_{ch} is:

$$V_{ch} = C_c + \Delta T_c - V_c = \left(1 - \frac{\beta}{\lambda_o}\right) T + \frac{1.4 \cdot c \cdot \beta \cdot T}{\lambda_o \cdot h_c} - V_c \tag{2.23}$$

Approximating the depth of the flexural compression zone with Eq. (2.14), the magnitude of V_{sh} is:

$$\begin{gathered} V_{sh} = V_{jh} - V_{ch} = \left[T - V_c\right] - \left[\left(1 - \frac{\beta}{\lambda_o}\right) T + \frac{1.4 \cdot c \cdot \beta \cdot T}{\lambda_o \cdot h_c} - V_c\right] \Rightarrow \\ V_{sh} = \frac{\beta}{\lambda_o}\left(0.7 - \frac{P}{f'_c \cdot A_g}\right) T \end{gathered} \tag{2.24}$$

The required amount of transverse reinforcements can be computed:

$$A_{jh} = \frac{V_{sh}}{f_{yh}} = \frac{A'_s}{A_s \lambda_o}\left(0.7 - \frac{P}{f'_c \cdot A_g}\right) \frac{f_y \lambda_o A_s}{f_{yh}} = A'_s \left(0.7 - \frac{P}{f'_c \cdot A_g}\right) \frac{f_y}{f_{yh}} \tag{2.25}$$

This equation points out that the amount of horizontal shear reinforcement depends on to the area of beam bottom longitudinal reinforcements. Although near the supports the beam top longitudinal reinforcement is able to carry a tensile force higher than bottom bars, it should be considered that, according to the assumption of this approach, only a fraction ΔT_c of the steel compression force C_s of the bottom beam reinforced is introduced to the strut by bond. The rest of the total compression force (assumed equal to the tension force) is introduced to the concrete strut mechanism. Thus, if the joint subassembly is subjected to a beam bending moment with beam top bar in tensions, the required amount of horizontal transverse reinforcements is governed by the area of beam bottom reinforcements and vice versa.

2.5 POORLY DETAILED BEAM-COLUMN JOINTS

As outlined in the previous paragraphs, large shear forces are introduced at the joint panel due to reverse seismic actions. If a proper amount of transverse reinforcement is not placed in the joint panel, a premature brittle failure may occur. This failure is often detrimental for the global seismic capacity. However, the joint panel transverse reinforcements have been introduced in design codes only in the recent years. Indeed, a relevant number of existing structural systems have lack of internal reinforcements in the joints.

The capacity models developed for joints with transverse reinforcement seems to be not appropriate for joint without transverse reinforcements. The absence of internal reinforcements and the reduced strength of concrete in tension do not allow the development of the truss mechanisms and the premature diagonal cracking of the joint panel can be observed. The cracked behavior of the joint panel is governed by resisting mechanisms that cannot be schematized with the strut mechanism, because the maximum strength may be governed by other phenomena such as the maximum shear on the cracks and the loss of equilibrium. To assess the seismic capacity of poorly

detailed beam-column joints, specific mechanical models have been recently developed.

2.5.1 Principal stresses approach

The joint panel is subjected to a significant and complex stress field generated by seismic excitation (bending moment, shear and axial load) (Figure 2.8a). The beams and columns introduce large shear forces in the concrete core. Replacing the flexural bending moments with the resulting tension , T, and compression forces , C, (Figure 2.8b), the joint shear force in the vertical, V_{jv}, and horizontal, V_{jh}, directions can be computed as shown in Figure 2.8c with the formulations reported in the sections 2.2 and 2.4.2. To satisfy rotational equilibrium, the vertical joint shear must be proportional to the horizontal shear; they are approximately in proportion by the joint dimensions, h_b /h_c. These large shear forces lead to diagonal compressive and tensile stresses in the joint core that may result in severe joint cracking (Figure 2.8a), especially in the case of under-designed beam-columns joints without a proper amount of internal stirrups (i.e. transverse reinforcement). A diagonal strut can be used to capture this effect. However, in the case of structural members dominated by shear, diagonal tension failure can govern over concrete strut crushing. This is particularly common on beam-column joints with a low amounts of transverse reinforcement. It would appear that more basic and relevant information could be obtained from examination of nominal principal tension and compression stresses in the joint.

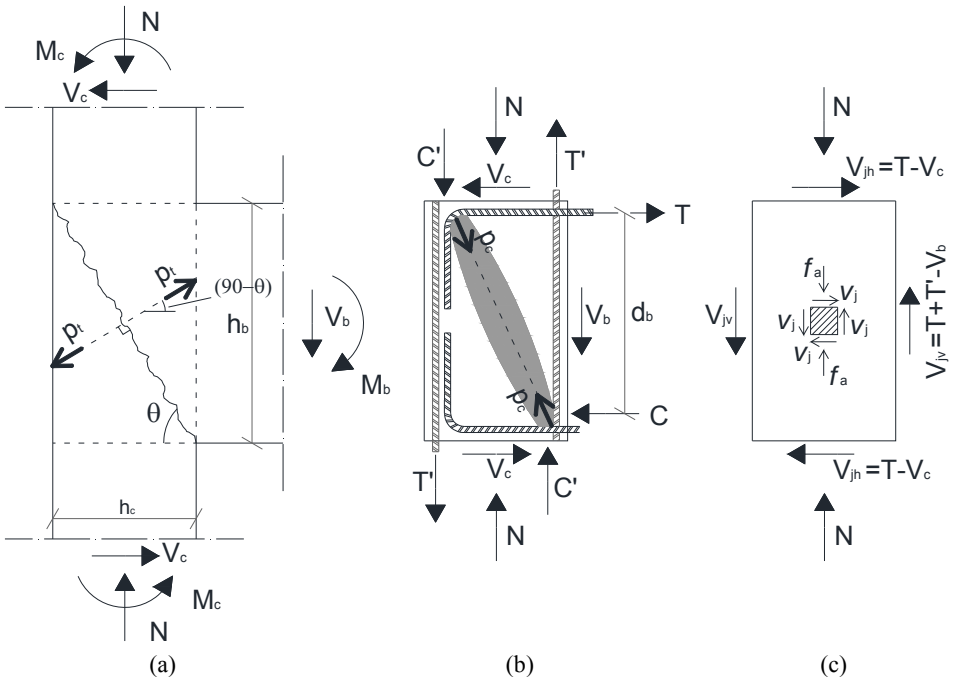

Figure 2.8 Actions and resisting mechanisms in corner beam-column joints (a), (b), (c).

These assumptions resulted in an analytical model (Priestley, 1997) based on the Mohr's circle of a typical stress field of the joint panels (Figure 2.8c) characterized by uniform shear stresses, $v_{jh} = V_{jh} / A_{col}$, and axial stress, $f_a = N / A_{col}$. Once the axial and shear stresses on two faces of the joint panel are known, the Mohr's circle can be derived computing the coordinates of the centre C [(σ_{11}-σ_{22})/2; 0] as difference between the normal stresses acting on two orthogonal sides of the joint panel. Because no axial load is transmitted by the beams, σ_{22}=0 and in turn, C is (f_a/2; 0). The radius of the circle is the distance between the centre C and a point with a known stress field P (f_a ; v_j). The Mohr's circle of a typical joint panel is depicted in Figure 2.9a along with the principal tension and compression stresses, p_t and p_c, respectively. Furthermore, the directions of principal tension and

compression stresses, inclined of $90°$-θ and θ, respectively, are depicted in Figure 2.9b with dashed line.

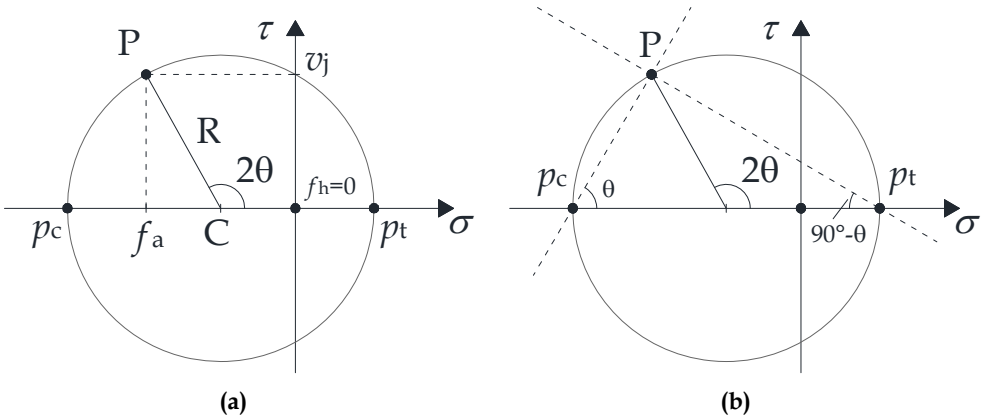

Figure 2.9 Mohr's circle of stresses for a typical joint panel: principal stresses (a) and principal directions (b).

The magnitude of the principal tension and compression stress can be easily derived by geometric consideration on the Mohr's circle, see Eqs. (2.26) and (2.27).

According to experimental evidence, Priestley suggested to limit the average principal stresses in tension Eq. (1) or compression Eq. (2) to values proportional to the concrete compressive strength (Priestley, 1997).

$$p_t = -\frac{f_a}{2} + \sqrt{\left(\frac{f_a}{2}\right)^2 + v_{jh}^2} \le k\sqrt{f_c} \tag{2.26}$$

$$p_c = \frac{f_a}{2} + \sqrt{\left(\frac{f_a}{2}\right)^2 + v_{jh}^2} \le 0.5 f_c \tag{2.27}$$

Here, k is a numerical coefficient which incorporates several mechanisms affecting the joint shear strength in tension. Number of parameters affects

the magnitude of this coefficient and the analysis of available literature studies can make this aspect clear.

2.5.2 Parameters affecting the joint shear capacity

Different mechanisms affect the joint panel shear strength in tension (i.e. maximum shear on the cracks, loss of equilibrium, local failures due to bar slip or anchorage opening). Difficulties arise detecting the failure mode and separating the effects because of the particular stress field of joint panel and the influence of local stresses. Thus, as initially proposed by Priestley et al. (1996), a numerical coefficient is commonly adopted to define the stress limits.

Several studies pointed out that this coefficient depends on the joint type, type of internal reinforcements, anchorage details, damage limit state and direction of loads. In particular, based on evidence of vast experimental programs (Kurose, 1987; Hakuto et al., 1995), Priestley (1996; 1997) formulated that the diagonal cracking in the joint panel is initiated when the principal tension stress is equal to $0.29\sqrt{f_c}$ (MPa). For beam bars bent down across the back of the joint, higher principal tension stresses are possible with a peak of $0.42\sqrt{f_c}$ (MPa) and $0.58\sqrt{f_c}$ (MPa) for exterior joints, and corner joints under biaxial response, respectively. Note that under biaxial response of corner joints, the joint shear force is formed from the vectorial addition of the orthogonal shears.

Furthermore, with the Mohr's circle approach, the direction of the principal compressive stress, θ, can be computed. This angle represents a key issue in the assessment of poorly detailed beam-column joints, because it identifies the crack direction. The experimental evidence (Figure 2.10) and field surveys (see Figure 1.1) showed that large diagonal corner-to-corner cracks characterize the failure mode of beam-column joint under cyclic horizontal actions (Calvi et al., 2002), regardless of the joint dimensions or longitudinal reinforcement details. In absence of stirrups, the principal compressive stress after cracking, can be assumed to be inclined at a

constant angle, θ, and, in turn, the direction of principal tensile stress is inclined at $90°-\theta$. The angle θ can be computed, as proposed by Paulay and Priestley (Paulay and Priestley, 1992), as function of the joint panel dimensions by Eq. (3):

$$\theta = const = atan\left(\frac{h_b}{h_c}\right) \tag{2.28}$$

After the joint first cracking, commonly characterized by hairline diagonal cracks, the joint panel exhibits a marked nonlinear behavior. Increasing stress levels are exhibited after the opening of cracks in both directions and the increase in crack width. At the peak strength, the crack pattern outlines the joint panel failure mechanism. The exterior beam-column joints are commonly characterized by a shear failure with the concrete core divided in four rigid bodies and concrete wedge spalling-off due to the opening of beam bar anchorages (see Figure 2.10).

(a) **(b)**

Figure 2.10 Joint panel diagonal tension failures: (Ilki et al., 2011) (a) and (Calvi et al., 2002) (b).

Referring to interior beam-column joints, they are characterized by different failure mechanisms. Because both the joint faces are confined by beams, the concrete spalling is prevented. Large stress level may be

achieved, but in available experimental tests the subassembly failure mode is often characterized by bond failure or flexural failure of framing beams. More details on stress and strain limits for interior connections are reported in Anderson et al. (2008).

The concrete crushing is not a severe limitation for the performances of poorly detailed joint, however the reduction of concrete compressive strength for cyclic diagonal cracks should be properly accounted for. Concerning the principal compression stress p_c (Eq. 2.27), an upper limit could be $0.50 \cdot f_c$ (MPa). This limit is significantly higher than the tension limits. However, it should be considered that the principal compression stress is more influenced by the axial stress than by the shear stress.

2.5.3 Joints with plain reinforcements

Significant slips characterize the cyclic behavior of RC members with plain longitudinal reinforcements (Verderame et al., 2008; Di Ludovico et al., 2014). It strongly affects the hysteretic behavior that commonly shows a significant rocking with low dissipation energy and a marked softening related to the progressive concrete crushing. In the beam-column joints the opening of shear crack strongly increase the bar slip. Calvi et al. (2002) pointed out that the use of plain bars, whose anchorage relies almost entirely on the end-hook, enhances the formation of the wedge mechanism, due to the detrimental effects of the concentrated beam-bar compression force transmitted by the end-hook to the concrete wedge. The premature cracking along with a fast strength degradation is achieved at stress levels lower than joints with deformed bars. Test results showed that for plain internal reinforcement the maximum peak strength is reached immediately after the joint cracking and k can be assumed equal to 0.20.

A summary of the limits to the principal tension stress and the typical joint failures are reported in Table 2.1 and Figure 2.11, respectively.

Table 2.1. Limits to the joint panel principal tension stress, value of coefficient *k*.

Joint type	Bar type	Long. bar anchorage	Actions	
			In Plane	3D
Exterior	Deformed	Bent-in	0.29 (cracking) 0.42 (peak)	0.29 (cracking) 0.58 (peak)
		Bent-out	0.29	-
	Plain	Hooked	0.20	-
Interior	All	Continuous	0.29 (cracking)	-

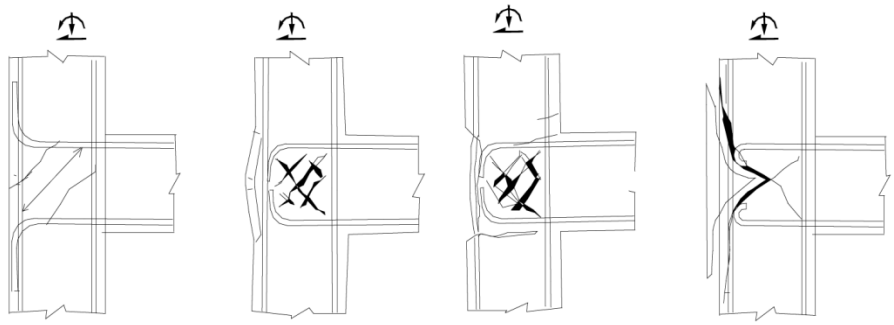

Figure 2.11 Summary of exterior joint shear failures (Calvi et al., 2002): (a) beam bar bent away from joint region; cover spalling (b); failure mode in joints with beam bar bent in the joint (c); concrete wedge mechanism in joints with plain bars (d).

2.5.4 The joint shear deformation

Minor importance has been reserved to the joint deformation and its effects on the frame global seismic response. This because of the predominant shear behavior of these structural elements and the difficulties in handle shear distortions. However, the joints have a key-role in the structural system and small joint shear deformations may have significant global effects. Although this aspect has been introduced by Priestley with the principal stresses approach (Priestley et al., 1996), recently the scientific community focused the attention on the role of joint shear deformations.

The joint shear deformations represent the complement of the joint shear strength. To be more precise, they are the effects of the shear stresses applied on the joint panel (see Figure 2.12). The joint panel stress field (reported in Figure 2.8c) imposes to the joint panel three main deformations: the axial compression, the horizontal shear deformation (Figure 2.12b) and vertical shear deformation (Figure 2.12c).

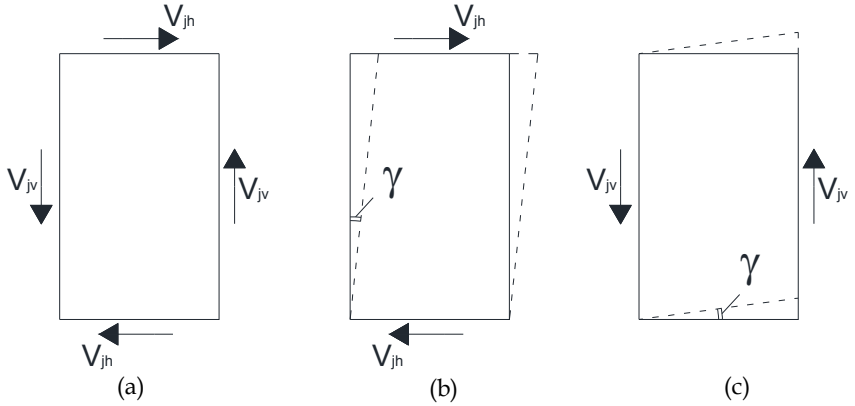

Figure 2.12 Shear stresses and shear deformations of a joint panel: joint panel shear stresses (a); horizontal shear deformation (b); vertical shear deformation (c).

An estimation of the magnitude of the shear deformations γ, assumed equal for the horizontal and vertical direction, was introduced by Priestly (Priestley et al., 1996). Based on experimental evidence, he provided shear strain limits at different stress levels (cracking, peak strength and joint collapse). Later, this model has been refined to include the relations for plain internal reinforcements (Calvi et al., 2002) (see Figure 2.13a). The authors also schematized the effects of the joint shear deformation on the interstorey drift (see Figure 2.13b). Recently, similar model has been proposed by Sharma et al. (2011) modifying the strain response according to recent experimental tests and accounting for different longitudinal beam bar anchorages.

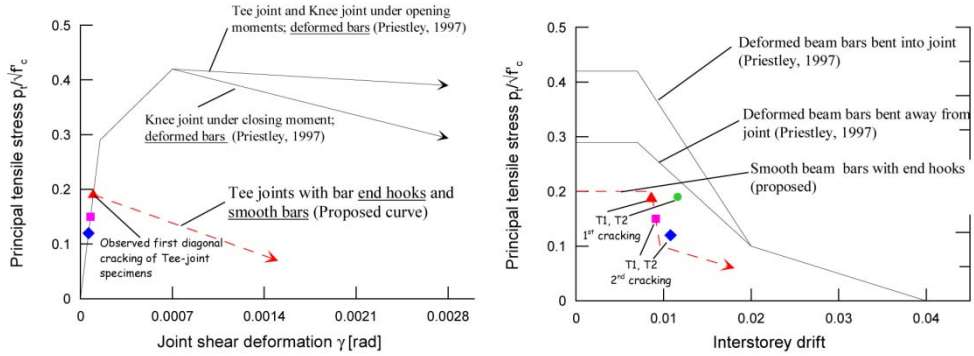

Figure 2.13 Deformability of poorly detailed beam-column joints (Calvi et al., 2002): joint shear deformation (a); effect of joint shear deformation on the interstorey drift (b).

Further limits to the joint deformability have been suggested by Pantelides et al. (2002). In particular, based on experiments on poorly detailed beam-column joints tested at different axial load levels, several limitations for the joint drift, crack width and shear strength have been provided at different performance levels (see Table 2.2). In particular five performance levels are proposed:

- Level I: is the first yielding of longitudinal reinforcements or hairline cracking;
- Level II: is the initiation of joint mechanism with visible cracks;
- Level III: full development of joint mechanism at the peak strength;
- Level IV: is the strength degradation with concrete spalling;
- Level V: is the total loss of gravity load.

Table 2.2. Limits to the joint panel shear strength and deformation (Pantelides et al., 2002).

(a) $0.1f'_cA_g$				(b) $0.25f'_cA_g$			
Performance Level	Drift ratio %	Crack Width (in)	γ (psi)	Performance Level	Drift ratio %	Crack Width (in)	γ (psi)
I	0.56	hairline	6.5	II	0.46	hairline	7.9
II	0.9	0.004	8.6	I	0.7	0.004	10.7
III	1.9	0.05	12.4	III	1.5	0.10	13.3
IV	2.5	≥0.18	10.5	IV	2.0	≥0.33	9.7
V	>3.5	—	<6.3	V	>2.7	—	<5.0

Refined analytical models have been proposed in the recent years. Based on a rigorous theory on the shear behavior of RC structures (Vecchio and Collins, 1986), Lowes & Altoontash (2003) proposed a macro-model that includes the effects of bond-slip of internal reinforcements and joint panel shear deformations. However, the application of this model needs to be implemented in a specific software.

Recently, simplified capacity models have been proposed based on large database of experimental tests. Lafave and Kim (2011), proposed a semi-empirical capacity model including formulations to predict both the shear strengths and deformations. In detail, a 3 points model (see Figure 2.14) with the coordinates in terms of shear stress, v_j, and shear deformation, γ, have been proposed.

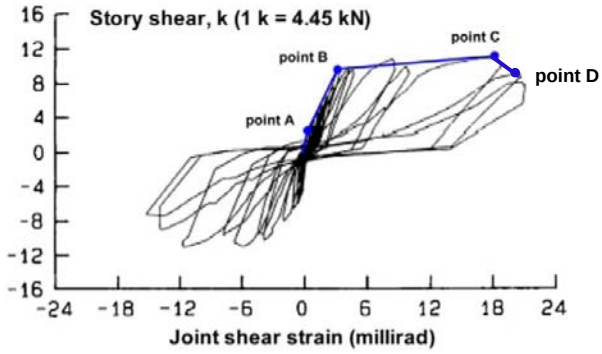

Figure 2.14 Analytical model for joint shear strength-deformation capacity (Lafave and Kim, 2011).

In particular:

- point *C* represents the subassembly peak strength; the joint shear stress and joint deformation can be derived with Eq. (2.29) and Eq. (2.30), respectively.

$$v_j = \alpha_t \cdot \beta_t \cdot \eta_t \cdot \lambda_t \cdot (JI)^{0.15} \cdot (BI)^{0.30} \cdot (f'_c)^{0.75} \,[\text{MPa}] \tag{2.29}$$

where: α_t is a parameter for in-plane geometry (1.0 for interior connections, 0.7 for exterior connections, and 0.4 for knee

connections); β_t is a parameter for out-of-plane geometry (1.0 for subassemblies with 0 or 1 transverse beams, and 1.18 for subassemblies with 2 transverse beams); $\eta_t = (1- e/b_c)^{0.67}$ describes joint eccentricity; and λ_t = 1.31; the joint transverse reinforcement index $JI = (\rho_j \cdot f_{yj})/f'_c$, in which ρ_j is the volumetric joint transverse reinforcement ratio in the direction of loading and f_{yj} is the yield stress of joint transverse reinforcement (for joints without transverse reinforcement $JI = 0.0128$); the beam reinforcement index $BI=(\rho_b \cdot f_{yb})/f'_c$, in which ρ_b is the beam reinforcement ratio and f_{yb} is the yield stress of beam reinforcement.

$$\gamma_j = \alpha_{\gamma t} \cdot \beta_{\gamma t} \cdot \eta_{\gamma t} \cdot \lambda_{\gamma t} \cdot (JI)^{0.10} \cdot BI \cdot \left(\frac{v_j}{f'_c} \right)^{-1.75} \quad [\text{Rad}] \quad (2.30)$$

where: $\alpha_{\gamma t} = JPRU^{2.10}$ is a parameter for in-plane geometry that depends also for the amount of transverse reinforcements, for $\beta_{\gamma t}$ is a parameter for out-of-plane geometry (1.0 for subassemblies with 0 or 1 transverse beams, and 1.18 for subassemblies with 2 transverse beams); $\eta_{\gamma t} = (1- e/b_c)^{0.67}$ describes joint eccentricity; and $\lambda_{\gamma t}$ = 1.31. JPRU was determined by dividing JPR by 1.2. In particular, for joints with lack of transverse reinforcements JPR= 1.0, 0.59, and 0.32 for interior, exterior, and knee joints, respectively.

- point *B* represents the yielding of joint transverse reinforcements or beam longitudinal reinforcements. In this case the joint shear stress and joint shear deformation can be derived as the product of numerical coefficients and Eq. (2.29) and Eq. (2.30).

$$v_j(B) = 0.89 \cdot v_j(C) \quad [\text{MPa}] \quad (2.31)$$

$$\gamma_j(B) = 0.36 \cdot \gamma_j(C) \quad [\text{MPa}] \quad (2.32)$$

- point *A* represents the joint panel first cracking. In this case the joint shear stress and joint shear deformation can be derived as the product of numerical coefficients and Eq. (2.29) and Eq. (2.30).

$$v_j(A) = 0.44 \cdot v_j(C) \quad [\text{MPa}] \tag{2.33}$$

$$\gamma_j(A) = 0.02 \cdot \gamma_j(C) \quad [\text{MPa}] \tag{2.34}$$

- point *D* is the post peak response at the 90%of the peak strength. In this case the joint shear stress and joint shear deformation can be derived as the product of numerical coefficients and Eq. (2.29) and Eq. (2.30).

$$v_j(D) = 0.90 \cdot v_j(C) \quad [\text{MPa}] \tag{2.33}$$

$$\gamma_j(D) = 2.02 \cdot \gamma_j(C) \quad [\text{MPa}] \tag{2.34}$$

In spite of the demonstrated effectiveness of the proposed model, particular care should be adopted in using this model for joints without transverse reinforcements. This is because of the small number of tests on poorly detailed beam-column joints available in the proposed database.

Based on large set of experimental data, Park and Mosalam (2012a) pointed out the main parameters affecting the shear strength of beam-column joints without transverse reinforcements. In particular, the amount of beam longitudinal reinforcements and the joint aspect ratio strongly affect the joint capacity. Furthermore, a new semi-empirical strength capacity model has been introduced. This model has been later modified to include a reasonable failure mechanism (Park and Mosalam, 2012b) and the subassembly deformations (Park and Mosalam, 2013). Using a strut and tie approach, a backbone curve is proposed to simulate the behavior of unreinforced corner and exterior joints (see Figure 2.15) under earthquake loading.

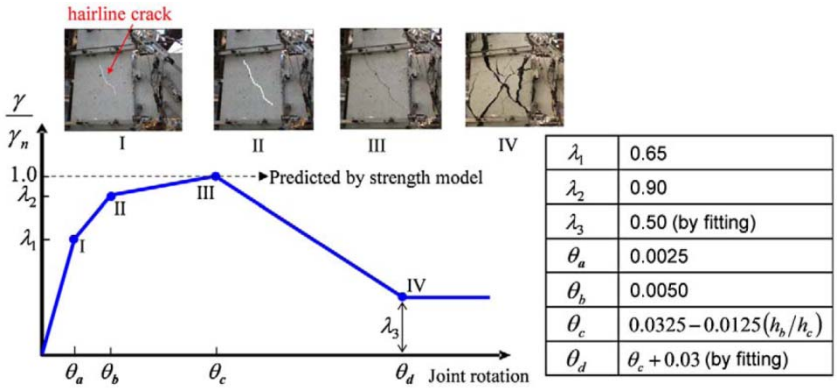

λ_1	0.65
λ_2	0.90
λ_3	0.50 (by fitting)
θ_a	0.0025
θ_b	0.0050
θ_c	$0.0325-0.0125(h_b/h_c)$
θ_d	$\theta_c+0.03$ (by fitting)

Figure 2.15 Backbone curve for T and corner joints (Park and Mosalam, 2013).

In particular, the shear stress is expressed in terms of the ratio $\lambda = \gamma/\gamma_n$, where $\gamma = v_{jh}/\sqrt{f'_c}$ and $\gamma = v_n/\sqrt{f'_c}$. The joint shear stress v_n , for T and corner joints, can be derived using the simplified strength capacity model:

$$v_n = \frac{V_n}{b_j h_c} = k\left[\sqrt{f'c}\,\frac{\cos(\theta)}{\cos(\pi/4)}\right] \quad [\text{MPa}] \tag{2.35}$$

where k can be derived by:

$$k = 0.4 + 0.6\left[\frac{SI_j - X_1}{X_2 - X_1}\right] \le 1.0 \tag{2.36}$$

The joint shear index can be derived by:

$$SI_j = \frac{A_s f_y}{b_j h_c \sqrt{f'_c}}\left(1 - 0.85\frac{h_b}{H}\right) \tag{2.37}$$

and:

$$X_1 = 0.33\sqrt{f'_c}\,\frac{\cos\theta}{\cos(\pi/4)} \quad \text{and} \quad X_2 = \sqrt{f'_c}\,\frac{\cos\theta}{\cos(\pi/4)} \tag{2.38}$$

The proposed backbone curve can be used to define the hysteretic behavior of a beam-column joint (see Figure 2.16a). In particular, the authors proposed to schematize the joint shear behavior with a rotational spring. To allow this simplification, the joint shear strength has been opportunely converted in the bending moment at the centre of the joint M_j.

The proposed model can be a reliable tool to include the joint capacity in terms of shear strength and deformation in the numerical simulation of RC building frames. Park and Mosalam (2013) demonstrated through nonlinear dynamic analysis that the joint deformability strongly affect the overall building response leading to interstorey drifts larger than models with rigid joints (Figure 2.16b).

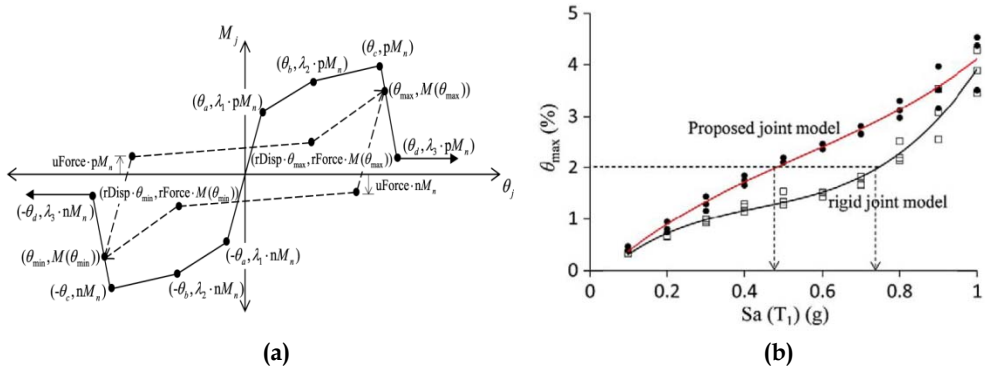

Figure 2.16 Analytical model of joint strength-deformation capacity (Park and Mosalam, 2013): joint capacity model (a); effect of joint shear deformation on the interstorey drift (b).

2.6 CODE REQUIREMENTS FOR BEAM-COLUMN JOINTS

The developments in the scientific research on the seismic behavior of beam-column joints took place after the severe seismic events in the 80's. Experimental and field evidence pointed out the role of internal transverse reinforcements improving the joint seismic performances. Before these events the joint shear reinforcements were almost never provided due to the lack of widely accepted theories. After a brief summary on the most

adopted theoretical approaches to design and assess the joint seismic capacity, the code provisions adopted in several national standards are reported herein. A distinction between the design approach and the code requirement to be used in the assessment procedure is needed.

2.6.1 Design of beam-column joints

The design of beam-column joints assumed significant relevance in modern seismic codes. The joint panel integrity should be guaranteed against seismic actions that produce severe joint shears. Thus the amount of transverse reinforcement in the horizontal and vertical directions should be properly designed. A summary on the developments in code provisions is reported herein.

- *Eurocode and Italian Building code approach*

Transverse reinforcements in the beam-column joints have been introduced in the Italian building code with the annex C.M.LL.PP. n°65 (MMLLPP, 1997) to the D.M. 1996 (MMLLPP, 1996). In particular, it has been prescribed to adopt in the joint panel at least the same amount of horizontal transverse reinforcements of the framing columns.
Recent developments in the scientific research on beam-column joints have been included in European standards EN 1998-1 (CEN, 2004) and in turn, in the new Italian building code D.M. 2008 (MI, 2008). These formulations are based on the principal stresses approach and assume that the stress field acting in the joint panel is the one proposed in Figure 2.8c. The effects of internal reinforcements can be schematized with an horizontal axial stress $\sigma_h=(A_{sh}\cdot f_{ywd})\ /b_j\cdot h_{jc}$. Using the Mohr's circle of stresses the principal tension stress is:

$$p_t = -\frac{f_a + \sigma_{sh}}{2} + \sqrt{\left(\frac{f_a + \sigma_{sh}}{2}\right)^2 + v_{jh}^2} \tag{2.39}$$

Assuming for design purpose that the principal tension stress cannot exceed the concrete tension strength f_{ctd}, the EN 1998-1 (CEN, 2004) formulation to design the amount of transverse reinforcements is:

$$\frac{A_{sh} \cdot f_{ywd}}{b_j \cdot h_{jw}} \geq \frac{\left(\frac{V_{jhd}}{b_j \cdot h_{jc}}\right)^2}{f_{ctd} + \nu_d f_{cd}} - f_{ctd} \tag{2.40}$$

Furthermore, it is prescribed that the diagonal compression induced in the joint by the diagonal strut mechanism shall not exceed the compressive strength of concrete in the presence of transverse tensile strains. Limiting the joint principal compression stress to value proportional to the joint compression strength, it results that:

$$\frac{V_{jhd}}{b_j \cdot h_{jc}} \leq \eta f_{cd} \sqrt{1 - \frac{\nu_d}{\eta}} \tag{2.41}$$

where η=0.6(1-f_{ck}/250) is a numerical coefficient accounting for the reduction in the concrete compression strength due to tension stresses or strains; ν_d is the normalized axial load; V_{jhd} is the joint shear (see Section 2.2). The concrete compressive strength should be reduced to 80% for exterior joint to account for the reduced degree of lateral confinement.

Alternatives prescriptions are reported both in the Eurocode (CEN, 2004) and Italian Building Code (MI, 2008). These prescriptions are based on the theoretical approach proposed by Paulay and Priestley (1992) that allows to separate the concrete strut and the truss contribution (see Section 2.4). In particular Eq. (2.15) and (2.24) have been modified considering the effective dimension of concrete strut and its variation due to reverse cyclic actions

(Fardis, 2009) in Eq. (2.42) and (2.43) for interior and exterior joints, respectively:

$$V_{sh} = A_{sh} f_{ywd} \geq \gamma_{Rd} \left(A_{s1} + A_{s2} \right) f_{yd} \left(1 - 0.8 \nu_d \right) \tag{2.42}$$

$$V_{sh} = A_{sh} f_{ywd} \geq \gamma_{Rd} A_{s2} f_{yd} \left(1 - 0.8 \nu_d \right) \tag{2.43}$$

Eq. (2.42) and (2.43) point out that the internal stirrups can be designed without consider the shear action on the joint panel. Indeed, the maximum joint shear force is reached at the yielding of the internal reinforcements. However, it should be noted that for the exterior joints, Eq. (2.43), the maximum shear force transferred to the stirrups is governed by the maximum bond on the longitudinal reinforcements in compression (see Section 2.4.2).

Fardis (2009) pointed out that there is a big discrepancy between the two design formulations proposed both by Eurocode and Italian standards. Furthermore, by comparing code predictions with experimental tests, a good agreement is reached only for medium-high values of the axial load ratio (ν>0.3). Indeed, it can be concluded that the joint shear reinforcement designed with these formulations should be adopted with confidence.

- *American standards*

The first provisions in the United States standards appeared in the ACI-ASCE 352 (1976) to limit the joint shear stresses in the joint panel. These limits were also adopted in the ACI 318 (1995). The nominal shear strength of the joint is limited to values proportional to the concrete compressive strength (expressed in MPa). The empirical values were calibrated on experimental tests of Guimaraes et al. (1989). In particular:

- for joints confined on all four faces ..... $1.7\, A_j \sqrt{f'_c}$
- for joints confined on three faces or on two opposite faces $1.2\, A_j \sqrt{f'_c}$
- for others ..... $1.0\, A_j \sqrt{f'_c}$.

Furthermore, a minimum amount of transverse reinforcement is required. It can be assumed at least equal to the half of transverse reinforcements in the framing columns or other members which are expected to yield. The same approach is reported in the current ACI 318 (2011) with more details for minimum amount of internal stirrups and anchorage of longitudinal reinforcements.

- *New Zealand and Japan standards*

A similar approach to the American standards have been adopted by the first version of the New Zealand standards NZS 3101 (1982).
A substantial improvement in the New Zealand standards was achieved after the development of the strut and truss theory by Paulay and Priestley (1992). Replacing the NZS 3101 (1982), based on the diagonal stress limitation, the NZS 3101 (1995) introduced new and simple formulations. These formulations can be derived by Eqs. (2.15) and (2.25) and allow to reduce the joint transverse reinforcements at least by 30% with respect to the previous code formulations. The same formulation have been adopted by the current NZS 3101 (2006).

Japanese standards AIJ (1989) essentially focused on the diagonal concrete strut failure, assuming that sufficient joint shear reinforcements were provided in order to avoid other premature mechanisms.

2.6.2 Assessment of existing beam-column joints

As discussed in the previous paragraphs, the seismic behavior of RC beam-column joints without transverse reinforcements should be considered apart from the behavior of well-detailed joints. In fact, existing structural members commonly have insufficient internal transverse reinforcements and premature failure mechanisms, such as shear failures in tension, may occur. Thus, in order to account for these premature failures,

the principal stresses approach is widely adopted in national standard for existing structures (CEN, 2004; MI, 2008; CS LL PP, 2009).

- *Eurocode and Italian Building Code*

European and Italian standards (CEN, 2005; MI, 2008; CS LL PP, 2009) adopt the principal stress approach to limit the joint panel shear capacity (see Section 2.5.1). The main difference in the two codes is represented by the stress limit to the principal tensile stress. Eurocode 8 (CEN, 2005) suggests to limits this stress to the tensile strength of concrete f_{ctd}. On the other side, the Italian building code imposes the limit of $0.3\sqrt{f_c}$. Although the two limits are quite similar, the Italian approach is more rigorous, because it empirically accounts for all the nonlinear phenomena and the possible failure modes of joint panels, and it is in compliance with experimental evidence (Priestley, 1997).

Further limitations are imposed on the principal compressive stress. The two codes prescribe different limitations as function of the concrete compressive strength. Commonly, the joint panel tensile failure is the more restrictive limit to the joint panel shear strength.

- *American standards*

The American standards ASCE/SEI 41-06 (2007) and ACI 369R-11 (2011) currently recommend empirical limit values of joint panel shear strength, V_{jh}, depending on joint type, load direction, orthogonal beam confinement, aspect ratio, and beam internal reinforcement. The nominal joint shear capacity can be computed by:

$$V_n = 0.083 \cdot \lambda \cdot \gamma \cdot \sqrt{f_c'} \cdot A_j \quad \text{[MPa]} \tag{2.44}$$

in which:

- λ is a numerical coefficient equal to 0.75 for lightweight aggregate concrete, otherwise 1.0;

- γ is an empirical coefficient that account for the joint geometry (see Table 2.3);
- f'_c is the nominal concrete compressive strength;
- A_j is the joint area computed according to previous paragraphs.

Table 2.3. Empirical coefficients for the joint nominal shear strength (ACI 369R-11, 2011)

ρ''	Value of γ				
	Interior joints with transverse beams	**Interior joint without transverse beams**	**Exterior joint with transverse beams**	**Exterior joint without transverse beams**	**Knee joint**
< 0.003	12	10	8	6	4
≥ 0.003	20	15	15	12	8

ρ'' = volumetric ratio of horizontal confinement reinforcement in the joint, knee joint = self-descriptive (with transverse beams or not)

Even though the empirical coefficients were calibrated on experimental datasets (Beres et al., 1996), the proposed formulation does not depend by the axial load. This is in contrast with all the theoretical approaches to the joint shear capacity and may led to not accurate estimation of the joint shear strength.

The American standards (ASCE/SEI, 2007) provides a capacity models which account for the joint deformation. It has been recently updated including more refined values of the joint shear deformation (ACI 369R-11, 2011). The joint shear distortions at the significant points of the nonlinear behavior are provided in function of the joint type, percentage of joint transverse reinforcement and axial load ratio. In particular, with reference to Figure 2.17, assuming that the joint nominal shear strength Q_y=V_n can be computed by Eq. (2.44), the extension of the plastic branch (a), the ultimate joint shear deformation (b) and the residual strength ratio (c) are suggested.

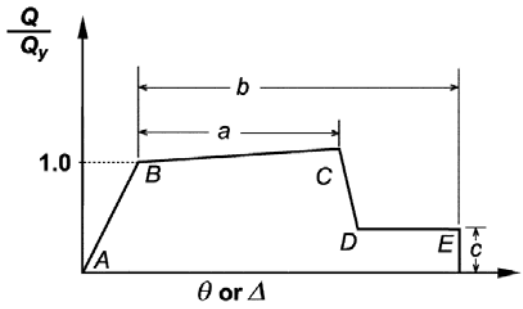

Figure 2.17 Analytical model of joint strength-deformation capacity (ACI 369R-11, 2011).

- *Japanese standards*

Japanese building code (AIJ, 1999) suggests an empirical formulation substantially similar to the one proposed by the American standards. In particular, the joint panel nominal shear strength can be calculated by:

$$V_n = 0.8 \cdot k \cdot \phi \cdot (f_c^{'})^{0,7} \cdot A_j \ \ [\text{MPa}] \tag{2.44}$$

in which:

- ϕ is an empiric coefficient which accounts for the confinement effects of transverse beams;
- k is an empiric coefficient which accounts for the number of structural members framing into the joint panel.

Table 2.4. Empirical coefficients for the joint nominal shear strength (AIJ, 1999).

loading direction	a.	b.	c.	d.	e.	f.	g.
AIJ Guidelines (1999)	$k = 0.4$ $\phi = 0.85$ 0.40	$k = 0.7$ $\phi = 0.85$ 0.70	$k = 0.7$ $\phi = 1.0$ 0.82	$k = 0.7$? $\phi = 1.0$ 0.82	$k = 1.0$ $\phi = 0.85$ 1.0	$k = 1.0$ $\phi = 0.85$ 1.0	$k = 1.0$ $\phi = 1.0$ 1.18

As already discussed for the American standards, also this formulation does not depend by the axial load.

2.7 FRP STRENGTHENING OF BEAM-COLUMN JOINTS.

Composite materials represent a big innovation in the modern engineering. The light weight and the high strength of these materials result in many advantages in terms of structural performances and reduction of global weight of the products. Indeed, composite materials were initially applied in the industrial engineering, where weight reduction goes along with high performances. The widespread of these materials and, in turn, the reduction in production costs strongly promoted their use in engineering applications.

In the construction practice, Fiber-Reinforced Polymers (FRP) adopted as externally bonded reinforcement (EBR) has emerged as a sound technique alternative to conventional materials and construction systems such as externally bonded steel plates (beton plaqué), steel or concrete jackets, and external post-tensioning (Bakis et al., 2002). Steel plates epoxy bonded to the external concrete surface in the tension zone of beams and slabs are traditionally adopted as a simple and cost-effective solution to upgrade their flexural capacity. However, this technique suffers from several disadvantages: bond deterioration due to steel corrosion, difficulty in manipulating the heavy steel plates at the construction site and limitation in available plate length. Steel or concrete jackets are mainly used to increase strength, stiffness and ductility of RC members, but they result in invasive and difficult applications, from a constructability standpoint with a lengthy disruption of the function of the building and for its occupants. Furthermore, the stiffness and weight increase commonly changes the seismic demand with a relevant impact in the design process and significant problems at the foundation system.

The use of FRP materials for repairing, strengthening, or retrofitting existing RC structures is becoming widely adopted around the world. Higher design loads, strength loss due to deterioration, design or construction deficiencies, damage caused by accidents and environmental

conditions, and seismic capacity increase to satisfy current code requirements, are typical situations in which a civil structure would require strengthening or retrofitting (Fib, 2003; Balsamo et al., 2012). Research effort in past decades and the recent development of standards and guidelines to support the design of FRP strengthening, strongly promoted the use of FRP materials in the current construction practice. The classic FRP applications (confinement and shear/flexural strengthening) are nowadays widely applied as a cost-effective solution for structural retrofit (Pampanin et al., 2007; M Di Ludovico et al., 2010; Balsamo et al., 2012). Furthermore, reliable formulations to proper quantify the benefits of these applications have been developed and recently adopted in current design standards and guidelines (DPC-ReLUIS, 2011; ACI 440, 2012; CNR-DT 200, 2013).

Although FRP systems are nowadays widely adopted in the seismic retrofit of RC members such as beams, columns and slabs, the seismic retrofit of beam-column joints is still a challenging task. In fact, the particular support geometry and the complex stress field make the mechanical behavior of FRP strengthened beam-column joints significantly different from all the other applications. Because the joint panel shear failure is often detrimental to the seismic performance of structural systems, recent research efforts have focused on developing sound, cost-effective retrofit strategies and techniques. In the recent years, large number of experimental tests have been carried out to investigate the benefits provided by fiber-reinforced polymer (FRP) systems as a strengthening solution for beam-column joints. Many experimental tests demonstrated at the subassembly level the effectiveness of the FRP strengthening improving the seismic capacity of poorly detailed beam-column joints typical of existing buildings (Gergely et al., 2000; Antonopoulos and Triantafillou, 2003; Prota et al., 2004; Ghobarah and El-Amoury, 2005; Akguzel and Pampanin, 2010). Further experimental tests and analytical studies on large structural systems pointed out that a significant improvement in the lateral displacement capacity and energy dissipation may be achieved with a local retrofit solution, by FRP strengthening deficient structural members (Pampanin et al., 2007; Di Ludovico et al., 2008; Frascadore et al., 2014). These studies

have been the driver behind the use of composites in the field of seismic retrofit of existing RC joints. In fact, FRP laminates on beam-column joints have been widely adopted in the L'Aquila aftermath as a local retrofit solution. Furthermore, proper guidelines (DPC-ReLUIS, 2011) have been developed to support practitioners in the design process of FRP strengthening in beam-column joints and to establish suitable field installation procedures. In this study, a review of the available literature studies and the main experimental findings on the FRP seismic retrofit of beam-column joints are reported.

2.7.1 Mechanical behavior of FRP strengthened joints

The mechanical behavior of FRP strengthened beam-column joints is characterized by a number of parameters larger than classic FRP applications (i.e. shear and flexural strengthening). This because of the complex stress field acting in the joint panel and the high variability of FRP systems in terms of mechanical properties and reinforcement layout. The effectiveness of externally bonded FRP systems was largely investigated in the past, pointing out the influence of the debonding phenomena (Yuan et al., 2004; Yao et al., 2005). The bond behavior strongly affects the FRP strengthening performances limiting the effective FRP strain to value far below their ultimate capacity. Indeed, if the interfacial shear stresses exceed the bond strength (in the adhesive or in the concrete support) a premature bond failure occurs. This failure is often detrimental for the FRP system performance because it is commonly associated with a sudden strength loss. Many studies pointed out the high variability of the debonding phenomena which are very sensitive to RC support characteristics, FRP mechanical properties, strengthening layout, surface preparation, bond length, use of mechanical anchorages and, above all, to the acting stress field. Number of experimental tests have been carried out to investigate and predict the effects of these variables. This effort resulted in clear guidelines for the FRP application and simple and reliable formulations to predict member

capacity increase. However, due to the complex stress field and the particular support geometry, the existing formulations, reliable for shear and flexural strengthening, cannot be extended to beam-column joints. Thus, the performance characterization for beam-column joints strengthened with EBR-FRP system is still a challenging task. In the recent years, number of experimental tests have been carried out to demonstrate the FRP effectiveness in the seismic retrofit of beam-column joints and point out the main parameters affecting the strengthening performances. A critical overview of the available experimental test is reported below.

- *Gergely et al.* (2000)

The first experimental program on beam-column joints retrofitted by FRP systems was carried out by Gergely et al. (2000). It aimed to identify the more efficient strengthening layout and basic design principles for the seismic retrofit of a bridge bent. A wide experimental program has been conducted on 14 beam-column joints without transverse internal reinforcements. The tested specimens were exterior T-joint representing the connection between internal column and the cap beam in a typical bridge bent. The analysis of the strength capacity and failure mode of four as-built tested specimens pointed out that the shear failure of the joint panel is detrimental for the subassembly performances. A proper FRP strengthening constituted by uniaxial carbon fibers (CFRP) inclined at 45° have been proposed. To improve the bond performance of the joint panel FRP strengthening the uniaxial fabric was wrapped around the columns, without any elongation on the beam. A more efficient mechanical anchorage has been provided by means of U-wrap along the columns. The adopted FRP strengthening layout is depicted in Figure 2.18. This study aimed to investigate the influence of the strengthening layout (varying the number of CFRP layers and fiber direction at 45° and ±45°), the support preparation technique and the curing temperature. The influence of the mechanical anchorages was also investigated by changing number, position and length

of U-wraps. The specimens were tested with a cyclic force applied at the beam tip. The column ends have been fixed to the strong floor by means of steel profiles restraining both the horizontal and vertical displacements.

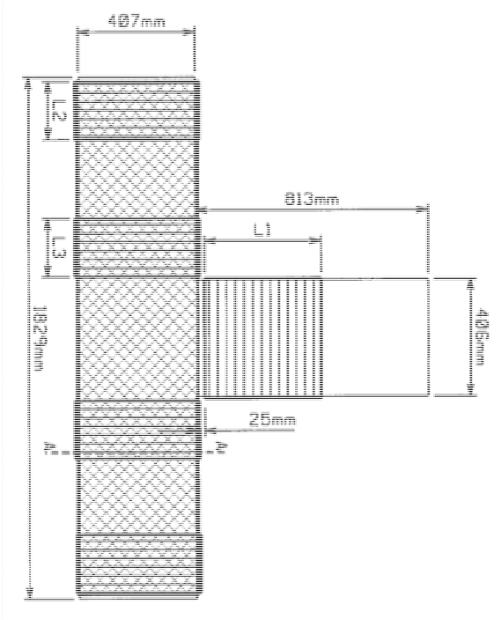

Figure 2.18 FRP strengthening layout for exterior T-joint of a typical bridge bent (Gergely et al., 2000).

The analysis of experimental results demonstrated the effectiveness of the proposed strengthening layouts improving the seismic capacity of shear deficient beam-column joints. In compliance with theoretical principles of shear strengthening, the FRP system performances are very sensitive to fiber inclination with respect to crack inclination. In fact, the specimens with fibers inclined of ±45° showed a significant strength increase both for push and pull loads. Reduced effects have been observed varying the curing temperature and additional mechanical anchorages. Indeed, the U-wrap anchorage systems seems to be redundant improving the fiber bond because the uniaxial fibers, constituting the joint panel shear reinforcement,

were already wrapped around the columns. Furthermore, the use of a significant amount of fibers (uniaxial CFRP with thickness of the dry fiber, t_f = 1.32mm) resulted in low working strains, only one third of the ultimate tensile capacity of fibers.

The experimental results for specimens strengthened with FRP system and an improved bond system (water jet for surface preparation and high performance structural adhesive) cannot be clearly interpreted because of significant torsional effects affecting the specimen performances.

- *Ghobarah & Said* (2002), *El-Amoury & Ghobarah* (2002) *and Ghobarah & El-Amoury* (2005)

Strong effort has been made by these researchers investigating the seismic behavior of beam-column joints strengthened with glass FRP (GFRP). The main goal of the experimental programs was to improve the strengthening layouts to prevent the joint panel shear failure promoting a more ductile flexural yielding of framing members.

Ghobarah & Said (2002) demonstrated that large strength and ductility increase may be achieved preventing the joint panel shear failure by using different FRP layouts (see Figure 2.19). The maximum recorded FRP strain on the specimen retrofitted with diagonal fabrics was about 0.3%.

El-Amoury & Ghobarah (2002) pointed out that the use of mechanical anchorages in the form of steel plate bolted in the concrete support allows to prevent the FRP end-deboning. However, due to the large amount of fiber adopted for the joint panel strengthening, maximum strains in the range 1/3 - 1/4 of the ultimate tensile strain have been recorded. Similar results have been outlined by Ghobarah & El-Amoury (2005).

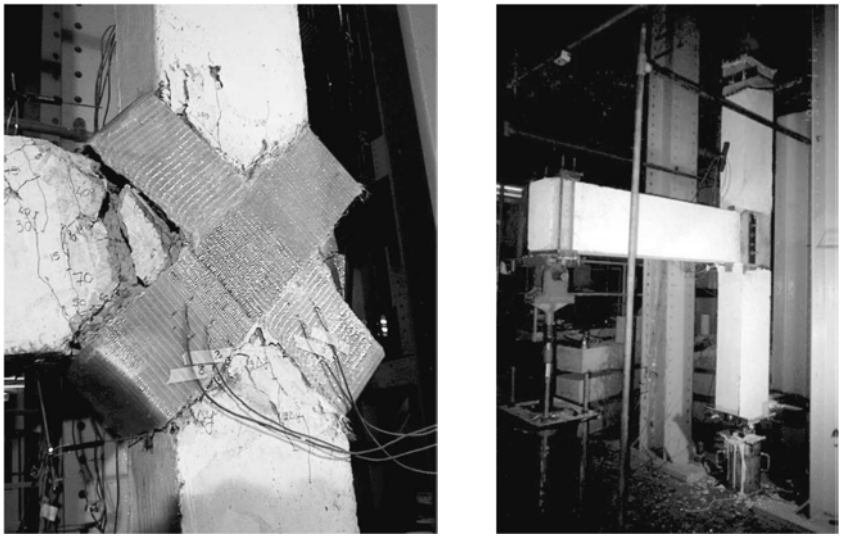

(a) (b)

Figure 2.19 Beam column joints retrofitted with FRP systems (Ghobarah and Said, 2002): (a) fibers in the diagonal directions; (b) use of mechanical steel anchorages for the joint panel FRP strengthening.

- *Antonopoulos and Triantafillou* (2003)

Antonopoulos and Triantafillou (2003) conducted the largest experimental program on poorly detailed exterior beam-column joints retrofitted with FRP systems. The main goal of this study was to investigate the influence of the strengthening layout on the seismic performance of joint subassemblies. A total of 18 specimens in 2/3 scale were constructed and FRP strengthened varying: the fiber inclination (two solutions were adopted: fiber in the column or beam direction), the number of layers, continuous fabric or strips, fiber materials (glass or carbon), presence of transverse beam, mechanical anchorages, axial load and strengthening application after initial damage. A summary of the tested FRP layouts is reported in Figure 2.20.

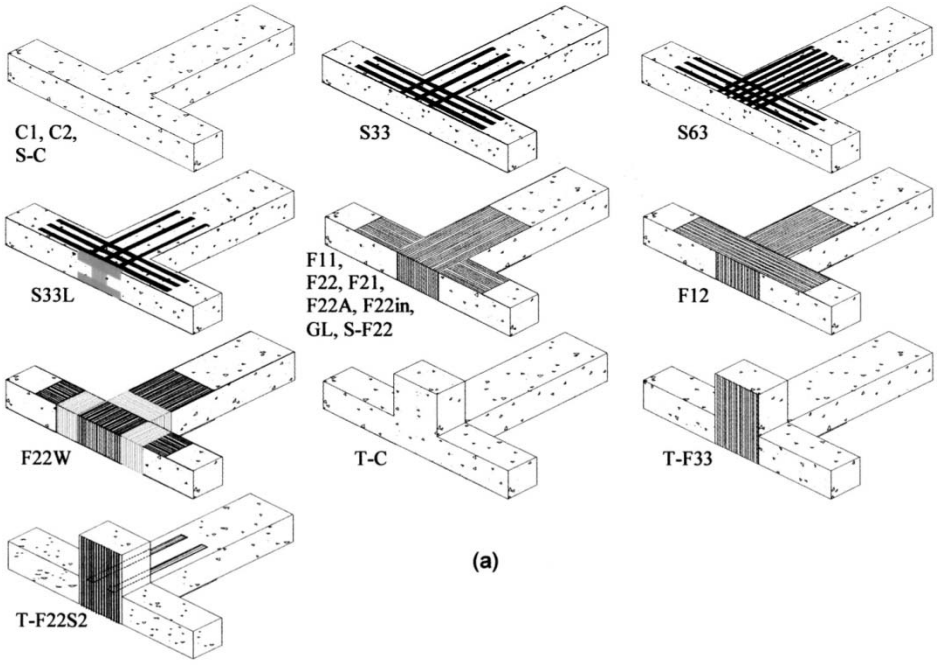

Figure 2.20 FRP strengthening layouts for exterior T-joints (Antonopoulos and Triantafillou, 2003).

This study demonstrated the effectiveness of FRP system increasing the subassembly strength and dissipated energy until the 70% higher than reference joint. Further relevant findings can be summarized in the following points:

- Joint performances increase with the amount of FRP fibers, but not with a linear proportion;
- The effectiveness of fibers changes with the fiber inclination: fiber parallel to the beam axis resulted more effective than those placed in the column; however, for an effective FRP strengthening a minimum amount of fiber in both directions is required;
- The flexible fabrics are more effective than strips, by using the same amount of fibers;

- The mechanical anchorages adopted in this study (FRP U-wrap at beam and column intersections) increased the performances of both fabric and strips. A notable result is that, only when mechanical anchorages have been adopted, the fiber tensile failure has been detected; in all the other specimen, FRP premature debonding strongly limited the strengthening performances;
- The presence of the transverse beam strongly affects the FRP effectiveness on beam-column joints. The confinement effect provided by this beam should be considered to be representative of a typical corner joint. Furthermore, in the case of corner joints only on side of the joint panel can be strengthened in shear with fibers;
- If the strengthened joint is damaged but not repaired, FRP materials are less effective in terms of energy dissipation and strength increase;
- The presence of axial load had a positive effects on the joint performances as already formulated in Eq. (2.26);
- The FRP effectiveness increases in the case of joint panel without internal stirrups.

- *Prota et al.* (2004)

One of the first study on the effectiveness of FRP system for interior joints (i.e. subassembly of perimetral frames with two beams and two column framing into the joint) was carried out by Prota et al.(2004). The tests aimed to validate the use of different FRP strengthening layouts (FRP fabrics, NSM FRP bars, and column wrapping) to increase the seismic performances of the whole subassembly. The experimental results demonstrated that the seismic retrofit with FRP systems can be an effective strategy also for exterior beam-column joints. The FRP-strengthening layout or the amount and location of FRP-strengthening systems may significantly affect the increase in beam-column joint capacity or modify its strength hierarchy leading to a more favorable ductile failure mode.

- *Parvin et al.* (2010)

Recently, six tests on full-scale RC beam-column joints, typical of existing buildings in the Mediterranean area, have been carried out by Parvin et al. (2010). The experimental program investigates the effects of the number of layers in the FRP retrofit scheme and the influence of the axial load on the joint shear strength and deformation capacity. All the tested joints failed due to end-debonding of uniaxial FRP fabric in the direction of the beam axis (see Figure 2.21). However, the specimens with the largest amount of fiber on the joint panel and an improved anchorage system (U-wrap) exhibited a significant strength and ductility increase with respect to the as-built specimens.

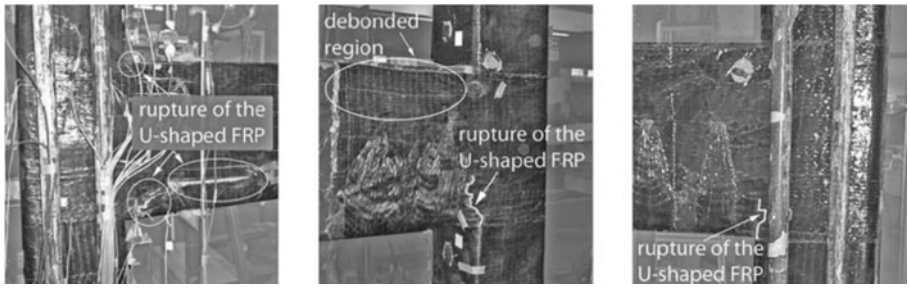

Figure 2.21 Failure mode of the FRP strengthened specimens (Parvin et al., 2010).

Furthermore, the proposed CFRP strengthening significantly reduces the joint panel shear deformations.

- *Akguzel & Pampanin* (2010)

In the recent years, a relevant experimental program has been carried out by Akguzel and Pampanin. The test program involved ten 2/3 scale beam-column joints, including four as-built specimens and six retrofitted specimens using externally bonded GFRP sheets. The joint subassemblies

are representative of old construction practice in Italy and New-Zealand with inadequate joint shear reinforcements (one stirrup in the set 1 or none stirrups in the set 2). Plain round steel bars were adopted for the longitudinal reinforcements anchored in the joint panel with end-hooks. The study aims to show the effects of varying axial and bidirectional loading on the seismic performance of deficient exterior RC beam-column joints before and after retrofit. A specific load protocol, consisting of an imposed displacement at the top column in both directions and variable axial load, has been applied to the specimens by means of the test setup depicted in Figure 2.22.

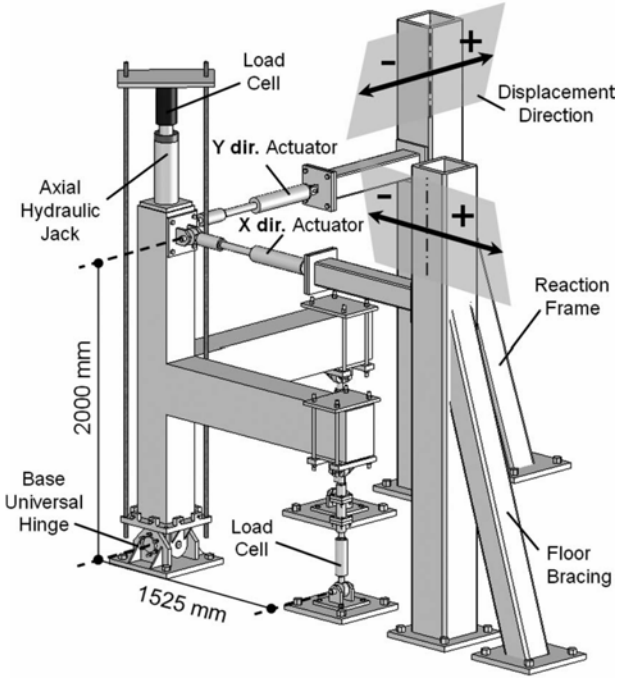

Figure 2.22 Test setup for the 3D tests on corner beam-column joints. (Akguzel and Pampanin, 2010).

The experimental tests demonstrated the effectinvess of the proposed FRP strengthening schemes improving the seismic capacity of poorly detailed beam-column subassemblies. Furthermore, the authors pointed out the

influence of the axial load variation and bidirectional loads on both as-built and GFRP strengthened joints. A significant reduction in the overall strength capacity and energy dissipation characterizes the specimens tested under bidirectional load and axial load variation with respect to unidirectional actions and constant axial load configurations. This because the bond degradation is anticipated if a multidirectional stress-field is applied. Another important experimental result concerns the effective FRP strains recorded during the tests. In fact, strain level higher than 0.4% have been recorded in almost all the tests. This results can be adopted to calibrate specific design formulations.

- *Al-Salloum et al.* (2011)

The most recent experimental program on RC beam-column joints strengthened with different techniques has been conducted by Al-Salloum et al. (2011). The main goal of the experimental program is to quantify and compare the benefits of the FRP strengthening (GFRP and CFRP fibers) and the textile-reinforced mortars (TRM) improving the seismic capacity of poorly detailed-beam column joints. Other relevant aspect of this study concerns the use of an efficient anchorage solution (U-wrap with steel plates at the ends) suitable for application on the beams with the slab at the top side (see Figure 2.23).

The experimental results demonstrated the effectiveness of both the proposed seismic retrofit solutions. Particular emphasis has been given to the performances of the TRM technique, which are comparable but still lower than FRP in the CFRP and GFRP configurations.

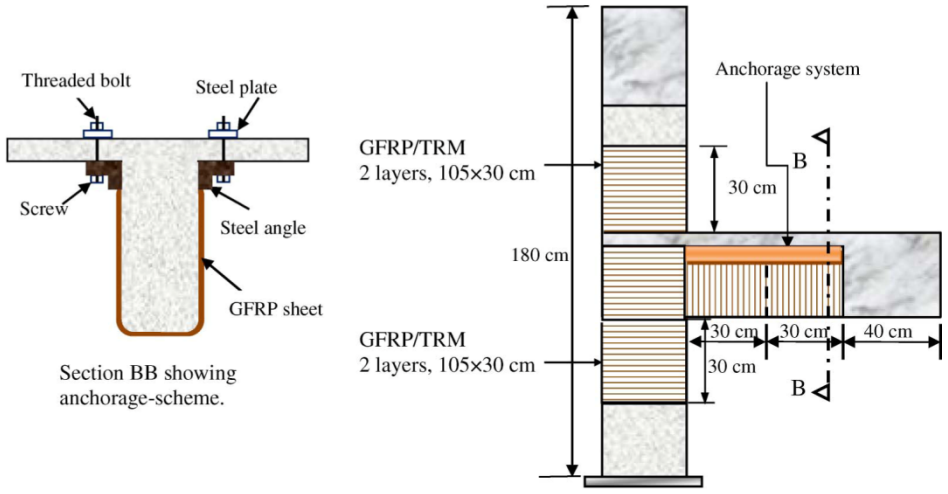

Figure 2.23 GFRP strengthening layout with the proposed anchorage solution (Al-Salloum et al., 2011).

Although relevant experimental programs have been carried out to investigate the effectiveness of FRP-based strengthening solutions on beam-column joints, there are not enough experimental data to calibrate the effective design strain of FRP joint panel strengthening. Thus, further experimental tests are needed in order to calibrate proper strain design limits based on experimental records. This may lead to developing a reliable and simple capacity model to be used by practitioners in the FRP-strengthening design process of beam-column joints.

2.7.2 Available capacity models for FRP strengthening

The widespread of composite materials in the structural retrofit of existing structural systems promoted large number of experimental tests aimed to investigate and quantify the benefits provided by the FRP systems. As outlined in the literature review on available experimental tests, the debonding phenomena represent the critical point of these applications. This is a common issue in the FRP strengthening of RC members as experimentally pointed out in classical applications (e.g. the shear or

flexural strengthening of RC and pre-stressed concrete (PC) members, (Khalifa et al., 1998; Triantafillou, 1998; M Di Ludovico et al., 2010)). To overcome the challenges of defining the exact FRP mechanical behavior, empirical equations to predict the effective strain of the FRP strengthening system can be determined from a large database of experimental results. In developing simple and reliable models for FRP strengthened beam-column joints, the nonlinearities associated with concrete core mechanical behavior and the high variability of the effective strains of the FRP strengthening system must be considered. The same aspects were identified as critical by Triantafillou (1998) and Khalifa et al. (1998) in the developing of design models for the shear strengthening of RC beams. Although the mechanical behavior of FRP system externally bonded on RC beam-column joints significantly differs from the shear strengthening of beams, these models need to be mentioned for the simple and clear approach adopted to simplify the complex mechanical behavior.

These studies pointed out that, due to concentration of stresses, the FRP systems may fail at stress levels far below their ultimate capacity. To account for this criticism, they proposed an experimental calibration of the effective FRP strains, back calculated from experimental tests. Then, the data were statistically fitted to obtain a theoretical formulation (see Figure 2.24).

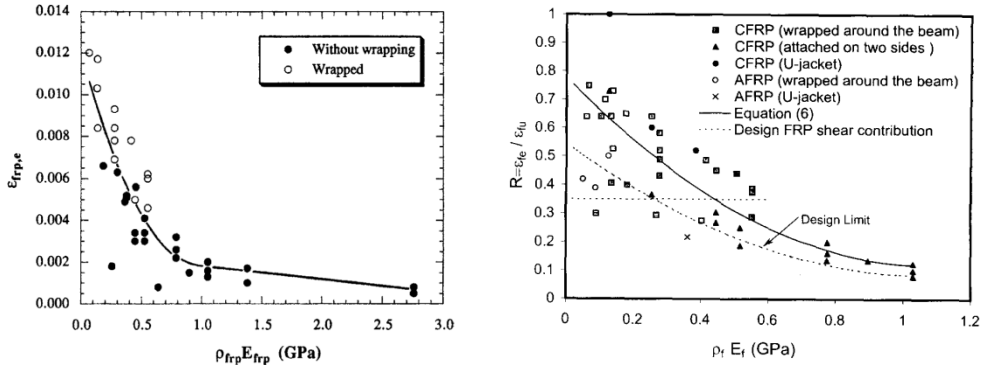

Figure 2.24 Proposed formulations for effective FRP strain in the shear strengthening of RC beams: (a) Triantafillou (1998); (b) Khalifa et al. (1998).

Due to the relevancy of these theoretical approaches, suggested by the CNR DT 200 R1 (2013) and ACI 440 (2012), a summary of the research study proposed by Triantafillou (1998) and Khalifa et al. (1998) is reported below.

Triantafillou (1998) observed that in the FRP shear strengthening of RC beams, the effective strain is a function of the axial rigidity of the FRP sheet expressed by the product $\rho_f E_f$. Indeed, experimental results demonstrated that, increasing the amount of FRP fibers or their elastic modulus, the effective FRP strongly decrease. It occurs because of the limited bond properties of the concrete supports. Furthermore, he pointed out the effectiveness of wrapping the fiber ends increasing the effective FRP strain. To obtain a simple design formulation, he plotted the experimentally determined FRP effective strains $\varepsilon_{frp,e}$ (back calculated from experimental shear strength using the proposed shear strength model) against the axial rigidity (see Figure 2.24a). The experimental results have been interpolated with a polynomial expression.

The same year, based on the impressing scientific contribution provided by the study of Triantafillou (1998), Khalifa et al. (1998) proposed a revised model in the ACI format (ACI 369R-11, 2011). They also simplified the expression for the effective FRP strain, expressed as a function of the ultimate tensile strain and limited the use of the formulation to FRP strengthening with axial rigidity conventionally adopted for practice applications ($\rho_f E_f$ <1) (see Figure 2.24b). Furthermore, a new bond-based design formulation has been suggested and specifically calibrated in order to include the concrete substrate mechanical properties. The proposed formulation is a recalibration of the bond-based formulation proposed by Maeda et al. (1997). According to the proposed formulation, the effective FRP strain is a function of the ratio $f'_c{}^{(2/3)}/(t_f\ E_f)$ and limited to 1/3 of the ultimate tensile strain for design purpose and to avoid the loss of aggregate interlock for the excessive crack width. In the final model for the shear strength of FRP strengthened RC beams, a reduction factor in the ACI format has been introduced to satisfy specific level of structural safety.

- *Antonopoulos and Triantafillou* (2002)

Significant effort in the development of a mechanical model to estimate the strength capacity of beam-column joints retrofitted by FRP systems has been made by Antonopoulos and Triantafillou (2002). The analytical model assumes that the directions of principal strains and stresses coincides. Thus, for each increment of the joint strain in each direction (only vertical and horizontal direction are considered in this model), the equilibrium relation, in the form of quadratic polynomial equation allow to compute the inclination of maximum principal strain and joint shear stress. For coupled problems, for example when FRP fabrics with fibers in multiple directions are used, the equations can be written in the matrix form, introducing the coupled matrix for stress and strain. The joint shear strength is assumed in correspondence of the first failure in the joint panel. The model accounts for different failures modes: concrete core web crushing, fiber rupture, fiber debonding and longitudinal reinforcement yielding. With reference to the FRP strengthening behavior, the debonding is considered by means of a fracture-based semi-empirical relation function of the anchorage length and the ratio $\sqrt{E_f \cdot f_{ctm} / t_f}$. The amount of FRP reinforcement is considered with the FRP reinforcement ratios in the vertical and horizontal direction. Although the model is effective in predicting the strength capacity of beam-column joint subassemblies retrofitted with fibers applied in the direction of the beam and/or column, an iterative complex procedure is required.

- *Tsonos* (2008)

Recently, Tsonos (2008) presented a different theoretical model where it is assumed that the FRP fibers oriented in the direction of the beam axis are equivalent to the steel hoops. The model provides the maximum strength capacity of the joint panel by solving a polynomial equation.

- *Akguzel and Pampanin* (2012)

In recent years, the Antonopoulos and Triantafillou model (2002) was simplified by Akguzel and Pampanin (2012) on the basis of experimental observations (Akguzel and Pampanin, 2010). In particular the authors assumed that the total joint shear strength is a combination of the strength of the as-built joint and the contribution of the composite materials for a given joint shear distortion. In this model the principal stress approach has been adopt to estimate the joint shear strength of the bearing joint. The FRP strengthening contribution is computed according to the original model (Antonopoulos and Triantafillou, 2002). The inclination of principal compression stresses, θ, can be computed by means of a quadratic polynomial equation. Furthermore, a new expression is proposed to account for the effective FRP reinforcement ratio, function of the number of joint panel sides covered with FRP. The FRP contribution to the shear strength can be evaluated increasing the strain parameter and computing θ. The procedure ends when the FRP failure (fiber rupture or debonding) or concrete compression failure is achieved. They also provided a simplified non-iterative procedure, to calculate the peak strength capacity, assuming the average strain equal to FRP ultimate strain. The model has been calibrated on experimental results of beam-column joints with plain round bars and end hooks and validated with an extended database of corner joint with deformed internal reinforcements and exterior X-joints. In spite of the model effectiveness, the wide validation and the strong effort in the model simplification, the proposed procedure remains complex to be applied in the design practice.

- *Bousselham* (2010)

To overcome the challenges of defining the exact FRP mechanical behavior, empirical equations to predict the effective strain of the FRP strengthening system can be determined from a large database of

experimental results (Khalifa et al., 1998; Triantafillou, 1998). This approach has been recently adopted by Bousselham (Bousselham, 2010).The author also suggested a simple procedure to calculate the FRP contribution to the shear strength of beam-column joints based on the principal stress approach (Priestley, 1997).

In developing simple and reliable models for FRP strengthened beam-column joints, the nonlinearities associated with concrete core mechanical behavior and the debonding effects have been considered in the effective strains of the FRP strengthening system. In particular, an experimental calibration of the effective FRP strains, back calculated from experimental tests, has been proposed. The data were then statistically fitted to obtain a theoretical formulation. Furthermore, to better correlate experimental results and predictions, it was then suggested that the effective FRP strain, $\varepsilon_{f,e}$, is limited to 0.4%. Further detail on this model are reported in Section 5.

2.7.3 Design provisions

In spite of the demonstrated effectiveness of FRP systems increasing the seismic capacity of existing structural systems, the mechanical behavior of unconfined RC beam–column joints externally bonded with FRP systems remains a critical issue. The large number of parameters involved makes the calibration of simple and reliable formulations difficult. Several models have been proposed in recent years but, in spite of their effectiveness, they implement complex solution procedures or can be applied only to specific joint types or FRP layouts. The difficulties in interpreting the mechanical behavior of FRP reinforcement, externally bonded on RC joint panels, are strongly related to the uncertainties of the effective FRP strain. Therefore, the available international guidelines and codes related to the use of externally bonded FRP laminates, FIB (2001), CNR-DT 200 NRC (2004), and ACI 440.2R-08 ACI (2008), do not provide expressions to determine the appropriate amount of FRP required for strengthening. For example, in CNR-DT 200 (2004) the FRP effective design strain is only suggested to be

limited to 0.4%, for design purpose. This value is commonly adopted to preserve the concrete integrity whenever the RC member is confined by externally bonded FRP systems. It does not seem to be appropriate for member that are governed by shear.

Because the post-earthquake *in situ* inspections on buildings damaged by L'Aquila earthquake clearly showed that local interventions on structural members may significantly increase the global seismic capacity of existing structures (Prota et al., 2014), proper guidelines were specifically drawn up to support engineers involved in the L'Aquila reconstruction process. The "Repair and strengthening of structural elements, infills and partitions" guidelines (DPC-ReLUIS, 2011) describes the local retrofit interventions, both for structural and non-structural members, illustrating the installation and calculation procedures. A wide section of the guideline focuses on the brittle failure mechanisms. In particular, according to experiences gained from examining the performances of RC structures after seismic events, a wide section focuses on the description of a strengthening scheme for partially confined joints by means of FRP laminates. The strengthening technique involves not only the shear strengthening of joint panels but also of each component of the beam-column joints in order to avoid premature failure mechanisms and, at the same time, to increase the structural local and global ductility. In particular, the shear failure prevention due to local effects of strong infills, the ductility increase of columns ends and the shear strengthening at ends of beams are accounted in the strengthening scheme. The strengthening scheme can be schematized in the following points:

i) beam column joint shear capacity increase against local effect of strong infills (see Figure 2.25): observation of post-earthquake damages confirms that the shear loading due to the infill strut force at column joint interface can cause significant damages to joint panel (i.e. pseudo-horizontal crack at the concrete construction joints or diagonal crack in the joint panel). In particular, in order to withstand the horizontal component of the infill strut force, Steel Reinforced Polymers (SRP) composites in the form of uniaxial systems can be installed around the beam-column joint both in the case of

corner or exterior joints (see Figure 2.26a). Such strengthening phase can be completed applying L-shaped quadriaxial FRP laminates at beams-column connection, see Figure 2.26b;

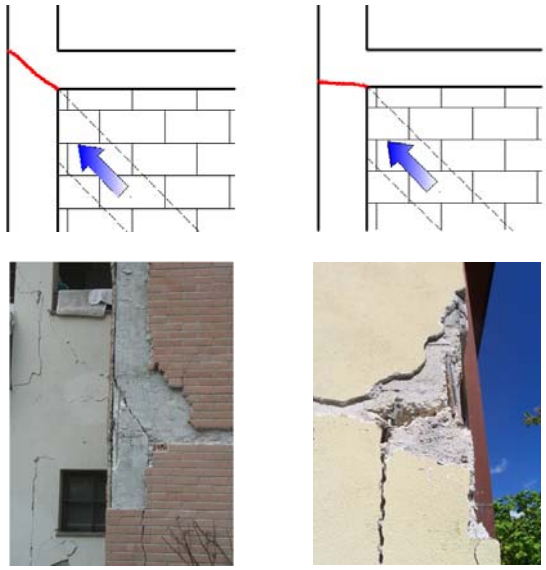

Figure 2.25 Effects of strong infills on the joint panel

ii) shear capacity increase of beam–column joint panel: the shear increase of beam column joint can be achieved through the application of composites with fibers placed along the principal tensile stresses (i.e. quadriaxial FRP laminates) as depicted in Figure 2.26c;

iii) columns ends confinement: it allows to significantly increase the deformation capacity in plastic hinges zones with a corresponding enhancement of global structural ductility. Indeed, FRP wrapping increases the ultimate compressive strain of concrete, thus determining an increase of cross-section ultimate curvature corresponding to a member rotational capacity increase. The confinement is also effective to prevent longitudinal bars buckling and to sustain the shear action, at the top of the column, due to the infill strut force. FRP uniaxial laminates can be installed as reported in Figure 2.26d;

iv) shear capacity increase of beams: the use of U-wrap FRP laminates can increase the shear capacity of beams at the ends (in the zone of maximum shear demand in case of seismic event) and, at the same time, can be very useful in order to provide a mechanical anchorage to the quadriaxial FRP panel sheet applied on the joint, see Figure 2.26e; they also allow to prevent the premature debonding of panel FRP external reinforcement and thus to increase the effectiveness of the whole strengthening scheme.

A view of a field installation of the proposed strengthening system is depicted in Figure 2.26f.

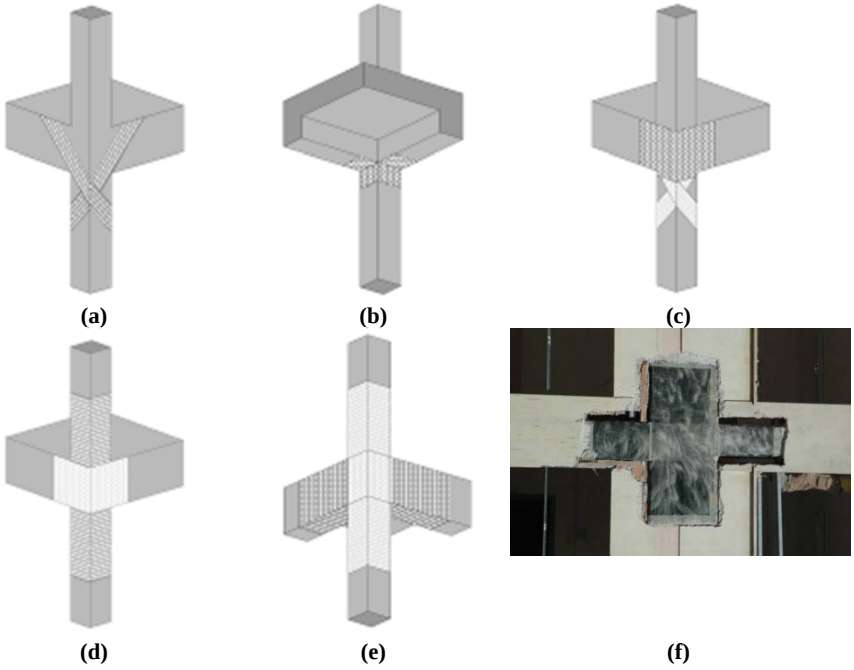

Figure 2.26 FRP strengthening system details (DPC-ReLUIS, 2011): SRP uniaxial system to sustain horizontal actions due to strong infills (a); L-shaped FRP laminates at beam column connection (b); Shear capacity increase of beam column joint panel (c); Columns ends confinement (d); Beam ends FRP wrapping (e); FRP strengthened joint (f).

Due to the complexity of available strength capacity models, a simple design formulation has been proposed. The theoretical approach suggested by Paulay and Priestley (1992) to design the amount of internal stirrups has been rearranged to consider the amount of FRP fiber on the joint panel.

In particular, in the expression 2.43 adopted by European and Italian building code (CEN, 2004; MI, 2008) the total shear force in the internal stirrups $A_{sh}f_{ywd}$ is assumed to be carried by FRP strengthening externally bonded on the joint panel. Assuming that a quadriaxial continuous fabric will be placed on the joint panel, the maximum shear force in the FRP system is:

$$A_{sh}f_{ywd} = t_f \cdot h_{beam} \cdot f_{fd} + 2 \cdot \left(t_f \cdot h_{beam} \cdot f_{fd} \cdot \cos 45° \right) \tag{2.45}$$

Substituting this term in Eq. (2.43), the required thickness of the FRP system on the joint panel which allows the yielding of beam longitudinal reinforcements can be computed with Eq. (2.46).

$$t_f \cdot h_{beam} \cdot f_{fd} + 2 \cdot \left(t_f \cdot h_{beam} \cdot f_{fd} \cdot \cos 45° \right) = \gamma_{Rd} A_{s2} f_{yd} \left(1 - 0.8 \nu_d \right) \tag{2.46}$$

Here, the FRP design stress f_{fd} can be computed according to the CNR DT 200 (2013) considering the design strain as the minimum between the ultimate strain and 0.4%. ν_d is the normalized axial load on the column.

CHAPTER 3
EXPERIMENTAL PROGRAM

Field observations in the aftermath of major seismic events and the review of available literature studies pointed out the high vulnerability of existing RC structures designed with obsolete code provisions. The absence of internal reinforcements makes the partially-confined beam-column joints vulnerable to seismic actions. Because the joint panel shear failure is often detrimental for the building seismic capacity, several strengthening techniques have been developed. In the recent years, several experimental tests demonstrated the effectiveness of FRP strengthening increasing the seismic performances of joint subassemblies and, in turn, the overall seismic capacity. This, along with the easy installation procedure, strongly promoted the field-applications in the aftermath of recent major seismic events as a sound-cost effective seismic strengthening technique.

In spite of the demonstrated effectiveness of FRP systems increasing the seismic capacity of existing structural systems, the mechanical behavior of unconfined RC beam-column joints externally bonded with FRP systems

remains a critical issue. The large number of parameters involved makes the calibration of simple and reliable formulations difficult. Several models have been proposed in recent years but, in spite of their effectiveness, they implement complex solution procedures or can be applied only to specific joint types or FRP layouts.

To support the research activities, a wide experimental program on full-scale beam-column subassemblies has been conducted. The test program involved poorly detailed corner joints, which represents the most vulnerable members of ordinary existing RC structural systems. The specimens were tested in the "as-built" and "FRP strengthened" configurations. The experiments had the main goal to investigate the principles of the mechanical behavior and the main parameters that play a key role in the resisting mechanisms. In order to provide further information to be used in the problem theorization, the joint panel stress and deformation capacity were closely monitored with particular care of the FRP mechanical behavior.

3.1 CHARACTERISTICS OF EXISTING BUILDINGS

The literature review on the available scientific studies and the analysis of the standard developments of the past century pointed out that there are many structural systems vulnerable to seismic actions worldwide. This is even more evident in the Mediterranean area where the largest development of constructions took place in the 60-90s (ISTAT, 2001) and the modern performance-based seismic design approach has been introduced in the Italian standard in the 1997 (MMLLPP, 1997). With reference to the Italian context, the seismic classification started in the 1915 and evolved in the years after catastrophic seismic events. Furthermore, the seismic actions, where prescribed, were frequently neglected in the design process. Thus, it can be assumed that large number of RC buildings were designed considering gravity load. This resulted in significant structural damage to

RC buildings during major seismic events due to not adequate design procedures (Ricci et al., 2011; Dolce and Goretti, 2015).

Concerning the evolution of Italian building code, several documents were approved in the past century. However, because the design practice was commonly based on guidelines and practice manuals, most of the existing structural systems were built with reference to only two main codes. Masi and Vona (2004a; 2004b) pointed out that significant differences in the Italian building code were introduced in the 70's years. Before this period the constructions were regulated by the Regio Decreto (1939). The main developments in the code prescriptions concerned the structural materials (the deformed steel bars were introduced). The minimum percentages of internal reinforcements were not significantly modified.

Furthermore, the analysis of the evolution of worldwide design standards pointed out that before the end of 80' years the joint shear reinforcements were almost never provided. They were introduced in Italian standard in the 1997 (MMLLPP, 1997).

In light of these considerations, the experimental program focused on RC frame buildings designed without seismic action and with lack of transverse reinforcements in the joint panel. With this purpose, the design process of an RC frame typical of existing residential buildings designed for gravity load, was reproduced.

3.2 RC FRAME CHARACTERISTICS

A detailed overview of the Italian RC construction practice is reported in Masi and Vona (2004 a; 2004 b). The analysis of typical construction practice pointed out that most of the residential building were designed regardless seismic actions. They also have uniform structural systems with moment resisting frames (MRF) in only one direction and perimetral frames in both directions to accommodate infill walls. The frame geometry is characterized by 5 meters span beams and 3 meters height columns with various number

of floors and bay ranging between 2-10 and 3-6, respectively (see Figure 3.1).

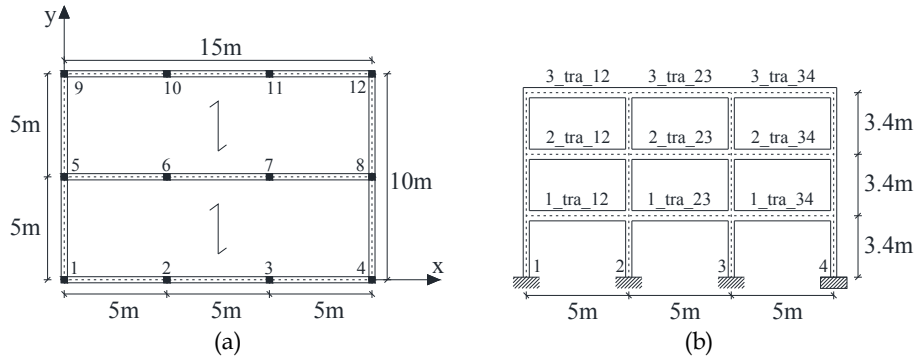

Figure 3.1 Geometry and details of a typical RC existing building: (a) plan; (b) lateral view of a typical resisting frame.

The RC structural system object of this study is a 3 floor buildings with MRFs in the x-direction and two perimetral frames in the y-direction. The main MRFs have 3 bay with 5 m span and 3 floors 3.4 m height. The slabs are 22 cm thick with rafters in the y direction.

In compliance with old design practice, the beams were designed considering a structural scheme of continuous beam on multiple supports with added bending moments on the external supports simulating the perimetral beams torsional stiffness.

According to Masi and Vona (2004), the Rck 250 concrete, with a cubic characteristic compressive strength of 25 MPa, was adopted in the design procedure. The 70's represent a period of transition from smooth internal reinforcement to deformed bars. However, as pointed out in the previous chapter, the members reinforced with smooth bars suffers from significant slip phenomena. Thus, a further variable may affect the joint behavior if this type of reinforcement are adopted. Because the influence of bar slip is out of the scope of this study, deformed reinforcements were adopted. In compliance with construction practice of the end of 70 years, FeB38k steel was selected. However, because this class of steel for internal reinforcements is not available nowadays, the FeB44k steel was adopted.

Rectangular beams 30 cm width and 50 cm height were designed according to the structural analysis considering design loads prescribed in the reference standard (D.M. 03/10/1978). The longitudinal reinforcement details are reported in Figure 3.2, along with the reinforcement details coming from the design drawings of a real existing building.

(a)

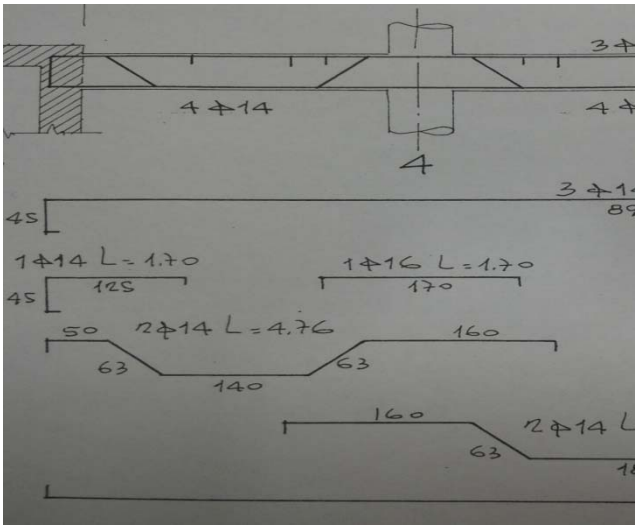

(b)

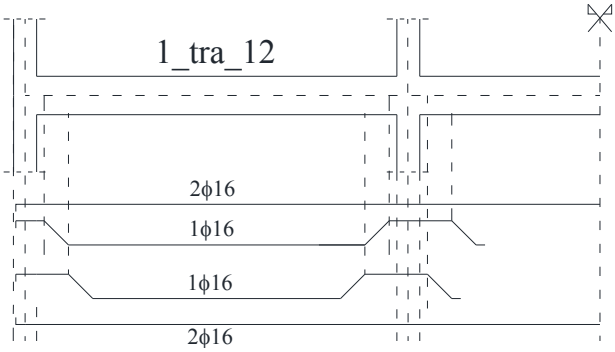

Figure 3.2 Longitudinal reinforcements of typical RC existing buildings: (a) original design scheme; (b) derived with the simulated design.

The analysis of design drawings of existing buildings built after the 70′ years pointed out several structural details commonly adopted in the design

practice. In particular, the shear action in correspondence of supports was resisted by internal stirrups (ϕ8, 20 cm spaced were commonly adopted) and also by means of diagonal transverse reinforcements coming from longitudinal reinforcement bents. This led to have a significant number of bars at the beam top side. Furthermore, the beam top and bottom reinforcements were commonly bent in the joint core to provide a satisfactory anchorage.

Columns were designed for gravity loads determined by means of a static analysis with design loads and including the axial load of upper floors. The adopted column cross-sections along with internal reinforcements (designed as the 0.8% of the concrete cross-section) are reported in Table 3.1 for the columns of the first floor. Due to the limited height of the reference building, the same cross-sections and internal reinforcements were adopted for the columns of the upper floors.

Table 3.1. Column cross sections and reinforcement details at the ground floor.

	Calculated				Adopted			
Column	N	σ_c *(k=0.7)*	A^*_b	A_f	A_{cls}	A_f	Cross-section	Reinf.
[-]	[kN]	[N/mm^2]	[mm^2]	[mm^2]	[mm^2]	[mm^2]	[cm]	[-]
1	337.7	5.95	56756	454	90000	804.25	30x30	4ϕ16
2	499.1	5.95	83880	671	90000	804.25	30x30	4ϕ16
3	499.1	5.95	83880	671	90000	804.25	30x30	4ϕ16
4	337.7	5.95	56756	454	90000	804.25	30x30	4ϕ16

This design approach resulted in square columns with 30 cm sides reinforced with only one bar in the cross-section corners. The columns were designed in axial compression only and, according to old design practice, ϕ8 stirrups, 20 cm spaced, were adopted for transverse reinforcements. Because joint transverse reinforcements were introduced in Italian standard in the 1997 (MMLLPP, 1997), the reference building has lack of joint reinforcements.

Nonlinear static analysis carried out in compliance with current code prescriptions (CEN, 2005; MI, 2008) and with analytical models suggested by Manfredi et al. (2007) points out a typical collapse mechanism of existing buildings. A soft storey mechanism interests the first floor of the reference structural system, with yielded columns at both ends (see Figure 3.3a). The failure mechanism is in compliance with failure mechanisms as typically found in the aftermath of major earthquakes (see Figure 3.3b).

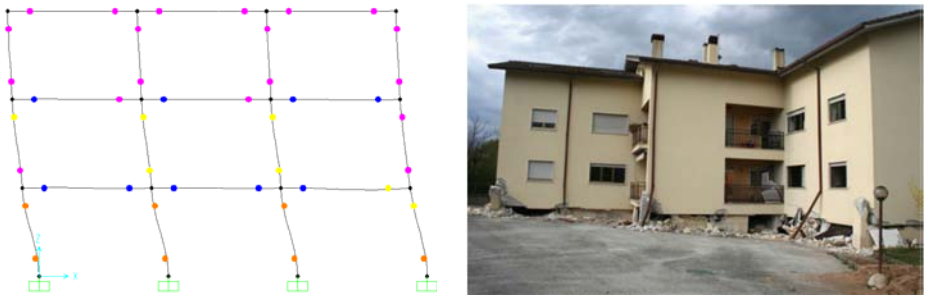

(a) (b)

Figure 3.3 Soft storey mechanism typical RC existing building: (a) results of Push-over analysis on the reference building; (b) collapsed building in the L'Aquila earthquake (2009).

3.3 JOINT SUBASSEMBLY

Poorly detailed beam-column subassemblies without stirrups in the joint panel were designed for the experimental program. The beam and column length were designed to allow for the typical story height and the portion of the beam up to the zero point of the bending moment diagram (about 1/3 of the span), respectively. The structural members under investigation are typical of frames designed for gravity loads. To represent a typical corner joint, an orthogonal beam stub, 35 cm long, was also designed to represent the transverse beam carrying the perimetral infill weight. The dimensions of members and the reinforcement ratios were chosen to reproduce

subassemblies with a weak column and strong beam, as pointed out by the nonlinear analysis on the whole structural system. Thus, a square column with a side length of 300 mm was adopted. The longitudinal reinforcement ratio is about 0.9%, corresponding to 4ϕ16 in the cross section corners. The beam cross section is 500 mm deep and 300 mm wide with 5ϕ16 on the top side and 3ϕ16 on the bottom side (reinforcement ratio of 0.7% and 0.4%, respectively). The beam longitudinal reinforcement is anchored in the joint panel with 90° standard hook (effective straight length equal to 200 mm). Internal reinforcements were slightly modified respect to the results of the simulated design process, in order to achieve shear failure in the joint panel prior to yielding of both beam and column reinforcements under simulated seismic action. This strategy was adopted in order to simplify the joint mechanical behavior avoiding to introduce further variables. The same is for the construction joints, not in the scope of this study. The specimen geometry and reinforcement details are reported in Figure 3.4.

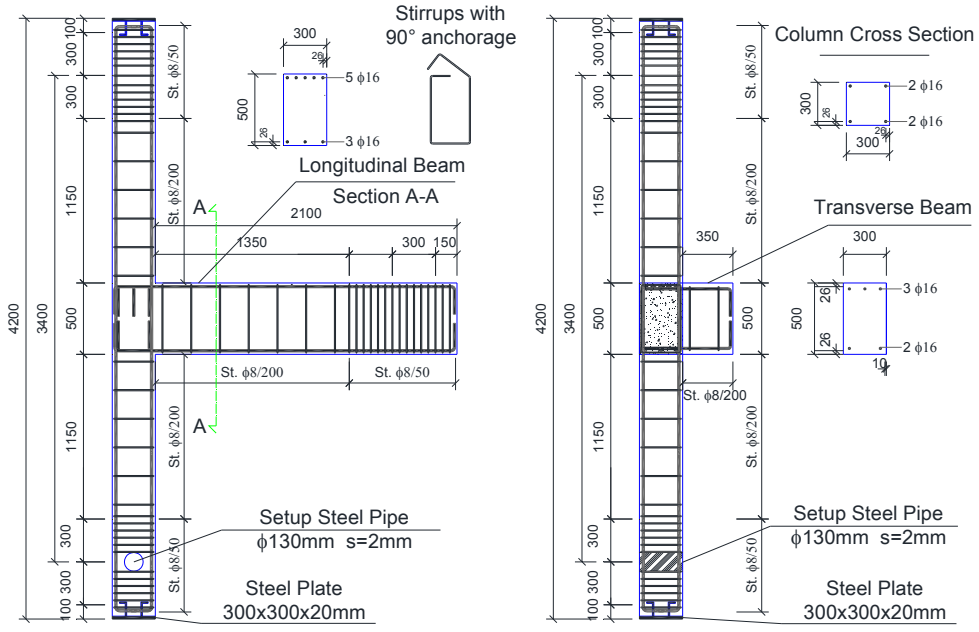

Figure 3.4 Tested specimens: geometry, internal reinforcements and details.

3.4 TEST SETUP

The specimen was constrained to the strong floor by two rigid steel frames and a steel roller placed inside the lower column end to simulate a pin connection. The top column was constrained to a rigid frame by two steel rollers that grabbed the column end externally and allowed top column elongation (Figure 3.5). As the specimen lay on the laboratory structural floor, spherical steel hinges were placed between the beam end and the floor to limit friction and allow free movement of the beam tip. Transverse cyclic loads were applied to the extremity of the beam to simulate seismic action along with a constant axial load on the top of the column applied by means of pre-stressed steel bars. The test setup was able to reproduce seismic action on beam-column subassemblies as theoretically formulated by Park (1994) and pointed out in several experimental studies (Beres et al., 1996; Prota et al., 2004). This test setup allows to simplify the real scheme (Figure 3.6a) applying the external forces/displacement to the beam tip (Figure 3.6b). This scheme allows to overcome several practice problems related to the application of lateral load/displacement at the same point of the axial load. However, a direct measure of the interstorey drift and column shear is not allowed with the alternative scheme. Subassembly drift can be computed as the ratio between the beam tip displacement (total displacement d minus gravity load displacement d_0) and the actuator distance from column axis, $L+h_c/2$ (L = 1650 mm and h_c = 300 mm, see Figure 3.5):

$$Drift(\%) = \frac{(d - d_0) * 100}{L + (h_c / 2)} \tag{3.1}$$

Column shear, V_c, can be computed as $F \cdot (L+h_c/2)/H_c$ with F, the beam shear force and H_c = 3400 mm, the distance between column reaction points.

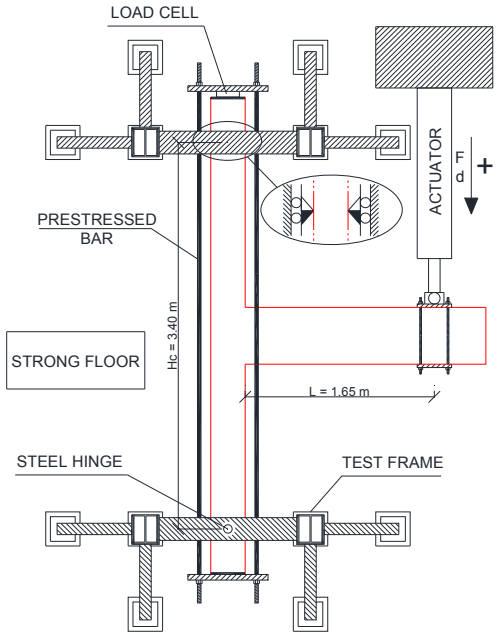

Figure 3.5 Test setup.

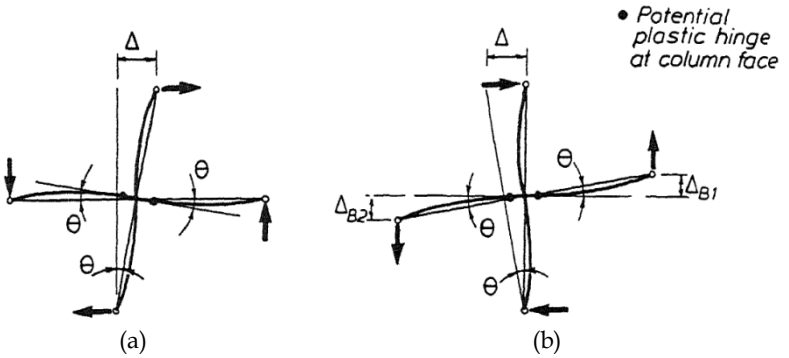

Figure 3.6 Equivalent schemes for beam-column joint tests (Park, 1994): (a) lateral loading causing displacements as in a frame; (b) alternative method of lateral loading.

The test setup arranged on the laboratory strong floor is depicted in Figure 3.7.

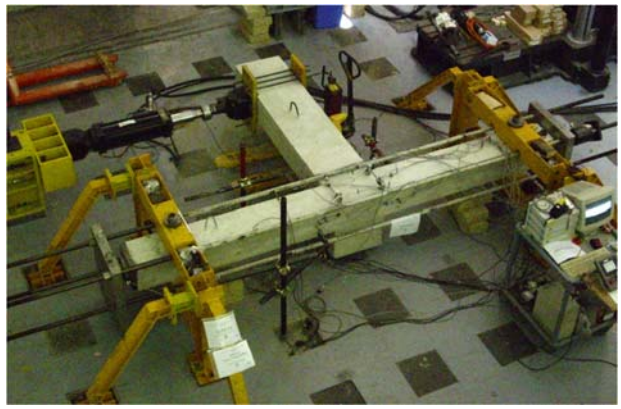

Figure 3.7 View of the test setup.

3.4.1 Design material properties

An average cylindrical concrete compressive strength ranging between 15 and 20 MPa was designed to represent existing RC buildings in which poor quality concrete is usually found. Furthermore, two joints were cast with a very poor concrete compressive strength (f_{cm} < 15 MPa) in order to study the influence of interface mechanical properties on the FRP debonding. A typical curve representing concrete mechanical behavior coming from compression tests on cylindrical coupons with 150 mm diameter and 300 mm height is reported in Figure 3.8.

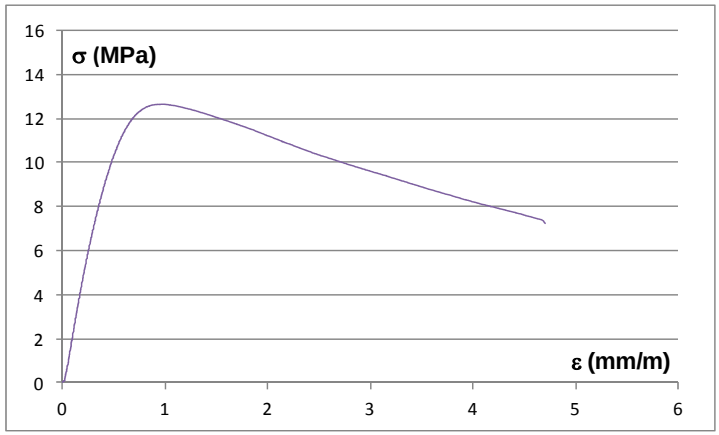

Figure 3.8 Stress-strain behavior of concrete used in this study.

Concrete casting and the experimental tests were carried out with the beam-column subassembly that was horizontally placed on a plane parallel to the strong floor (see Figure 3.7) More details about the concrete compressive strength specific for each of the tested subassemblies are reported in the next paragraphs.

Reinforcing steel FeB44k was adopted for internal longitudinal and transverse reinforcements. Tensile tests were performed on sample coupons extracted from the different batches used to build the joint subassemblies. A typical stress strain behavior is reported in Figure 3.9. The test results for all the coupons are resumed in Table 3.2.

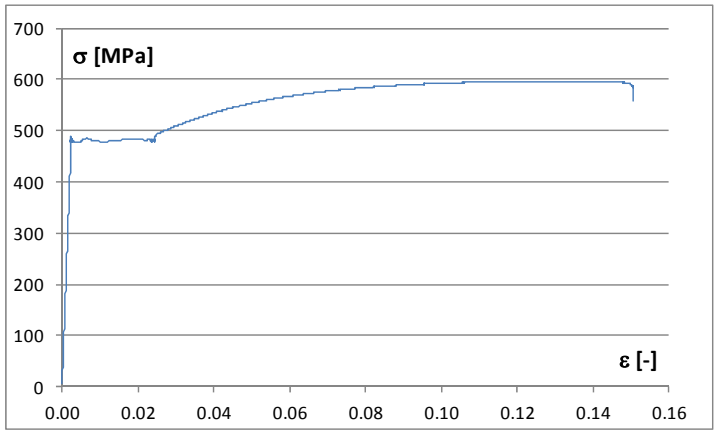

Figure 3.9 Stress-strain behavior of adopted longitudinal steel reinforcements.

Due to the homogeneity of test data, they can be accurately represented by their average value.

Table 3.2. Summary of tensile tests on longitudinal steel reinforcements.

Batch	spec.	ϕ	σ_y	ε_y	E	ε_h	ε_{max}	σ_{max}
[-]	[-]	[mm]	[MPa]	[-]	[MPa]	[-]	[-]	[MPa]
1	1	16	457.9	0.002238	204613	-	-	-
	2	16	452.4	0.002184	207179	-	-	-
2	1	16	497.0	0.002461	201951	0.023	0.175	596.8
	2	16	488.3	0.002447	199580	0.023	0.150	596.8
	3	16	493.6	0.002487	198478	0.0235	0.220	601.8
3	1	16	462.7	0.002281	202851	0.0232	0.210	601.8
	2	16	466.6	0.002303	202646	0.0233	0.212	603.3
	3	16	468.5	0.002257	207551	0.0234	0.220	606.8
Average		16	473.4	0.002332	203106	0.0232	0.201	601.2

The average yield stress is about 470 MPa, the average yield strain ε_y = 0.24% and the average maximum strength is 600 MPa (maximum strain ε_u = 20%).

3.4.2 Failure sequence

Several theoretical capacity models (Priestley, 1997; ASCE/SEI, 2007; ACI 369R-11, 2011; Lafave and Kim, 2011; Park and Mosalam, 2012b) were used to predict the strength capacity of beam-column joints and the subassembly failure sequence. According to theoretical analyses and assuming the joint shear capacity provided by Priestley (1997), the failure sequence was determined. In the calculations, it should be accounted for a preload of 19.2 kN applied at the beam tip to represent the gravity load. Thus, the analytical determined failure sequence, assuming f_{cm}=16.4MPa, is:

1. Joint panel shear failure: the joint shear capacity V_{jh}, corresponding to the principal tension stress $p_t = 0.42\sqrt{f_{cm}}$ (Priestley, 1997), is reached at a column shear of V_c = 42.8 kN (see Figure 3.10, step1);
2. Yielding of top column bars at V_c = 55.9 kN;
3. Yielding of beam bars at V_c = 43 kN (due to a preload in the positive direction about 19.2kN, ΔV_c = 43+13 kN=56 kN).

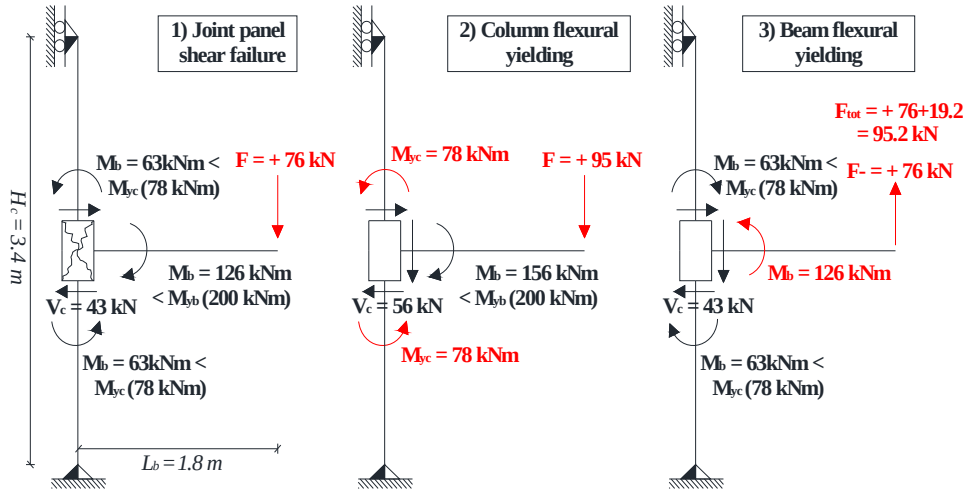

Figure 3.10 Joint subassembly failure sequence.

Furthermore, the joint panel first cracking, corresponding to the principal tension stress $p_t = 0.29\sqrt{f_{cm}}$ (Priestley, 1997), is reached at a column shear of V_c = 34 kN. At this step, the imposed displacement at beam tip is about 15 mm.

3.4.3 Load protocol

The load protocol consisted of three consecutive cycles (see Figure 3.11). The displacement amplitude in each direction was progressively increased by 5 mm (up to 30 mm) or 15 mm (up to failure). The incremental step was set in order to achieve the joint first cracking (d=15 mm) in three steps. For large imposed displacements, the incremental step was increased to 15 mm in order to reduce the total duration of the tests. To simulate gravity loads, a preload of 19.2 kN (d_0=5mm) was applied to the beam along with a constant axial load ($\nu = P/A_g f_c = 0.2$) to the column. The test setup was able to reproduce seismic action on beam-column subassemblies as pointed out in several experimental studies ((Beres et al., 1996; Prota et al., 2004)).

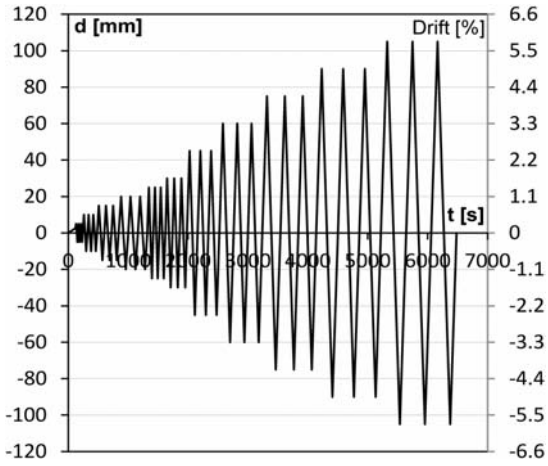

Figure 3.11 Load protocol.

3.4.4 FRP Strengthening

The experimental program involved six tests on as-built and retrofitted beam-column specimens. The specimen label is T_XYZ: T is the joint type (T joint); X is the joint configuration: C for control specimens with a progressive number (1, 2, 3) or F for FRP strengthened specimens; Y is the strengthening configuration (Figure 3.12), L (Light) or S (Strong); Z is the number of carbon FRP (CFRP) quadriaxial sheet layers on the joint panel (1 or 2). Concrete mechanical properties were designed to simulate existing RC constructions. Two joints (T_C1 and T_FL1) had a poor concrete compressive strength (f_{cm} < 15 MPa) and four others (T_C2, T_C3, T_FS1, T_FS2) had a concrete compressive strength ranging between 15 and 20 MPa. Of a total number of six subassemblies, three specimens were tested in the as-built configuration, defined as T_C1, T_C2, and T_C3. Three specimens (T_FL1, T_FS1, T_FS2) were strengthened to investigate the benefits provided by different FRP layouts. The FRP-strengthening strategy aimed to avoid joint brittle failure (T_FL1) and increase the subassembly dissipation capacity (T_FS1 and T_FS2). Indeed, inspections of RC structures after seismic events indicate that the most common collapse mechanism results from premature shear failures. Once the potential brittle failure has been avoided, the structural global dissipation capacity can be increased by using FRPs at the location of potential plastic hinges (usually at the ends of columns, especially in existing RC structures designed to sustain only gravity loads). This goal can be pursued without changing the plastic hinge position or relocating the potential plastic hinges following the capacity design criterion. The former strategy was pursued in the experimental program. Thus, the effectiveness of FRP wrapping on plastic hinge zones (i.e., column ends) was investigated on Specimens T_FS1 and T_FS2. According to these criteria, the joint panel was strengthened by quadriaxial FRP sheets (to sustain the shear demand), and the column ends were wrapped by uniaxial FRP sheets (to increase the subassembly dissipation capacity). Furthermore, the use of uniaxial FRP sheets at the end of the beams was aimed at delaying FRP joint panel reinforcement

debonding. This intervention may also be effective at increasing the shear capacity of beam at the location of maximum shear demand (e.g., in the case of an existing structure with insufficient shear reinforcement on the beams).

The first strengthening solution, termed Light (Scheme 1), was adopted for the T_FL1 specimen. It involved one layer of quadriaxial carbon fibers, CFRP, applied to the joint panel and slightly extended to the beams (i.e., 200 mm, Figure 3.12a). Panel strengthening was anchored by means of uniaxial U-shaped CFRP wraps on the beam ends for 200 mm.

T_FS1 and T_FS2 were strengthened by means of a Strong configuration as depicted in Figure 3.12b,c, respectively. Also, in this case, quadriaxial CFRP sheets were applied on the joint panel and extended to the beam ends for 200 mm. Two layers were adopted for T_FS2 on which the joint panel strengthening was also extended for 200 mm to column ends. This extension was made to increase the FRP joint panel bond length; it was not designed to move the first yielding from the column to the beam. On both T_FS1 and T_FS2 specimens, U-shaped uniaxial CFRP wraps were used to anchor the joint panel strengthening mechanically. They were extended 750 mm to the beams (instead of 200 mm as in T_FL1) to simulate in situ strengthening. In such cases, an increase in shear capacity could be necessary at the extremity of the beam (Di Ludovico et al., 2008). On T_FS2, the U-shaped uniaxial sheet was also wrapped around the top side of the beam to improve the anchoring system (Figure 3.12c). Finally, the CFRP wrapping of column ends (750 mm) was also adopted for both T_FS1 and T_FS2.

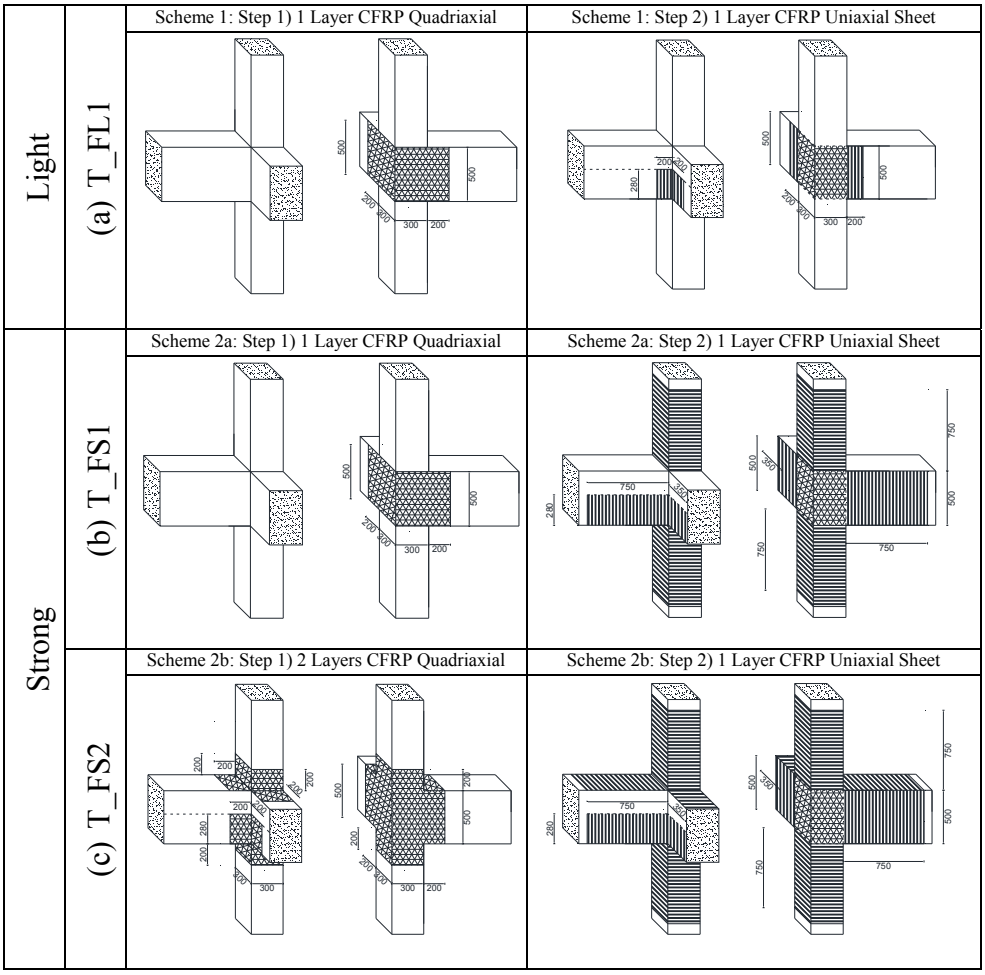

Figure 3.12 FRP strengthening layouts (dimensions in mm).

Uniaxial CFRP sheet with a unit weight of 300 g/m² and thickness of dry fibers, $t_{f,eq}$, of 0.166 mm was used to anchor the joint panel reinforcement and for column confinement. Tensile tests were performed on 12 CFRP coupons made of uniaxial sheets to determine their mechanical properties. The average tensile strength and ultimate strain of uniaxial CFRP laminates were 254 MPa and 1.6%, respectively. Quadriaxial CFRP sheets with a unit weight of 380 g/m² and thickness of dry fibers, $t_{f,eq}$, of 0.053 mm were used

for joint panel strengthening. The sheet properties were provided by the manufacturer: Young's modulus of 230 GPa and ultimate strain of 1.5%.

T_RFL1 specimen is the specimens tested in as-built configuration, T_C2, firstly repaired by using epoxy resin injections and controlled-shrinkage fiber reinforced fluid mortar and then retrofitted by using one layer of quadriaxial CFRP sheet on the joint panel (Light configuration). The main repair and retrofit phases are reported in Figure 3.13. R4 class, according to EN-1504-3 (2005), controlled-shrinkage fiber-reinforced fluid mortar was used for concrete repair on the damaged and retrofitted joint. Two-component super fluid epoxy resin was used for cracks sealing with Youngs' modulus of 3.4 GPa, ultimate axial strain 1.0%, tensile strength 44 MPa, compressive strength 100 MPa.

(a) (b) (c) (d)

Figure 3.13 Repair and retrofit of specimen T_RFL1: concrete cover and damaged concrete removal (a); controlled-shrinkage fiber-reinforced fluid mortar casting (b); super fluid epoxy resin injection (c); and FRP panel installation (d).

3.4.5 Instrumentation

The structural response was measured in real time with an electronic data acquisition system. Linear variable displacement transducers (LVDTs) were used to monitor the specimen's deformed shape, joint panel shear strain, joint drift and curvatures at end cross-sections of beam and columns. The effective beam tip displacement was recorded by means of a

potentiometer. Strain gauges were installed on the different directions of FRP fibers of the joint panel strengthening sheet to record the strain attained on the fibers.

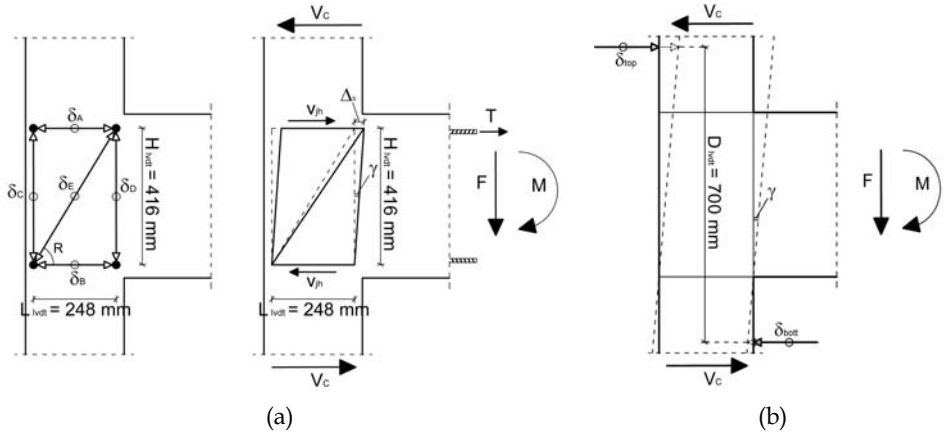

(a) (b)

Figure 3.14 LVDT layout to monitor: a) joint shear deformations; b) joint drift.

Major importance was reserved to the joint panel shear deformation. Indeed, six LVDTs were installed on the joint panel to monitor horizontal, vertical and diagonal deformations (see Figure 3.14a).

Using the records of the four LVDTs in the horizontal and vertical directions, plus one of the two diagonals, the joint panel shear deformation can be calculated by:

$$\gamma = arctg\left(\frac{\Delta_s}{H_{LVDT}}\right) \quad [rad] \tag{3.2}$$

Where Δ_s can be calculated as reported in Figure 3.15 and H_{LVDT}=416mm.

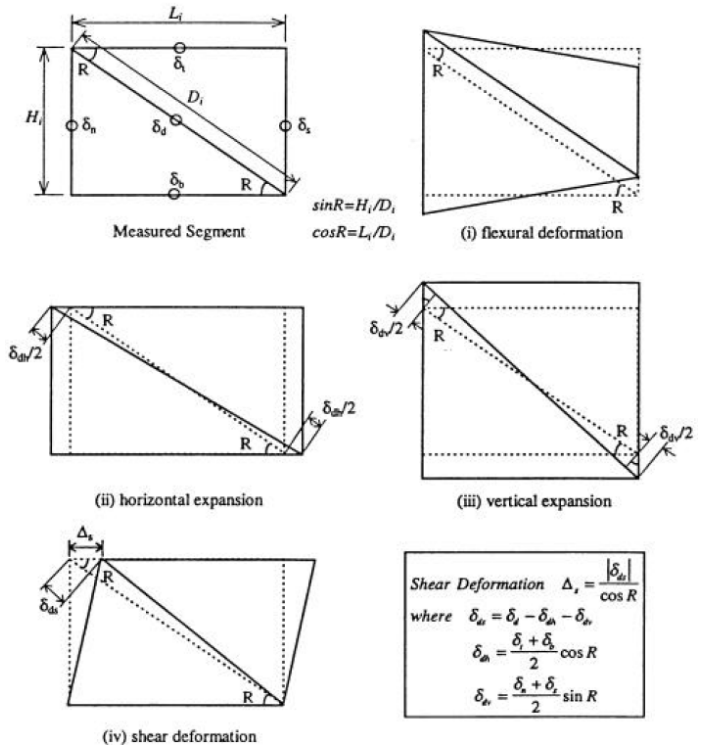

Figure 3.15 Joint shear deformation computed from LVDTs on the joint panel (Moratti, 2000).

A further expression to calculate the joint shear deformation was derived. This expression may be needed when the records of all the four LVDTs on the joint panel frame are not available due to the loss of LVDT support because of the joint cracking.

$$a^2 = b^2 + c^2 - 2 \times b \times c \times \cos(\alpha) \Rightarrow$$
$$\alpha = \arccos\left(\frac{b^2 + c^2 - a^2}{2 \times b \times c}\right) \Rightarrow \quad (3.3)$$
$$\gamma = 90 - \alpha$$

Where *a*, *b*, *c*, are the LVDT recorded deformations in the diagonal, horizontal and vertical direction, respectively. Thus, with this method only 3 LVDT records are needed.

The effects of joint shear deformations of the interstorey drift (i.e. the joint drift) can be quantified monitoring the lateral displacement close to the joint panel. For this reason two LVDTs were installed at the column-to-joint interface (see Figure 3.14b). The joint drift can be evaluated as the sum of the two LVDT records divided by the LVDT distance, D_{LVDT}=700 mm.

3.5 EXPERIMENTAL RESULTS

The experimental results are discussed with reference to: (1) global behavior (crack patterns, failure mode, column shear-drift hysteresis loop, subassembly energy dissipation and stiffness); and (2) local behavior (moment curvature relationship for the column base cross-section, stress-strain evolution of the joint panel, strain on the internal steel bars and on the joint panel FRP sheet).

The main experimental results for both positive and negative load actions are reported in Table 3.3 in terms of the maximum column shear, $V_{c,MAX}$, and the corresponding Drift ($V_{c,MAX}$). The average compressive strength of concrete was determined on the basis of three tests made on cylindrical samples that had been cast during the preparation of the specimens; the average strength reached 28 days after casting is also reported Table 3.3. The hysteretic behavior resulted from experimental tests are reported in Figure 3.16 and Figure 3.17. The experimental findings will be discussed in the next sections. To further aid evaluation of specimen performance under different retrofit schemes, the cumulative energy dissipation at each cycle, E_{tot}, was also computed by totaling up the areas under hysteretic cycles of the column shear-drift relationship (see Table 3.3). The strains, recorded on the strengthening system of the FRP joint panel at $V_{c,MAX}$, are reported in the last column of Table 3.3.

Table 3.3. Test matrix and experimental results.

Spec.	f_{cm}	$t_{f,eq}$	Load sign	$V_{c,MAX}$	ΔV_c	Drift ($V_{c,MAX}$)	Failure Mode	E_{tot} (Drift=3.3%)	ΔE_{tot}	ε_{FRP} (max)
[-]	[MPa]	[%]	[-]	[kN]	[%]	[%]	[-]	[kN*mm]	[%]	[με]
T_C1	12.6	-	+	33.2	-	1.1	JS	7406	-	-
			-	27.6	-	1.3				
T_C2	16.4	-	+	42.6	-	1.3	JS	n.a.[a]	-	-
			-	34.4	-	1.3				
T_C3	16.3	-	+	43.8	-	1.3	JS	10237	-	-
			-	36.9	-	1.3				
T_FL1	13.5	0.053 (scheme 1)	+	38.8	17.0[b]	1.3	FD /JS	8596	16.1[b]	7.3
			-	33.1	19.8[b]	1.3				
T_FS1	17.7	0.053 (scheme 2a)	+	56.1	29.9[c]	2.4	CH /FD	12225	19.4[c]	10.2
			-	45.2	26.6[c]	2.4				
T_FS2	16.4	0.106 (scheme 2b)	+	65.3	51.2[c]	2.3	CH /FC	13460	31.5[c]	6.7
			-	50.1	40.6[c]	1.3				
T_RFL1	16.4	0.053 (scheme 1)	+	45.4	6.4[c]	2.4	FD /JS	10190	-	4.5
			-	35.0	1.7[c]	2.4				

Note: JS = joint shear; CH = column flexural hinging; FD = FRP debonding; FF = tensile failure of FRP fibers.

[a] This test was stopped at a drift of 2.39%; [b] Computed for T_C1; [c] Computed for the average T_C2 and T_C3.

3.5.1 As-built specimens

Although characterized by different concrete compressive strengths, the as-built specimens (T_C1, T_C2, and T_C3) showed a similar joint panel crack pattern and failure mode Figure 3.18 and Figure 3.19. Observed joint panel failure was characterized, in each case, by large deep diagonal cracks and concrete wedge spalling-off, as commonly observed in post-earthquake inspections and in several experimental tests (Priestley, 1997; Pantelides et al., 2002; Antonopoulos and Triantafillou, 2003). The cyclic behavior (T_C1, T_C2 and T_C3 in Figure 3.16) was asymmetrical because beam internal top and bottom reinforcements differed (i.e., 5ϕ16 on the top side and 3ϕ16 on the bottom side). Furthermore, the higher peak shear values were always attained in the positive load direction because of the initial positive preload on the beam used to simulate the existing gravity loads (i.e., 19.2 kN).

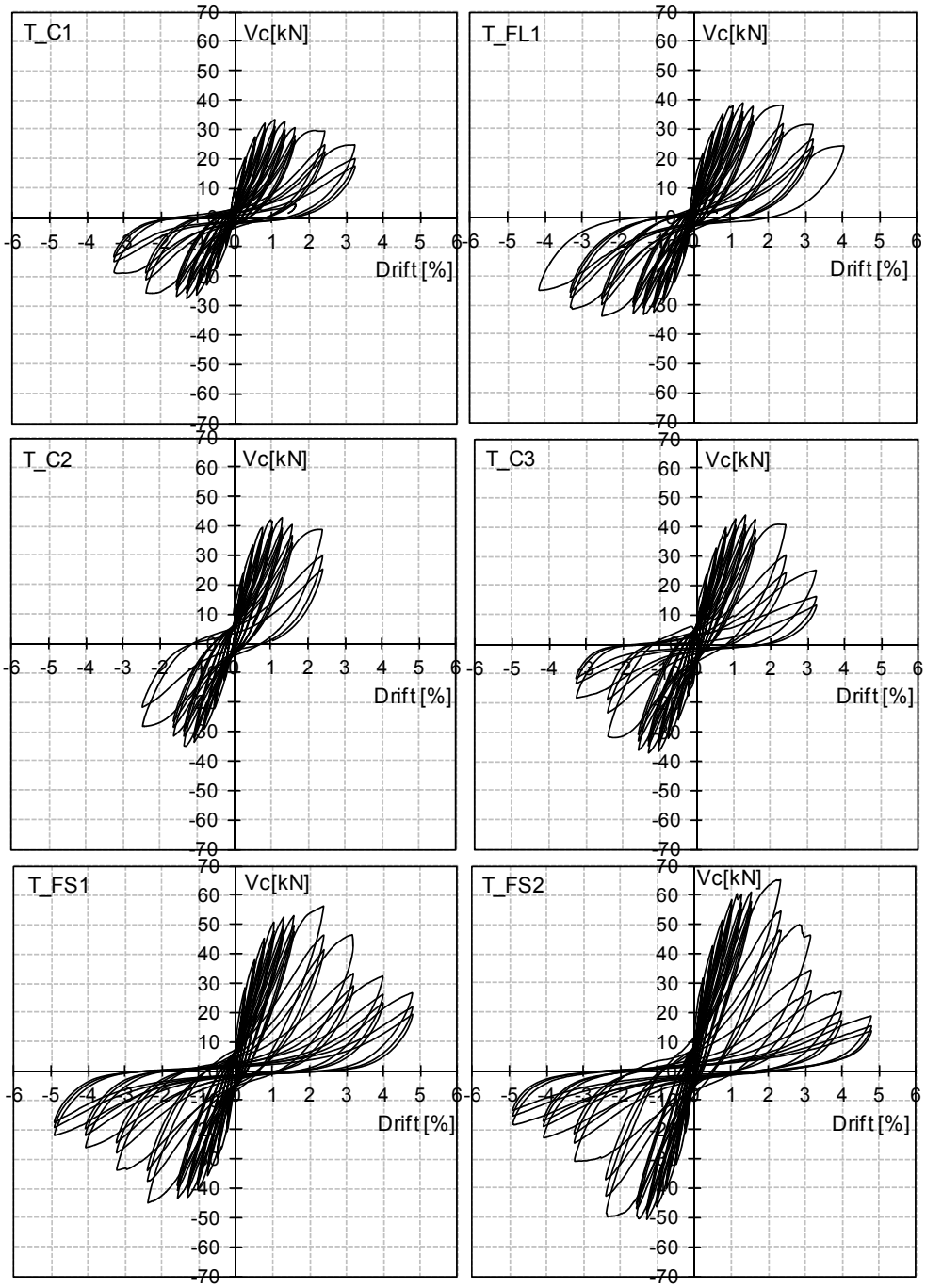

Figure 3.16 Cyclic hysteresis loop of tested specimens.

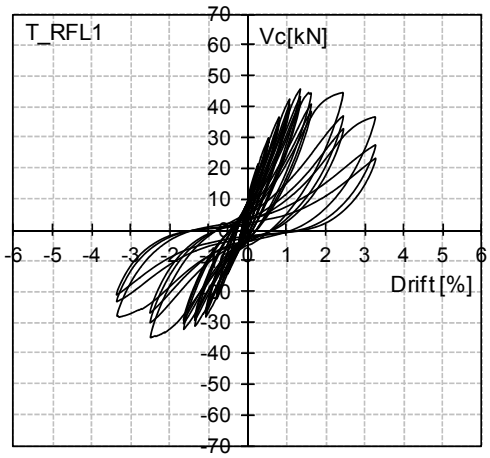

Figure 3.17 Cyclic hysteresis loop of T_RFL1 specimen.

The initial hairline cracking in the joint panel of as-built specimens started at the beginning of the third load cycle for an imposed drift, approximately equal to 0.5% and corresponding to a column shear of approximately 27 kN for T_C1 and 33 kN both for T_C2 and T_C3. The first diagonal cracking of the joint panel can be easily observed in the v_j–γ envelope curve reported in Figure 3.20 for Specimen T_C3 (experimental trends for T_C1 and T_C2 are partially available because the LVDTs stopped functioning when excessive cracking of the joint panel was attained). Indeed, a strong change in slope in the diagram of the joint panel shear stress-strain is visible at γ = 0.0009 rad, corresponding to a computed shear stress of 2.34 MPa (Figure 3.20, Level II point). Comparison of γ and Drift values reached at the first cracking of the joint with the values recorded by Pantelides et al. (2002) is reported in Table 3.4. In the drift range 0.78–1.31%, the joint panel cracks rapidly increased in number and width (Figure 3.18), leading to a significant degradation of subassembly stiffness. Concrete strength considerably affected the subassembly peak strength (see Table 3.3) that was attained for a drift of 1.1% for T_C1 and 1.31% for both T_C2 and T_C3. At this stage, deep wide cracks developed on the joint panel in both principal directions (γ = 0.0083 rad and v_j = 2.95 MPa, Level III in Figure 3.20), shear failure was attained, and a descending trend of the V_c-Drift branch started. Good agreement was

found with the experimental values reported by Pantelides et al. (2002), as shown by Table 3.4. The post-peak stage was characterized by a significant opening of the anchorages of beam bars bent into the joint. This led to concrete wedge spalling-off (see Figure 3.18b and Figure 3.19a) that became significant for a drift of 2.39%. At this stage, the specimen behavior was characterized by a strength degradation related to the concrete core fracture in the joint panel. For an imposed drift of 3.3%, the opening of the anchorages of beam bars led to complete concrete spalling and to significant shear strains in the joint panel (i.e., γ = 0.0226 rad on T_C3, Figure 3.18b,c, Figure 3.19b and Figure 3.20 Level IV). The experimental evidence showed that a joint panel shear failure was attained on the as-built specimens at a drift of approximately 1.1–1.3%. A significant joint strength degradation has been achieved as shown in Figure 3.16, for T_C1, T_C2 and T_C3 specimens.

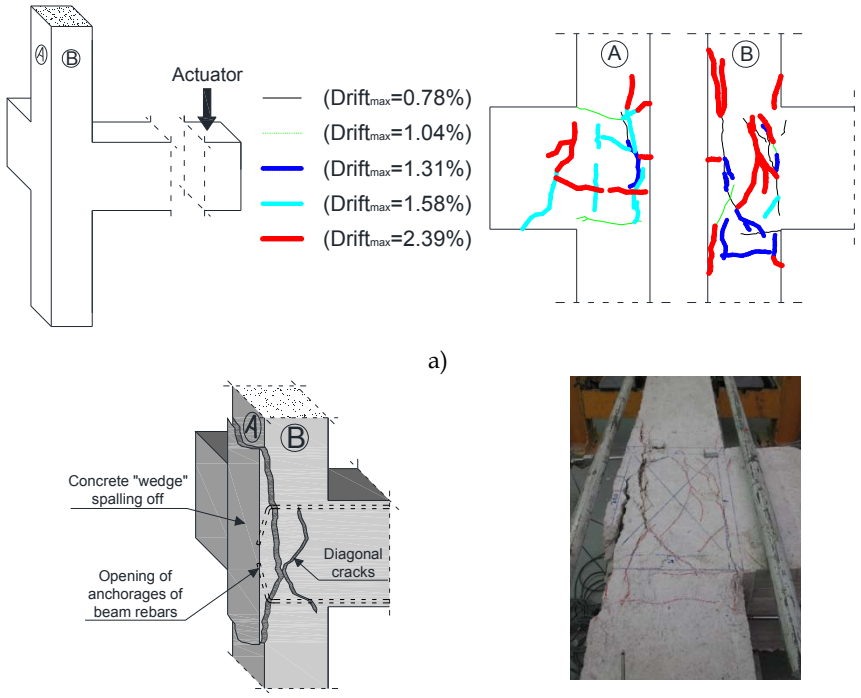

Figure 3.18 Specimen T_C1: crack pattern (a); failure mode (b); final damage report (c).

The hysteresis loops were characterized by a significant pinching effect because of residual shear strains in the joint panel.

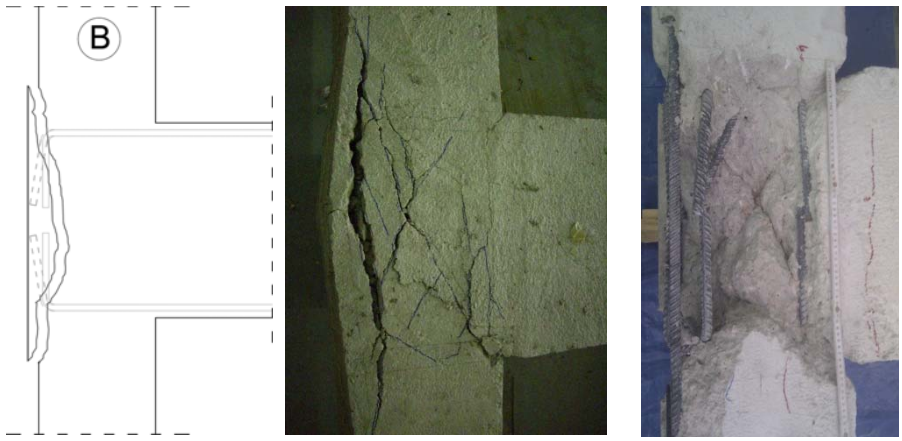

(a) (b) (c)

Figure 3.19 Specimen T_C3 crack pattern (a); failure mode (b); final damage report (c).

To examine the crack dimensions in the joint core, the damaged concrete was removed after each test. The core inspections showed two deep diagonal cracks that led to joint panel splitting in four parts (see Figure 3.19c). The experimental failure modes showed the premature shear failure of the joint panel without the internal bars yielding, as confirmed by strain gauges placed on the bars at the section interface between beam or columns and joint panel. In each test, the maximum recorded strains were significantly lower than the yield strain.

Table 3.4. Joint panel shear-strain literature comparisons for specimen T_C3

		Experimental		Pantelides et al. (2002)	
Level	Performance description	Drift	γ	Drift	γ
[-]	[-]	[%]	[rad]	[%]	[rad]
I	Beam bar yielding	-	-	0.66	0.0018
II	Joint significant cracking	0.52	0.0009	0.48	0.0010
III	Joint shear mechanism	1.31	0.0083	1.43	0.0085
IV	Significant concrete spalling	2.39	0.0226	1.84	0.0264

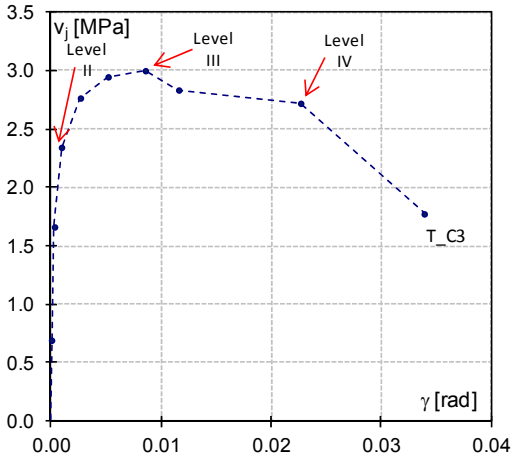

Figure 3.20 Experimental versus theoretical joint shear stress-strain for T_C3.

3.5.2 FRP strengthened specimens

The main experimental parameters related to tests on FRP strengthened specimens are reported in Table 3.3. The hysteresis loops are depicted in Figure 3.16 and Figure 3.17. The T_FL1 hysteresis loop showed that the column shear peak of 38.8 kN (17% higher than the peak strength on the as-built Specimen T_C1) was attained at 1.3% drift. At 2.39% drift, the strength remained almost constant both in the positive and negative load directions. At this stage, a significant drop in strength was attained because of FRP end debonding. A trend very similar to that observed on the as-built T_C1 specimen was then observed. The failure mode was given by FRP debonding as shown in Figure 3.21a. In particular, initial intermediate debonding was detected on the quadriaxial CFRP joint panel strengthening at a drift level of 1.1%. This result is confirmed by the FRP tensile strain trend reported in Figure 3.22. The figure shows the tensile strain on the FRP quadriaxial sheet, ε_{max}, corresponding to different drift levels (i.e., maximum drift of each load cycle). At an imposed drift of 1.1%, a contraflexure point can be observed in the strain drift trends (Figure 3.22a). It could be representative of an initial debonding phenomenon. The end anchorage

system (i.e., U wraps) delayed the full FRP debonding and avoided sudden strength degradation. Full FRP panel debonding was achieved at drift 3.3% with a maximum strain on the FRP reinforcement of approximately 0.6–0.7% in the diagonal fiber directions (strain gauge s.g.f.#2, 4, Figure 3.22a,b) and approximately 0.4% in the horizontal fiber direction (strain gauge s.g.f.#1, Figure 3.22c). Thus, premature debonding strongly reduced the effectiveness of FRP strengthening. Indeed, the FRP joint panel strains at failure were significantly lower than the ultimate FRP strains. This result was also found by Gergely et al. (2000). However, the experimental FRP maximum strain on the joint panel was higher than 0.4%, which is suggested by CNR-DT 200 (2013) as the maximum FRP strain for design purposes. Starting from a drift level of 2.39%, column concrete crushing was also observed (Figure 3.21).

(a) (b)

Figure 3.21 T_FL1: failure mode a); crack pattern after FRP removal b)

On the T_FS1 specimen, initial FRP debonding was attained at a drift level higher than in the case of T_FL1, even if the anchorage length of the quadriaxial sheet was 200 mm as in T_FL1. Initial debonding started at a positive drift of 1.58%. This confirmed that the quality of the concrete significantly affected the strengthening system efficiency by delaying cohesive intermediate debonding, thanks to higher substrate mechanical properties.

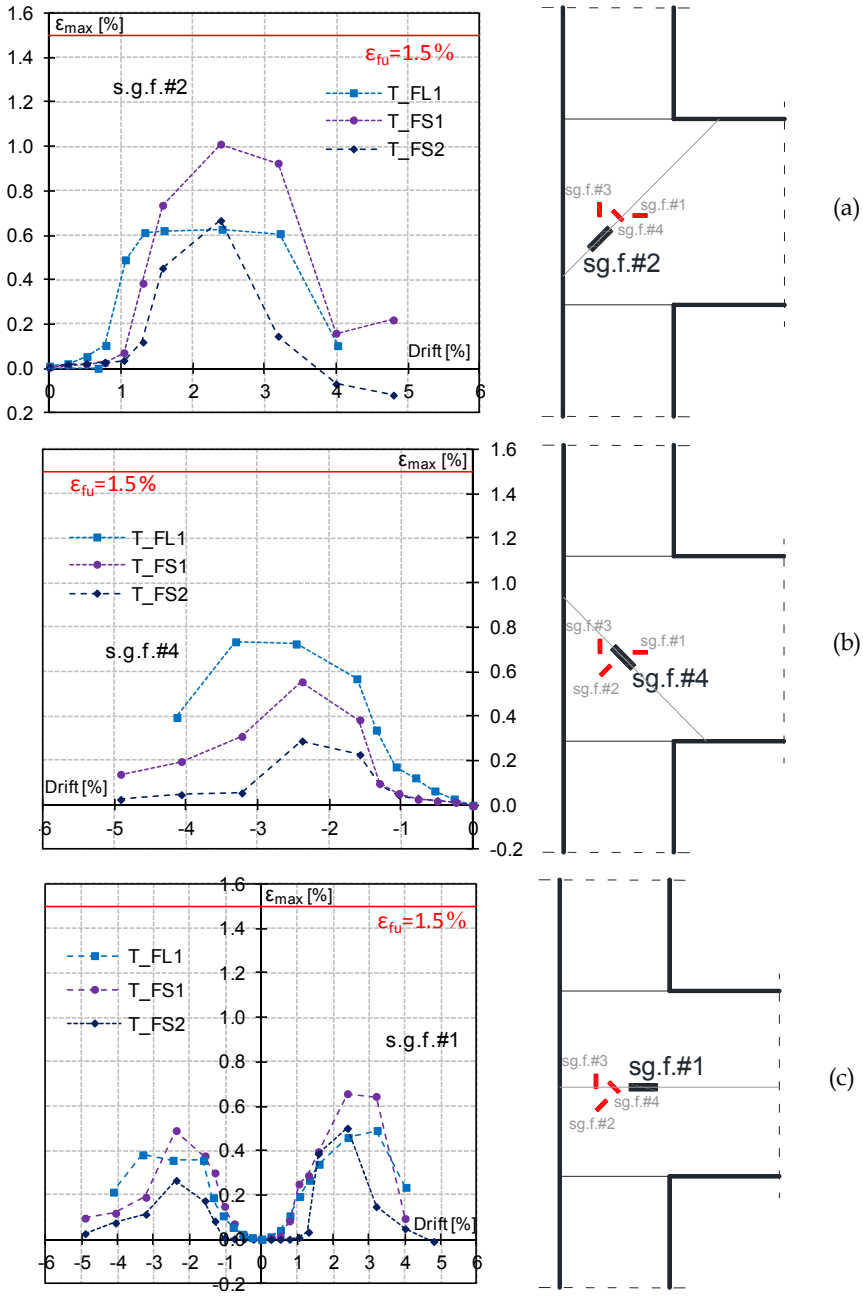

Figure 3.22 Joint panel FRP strains.

The maximum strain recorded on T_FS1 was higher than that related to T_FL1: 1.0% in the diagonal fiber direction (s.g.f.#2) at 2.39% drift for a positive load action (Figure 3.22a). Lower strain levels were attained on the opposite diagonal fiber at the same drift level because the initial debonding had already started during positive load action. The higher peak strain on FRP resulted in a significant subassembly strength enhancement compared to the peak strength of as-built Specimen T_C3 (i.e., slightly less than 30%, see Table 3.3). Once peak strength had been attained, a sudden strength drop was observed (see Figure 3.16, T_FS1). Full debonding occurred at the extremity of the joint panel at 3.3% drift (Fig. 8). FRP full debonding is shown in Figure 3.23 along with the concrete surface after FRP removal. The figure shows that debonding started from the extremity of the quadriaxial FRP sheet, as what happened with T_FL1. However, the tensile failure of quadriaxial fibers on the joint panel corner was also detected on this specimen. The failure of these fibers occurred because the outer fibers on the joint panel still had an effective anchorage length even after first debonding of the FRP quadriaxial free end.

(a) (b)

Figure 3.23 T_FS1: failure mode a); crack pattern after FRP removal b)

T_FS2 column shear versus the drift curve is reported in Figure 3.16. The experimental test showed the effectiveness of the new anchoring solution

(Figure 3.12c) that prevented full debonding and led to the tensile failure of quadriaxial fibers on the joint panel (Figure 3.24).

(a) (b)

Figure 3.24 T_FS2: failure mode a); crack pattern after FRP removal b)

In particular, the anchorage provided by the uniaxial FRP sheet wrapped up to the beam top side protected the quadriaxial laminates from full debonding of the FRP end. Initial debonding started again in the drift range of 1.57–2.42%, as for T_FS1, but it stopped when the anchorage provided by the uniaxial sheet became effective. At a drift of 2.42%, the tensile failure of CFRP quadriaxial fibers was reached on the joint panel perimeter. Tensile failure occurred even if the maximum strain recorded was approximately 0.6% (Figure 3.22a). This may be related to high stress concentrations on the beam-joint panel interface. The lower strain level than recorded on Specimen T_FS1 may be related to a larger amount of FRP fibers on the joint panel, as also confirmed by Akguzel and Pampanin (2010). Because full debonding was prevented on this specimen, maximum strength increase was attained with respect to as-built joints (i.e., 51 and 41% for positive and negative load actions, respectively, see Table 3.3). In contrast, the brittle failure mode due to the tensile failure of fibers (at a drift of 2.4%) did not allow the FRP to increase subassembly global ductility significantly. Strength degradation was faster than that recorded on the other specimens because of brittle failure of CFRP fibers. The debonding phenomena

detected on both T_FS1 and T_FS2 were also found in the tests carried out by Antonopoulos and Triantafillou (2003). The tests showed that even if end debonding is avoided by adopting a proper anchorage solution, intermediate debonding can be achieved. Thus, the adoption of discrete restraint points in the joint region, as proposed by Ghobarah and El-Amoury (2005), may prevent FRP intermediate debonding. Maximum strain records on the FRP joint panel (Figure 3.22) pointed out that on each strengthened specimen, the maximum strains were recorded on diagonal fibers (see s.g.f.#2, 4 in Figure 3.22a,b). The FRP joint panel was removed after tests on T_FL1, T_FS1, and T_FS2. Views of the concrete substrates are reported in Figure 3.21, Figure 3.23 and Figure 3.24. These figures show that once FRP was removed, the cracks on concrete were more diffused on the joint panel surface and characterized by a lower depth with respect to as-built specimens T_C1, T_C2, and T_C3.

(a) (b)

Figure 3.25 T_RFL1: failure mode a); crack pattern after FRP removal b).

On the repaired and FRP retrofitted joint, T_RFL1, and FRP strengthened one, T_FS1, a premature debonding of the panel reinforcement was attained starting from the free end of U-shape anchorage system (see Figure 3.25a). Thus, the limited width of the anchorage system adopted in the strengthening layout strongly affected the strengthening response. After the test, the FRP reinforcement was removed to investigate on the internal

concrete damages; the inspections showed that several cracks developed in the joint core characterized by a lower width and depth with respect to those observed on control specimens (see Figure 3.25a). Although the FRP debonding limited the FRP effectiveness, the FRP retrofitted specimen, T_RFL1, was able to recover both original strength and deformation capacity without a significant stiffness reduction.

Comparisons on performances of the different strengthening layouts are reported in the next chapter.

CHAPTER 4
DISCUSSION ON EXPERIMENTAL RESULTS

The experimental tests performed on RC beam-column corner joints demonstrated the seismic vulnerability of poorly detailed joint subassemblies and the effectiveness of FRP strengthening. In order to identify the main parameters affecting the mechanical response of RC beam-column joints and the FRP strengthening, a comparison between the experimental results is presented in this chapter. Furthermore, the accuracy of the available capacity model predicting the joint shear strength and deformation is assessed. This is very important to reliably identify the contribution of the concrete mechanisms to the shear strength of FRP retrofitted joints.

4.1 AS-BUILT SPECIMENS STRENGTH

To assess the reliability of available capacity models for poorly detailed exterior beam-column joints, it is presented a numerical comparison

between theoretical and experimental column shear strength at the first cracking of the joint panel, $V_{c,pr,f.c.}$ (computed according to Priestley (1997), by assuming k = 0.29) or at subassembly peak strength, $V_{c,pr}$. The results are summarized in Table 4.1. $V_{c,pr}$ is computed as the difference between the total tensile force in beam internal bars T (computed from the beam end cross-section equilibrium at the rotation) and the joint panel shear $V_{jh,pr}$ (computed according to the theoretical formulations). In particular, in the ASCE/SEI 41-06 (2007) and AIJ (1999) formulations, two different values are adopted for the coefficients that account for the confinement provided by transverse beams (6 and 8 for coefficient $\bar{\gamma}$ in the former and 0.85 and 1 for coefficient φ in the latter). An absolute maximum scatter of 10% between the theoretical and experimental strength capacity was found by using models available in the literature (Priestley, 1997; Park and Mosalam, 2012b).

Table 4.1. Shear strength literature comparisons

	Priestley (1997) k=0.29		Priestley (1997) k=0.42		Park and Mosalam (1997)		AIJ (1999)		ASCE 41-06 (2007)	
Spec.	$V_{c,pr,f.c}$	Δ^*	$V_{c,pr}$	Δ^{**}	$V_{c,pr}$	Δ^{**}	$V_{c,pr}$	Δ^{**}	$V_{c,pr}$	Δ^{**}
[-]	[kN]	[%]	[kN]	[%]	[kN]	[%]	[kN]	[%]	[kN]	[%]
T_C1	28.3	3.6	36.0	8.5	34.2	3.1	35.8 (φ = 0.85)	7.8	25.4 ($\bar{\gamma}$ = 6)	-23.5
							42.0 (φ = 1)	26.5	33.9 ($\bar{\gamma}$ = 8)	2.2
T_C2	33.6	1.3	42.7	0.1	39.3	-7.8	42.5 (φ = 0.85)	-0.2	29.0 ($\bar{\gamma}$ = 6)	-31.9
							50.3 (φ = 1)	17.5	38.6 ($\bar{\gamma}$ = 8)	-9.8
T_C3	33.5	4.0	42.6	-2.7	39.3	-10.2	42.4(φ = 0.85)	-3.1	28.8 ($\bar{\gamma}$ = 6)	-34.2
							50.2 (φ = 1)	14.6	38.4 ($\bar{\gamma}$ = 8)	-9.8

Note: * computed for joint panel first cracking (27.3kN for T_C1; 33.3kN for T_C2 and T_C3); ** computed for as-built joint $V_{c,MAX}$, reported in Table 3.3.

The minimum difference was obtained according to the approach reported in Priestley (Priestley, 1997). The ASCE/SEI 41-06 (2007) and AIJ (1999) design expressions proved less accurate than the formulation to predict experimental strength capacity of Priestley (1997). In particular, the ASCE/SEI 41-06 (2007) formulation may lead to very conservative strength capacity predictions if the confinement effect of the transverse beam is

neglected (i.e., by using $\bar{\gamma}$ = 6). By contrast, the AIJ (1999) expression may significantly overestimate the joint strength capacity if a significant confinement effect coefficient (i.e., φ = 1) is taken into account. The EN 1998-1 (CEN, 2004; Fardis, 2009) design expression supplies the joint shear design capacity as that obtained at joint panel first cracking, providing a very conservative prediction (i.e., an average of 30% lower than the experimental maximum strength capacity).

4.2 AS-BUILT SPECIMENS SHEAR DEFORMATION

The experimental tests showed that joint strength capacity was attained for significant shear deformations. This should be appropriately taken into account in the structural assessment of RC buildings. Thus, the research community has undertaken major efforts to calibrate suitable capacity models for joint shear deformability. To assess the reliability of such models, also in the case of poorly detailed beam-column joints designed according to obsolete seismic codes, a comparison between the experimental results and the models set up by Priestley et al. (1996), ACI 369R-11 (2011), and LaFave and Kim (2011) is reported in terms of v_j–γ in Figure 4.1. The figure shows that: (1) ACI 369R-11 (2011) predictions were very conservative both in terms of peak and ultimate shear stress and strain; (2) the trilinear theoretical curve provided by Priestley et al. (1996) strongly underestimated the experimental strains but matched the experimental joint shear stresses better; and (3) albeit conservative, the LaFave and Kim (2011) model provided the best approximation of experimental behavior in terms of shear strains at peak strength.

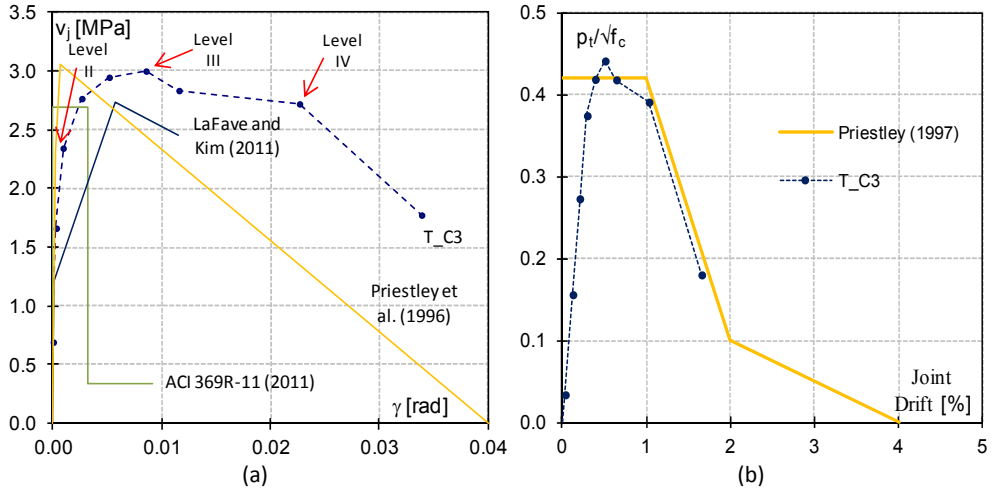

Figure 4.1 Experimental vs. theoretical as-built joint shear stress-strain (a); joint drift (b)

Available literature studies (Calvi et al., 2002; Park and Mosalam, 2013) pointed out that the joint shear deformations may significant affect the seismic response of the overall structural system. In order to quantify these effects, the joint drift, a representative parameter of the overall structural response, has been monitored during the tests. The experimental trend is depicted in Figure 4.1b against $p_t/\sqrt{f_c}$. The experimental behavior shows that the effects of the joint deformation on the joint drift increases almost linearly with the principal tension stress until 0.3% (on a total drift of 1.0%, see Figure 3.16). Thus, the experimental tests demonstrate that also at the pre-cracking stages, the joint shear deformations have to be accounted in the global structural analysis, because they affect the global deformability of about the 30%. After the joint first cracking, the joint drifts significantly increases until 1.7% at the subassembly collapse. In the nonlinear stage, the effects of joint deformability become even more significant (i.e. the 50% of the global subassembly deformation). This experimental trend can be reliably predicted by the theoretical degradation model proposed by Priestley (1997) as depicted in Figure 4.1b, for Specimen T_C3.

4.3 FRP STRENGTHENED SPECIMENS

The FRP-strengthened specimens showed a significant strength enhancement compared to as-built joints: approximately 18, 28, and 46% on average for T_FL1, T_FS1, T_FS2, respectively (see Table 3.3 and Figure 4.2). Although the same joint panel strengthening system was adopted on T_FL1 and T_FS1, a different mechanical behavior was observed on such specimens. Indeed, the poor quality concrete of T_FL1 led to premature intermediate debonding that substantially reduced the potential benefits provided by the CFRP joint panel reinforcing system. The same phenomenon limited the performances of the FRP strengthening on T_RFL1 specimen. The proposed repair and retrofit solution, was able to recover both original strength and deformation capacity without a significant stiffness reduction. Concrete crushing detected at the column-joint interface on T_FL1 demonstrated the need to confine the column ends to increase plastic hinge ductility. Although the strengthening scheme adopted in T_FS1 provided a significant strength increase with respect to the as-built specimens, it was unable to avoid the subassembly brittle failure mode (i.e., joint panel shear failure after FRP debonding). Indeed, top column yielding was not attained on this specimen.

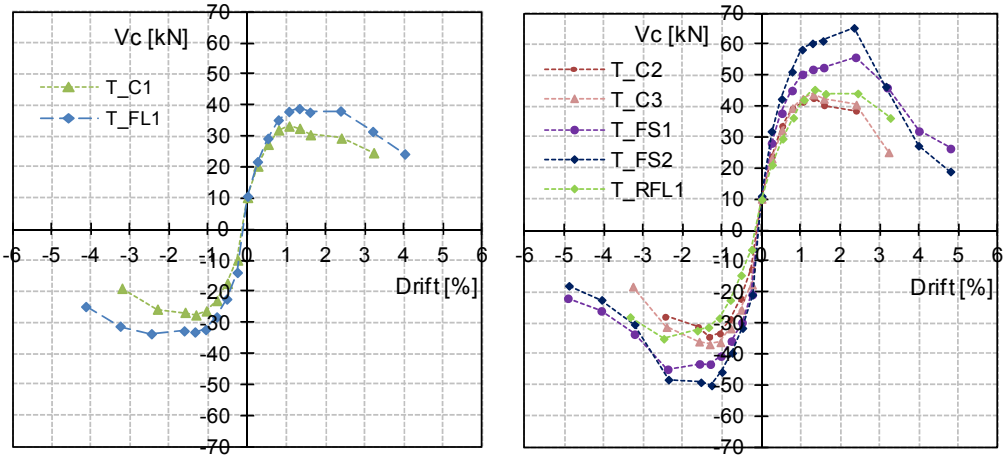

Figure 4.2 Comparisons of experimental skeleton curves.

To analyze the top column plastic deformations, experimental curvatures at the column joint interface cross-section were computed by means of LVDT records. In Figure 4.3, the experimental moment curvature relationships are compared to the theoretical ones. The theoretical curves were computed with reference to the cross-sections reported in Figure 4.3c,d by using an iterative procedure (Marco Di Ludovico et al., 2010).

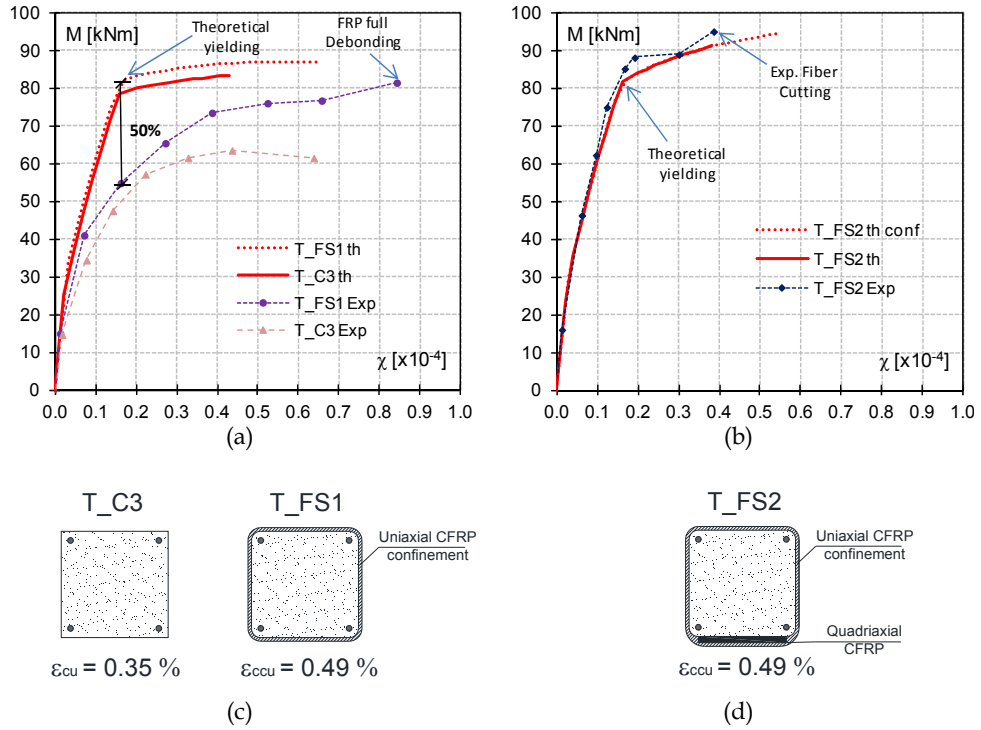

Figure 4.3 Moment-curvature relationships (a), (b); column cross section details (c), (d)

Figure 4.3a shows a considerable gap (50%) between theoretical and experimental acting moments at the theoretical yielding curvature of the T_FS1 column-joint interface cross-section. A bending moment capacity that is comparable to the theoretical yielding was reached in the next load stages. However, considerably higher curvatures than the theoretical ones were recorded. This result may be related to the inadequate amount of FRP panel reinforcement (i.e., only one layer). This strengthening solution

strongly delayed subassembly shear failure thanks to the joint panel confinement effect, but it was unable to modify the failure mode. Indeed, subassembly failure was due to shear with significant joint shear strains. Therefore, column yielding was primarily due to the joint's high deformability. The use of two CFRP plies to increase joint panel shear capacity, combined with a stronger anchorage solution (T_FS2), prevented joint shear failure and allowed top column yielding. The joint panel deformations were reduced, leading to plastic hinge development on the top column Figure 4.3b. The moment-curvature diagram, reported in Figure 4.3b, shows a good match between experimental and theoretical predictions. However, because of quadriaxial CFRP failure, the ductility reserves of the confined column were not fully exploited. In terms of stiffness, Figure 4.2a shows that no significant influence was provided by FRP strengthening on the initial behavior of Specimen T_FL1 (i.e., up to 0.5%). In subsequent cycles, the strengthening system allowed more gradual stiffness degradation compared with T_C1. This finding was confirmed by FRP strain records (Figure 3.22): the FRP system becomes effective from drift values of 0.5%, which corresponds to the first cracking of the as-built specimen joint panel. The same trend was observed in T_FS1 and T_FS2 (Figure 4.2b). Experimental comparisons in terms of cumulative energy dissipation (E_{tot}) are reported in Table 3.3 and Figure 4.4. The maximum increase in energy dissipation was approximately 16% for T_FL1 compared with T_C1 and approximately 20% and 30%, respectively, for T_FS1 and T_FS2 compared with T_C3. These values refer to the ultimate drift reached on as-built specimens (i.e. 3.3%).

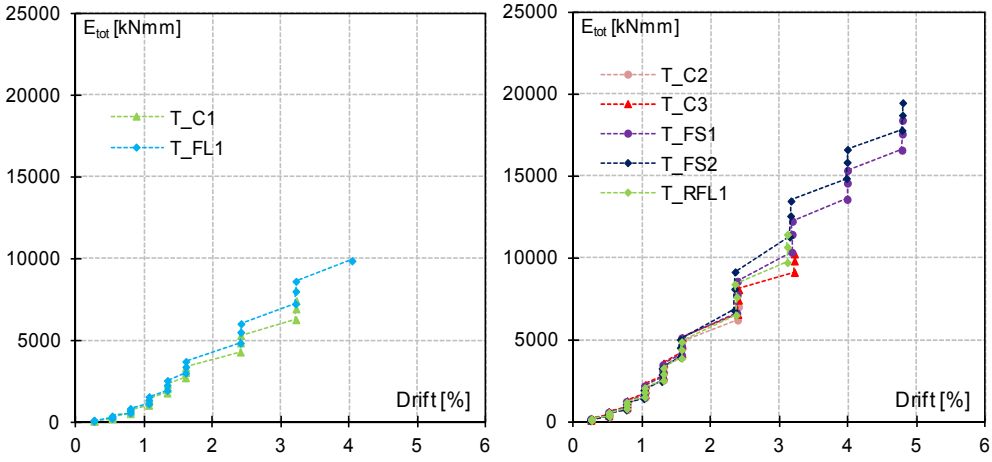

Figure 4.4 Comparisons of energy dissipation in the tested specimens.

In conclusion, the analysis of the joint panel deformability in terms of joint drift is presented comparing the as-built specimen (T_C3) with the two FRP strengthened specimens. It should be noted that the use of FRP strengthening system strongly reduces the joint panel deformability making the joint more rigid. However, this difference is not relevant in terms of the global subassembly initial stiffness (see Figure 4.2b). In compliance with the previously discussed moment-curvature diagrams (see Figure 4.3), the relationships reported in Figure 4.5 point out the importance to account for joint panel deformability in the design of the FRP strengthening system.

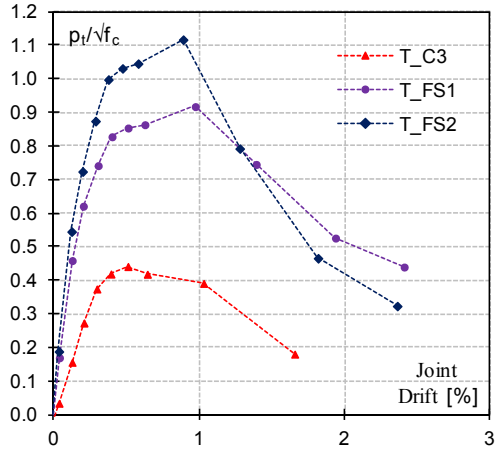

Figure 4.5 Comparisons of measured joint drifts.

Indeed, significant joint shear deformations are associated to high shear strength also in the retrofitted specimens. This deformation may strongly affect the overall seismic response of the structural system and should be properly accounted in the analysis. The assumption of rigid joint panel, commonly adopted in practical application, should be verified. To overcome this important issue, a proper design limit to the shear strength can be calibrated on available experimental tests.

CHAPTER 5
ANALYTICAL MODEL FOR FRP STRENGTHENING OF EXTERIOR JOINTS

The use of FRP systems is widespread in the seismic strengthening of beam–column joints. In spite of the demonstrated effectiveness of FRP systems increasing the seismic capacity of existing structural systems, the mechanical behavior of unconfined RC beam–column joints externally bonded with FRP systems remains a critical issue. The large number of parameters involved makes the calibration of simple and reliable formulations difficult. Several models have been proposed in recent years but, in spite of their effectiveness, they implement complex solution procedures or can be applied only to specific joint types or FRP layouts. The difficulties in interpreting the mechanical behavior of FRP reinforcement, externally bonded on RC joint panels, are strongly related to the uncertainties of the effective FRP strain. Therefore, the international guidelines and codes on the design of FRP retrofit systems currently do not provide specific formulations to account for the FRP contribution to the

shear strength of beam–column joints. Based on recent experimental observations, a new strength capacity model is proposed in this work.

5.1 PARAMETERS AFFECTING THE FRP RESPONSE

Number of parameters affect the cyclic response of RC beam-column joints strengthened with FRP systems. A summary of the main experimental findings and analytical modelling developments are reported in (Bousselham, 2010) and also summarized in the Section 2.7 of the present study. Among the existing capacity models, Bousselham (2010) suggested a simple approach to compute the shear strength increase provided by FRP strengthening systems. In particular, it considers the contribution of the FRP fibers inclined at an arbitrary angle, β, to the principal tensile stress, inclined of $90° - \theta$. Because of the main stiffness in the axial direction, the contribution of the FRP fibers can be assumed to be equal to the component of the fiber axial stress in the direction of the principal tensile stress in the joint panel. This model also accounts for the elastic modulus, E_f, of different types of fibers (carbon, CFRP, or glass, GFRP), the amount of fibers on the joint panel, ρ_f, and the substrate mechanical properties, f_c. In spite of the model effectiveness predicting the experimental joint shear strain, several criticisms can be observed in the Bousselham's design approach (2010). In particular, the comparison between the predicted FRP strains with those related to an enlarged experimental database (experimental data used by Bousselham (2010) and experimental tests reported in section 3) shows that FRP performances are, in most cases, significantly underestimated; this is because of the FRP strain limitation at 0.4% (see Figure 5.1). Such underestimation (continuous line instead of dashed line) led to reduce the potential benefits provided by the FRP in strengthening the joint shear capacity. Furthermore, the experimental strain records on FRP panel strengthening (see Section 4) showed that the FRP fiber effectiveness starts at the joint panel cracking (theoretically predictable by Eq. (2.26), see Section 2). This is in contrasts with Bousselham's hypothesis in the calculation of the effective FRP strain; indeed in the model it has been assumed that the

FRP starts to be effective at the joint panel peak strength. Several experimental tests showed the effectiveness of FRP strengthening layouts with multidirectional fibers (Antonopoulos and Triantafillou, 2003). Test results reported in section 3 and available literature studies showed that due to the limited joint panel dimensions, FRP strengthening systems are frequently subjected to end debonding (Ghobarah and Said, 2002; Antonopoulos and Triantafillou, 2003). They also demonstrated the effectiveness of different FRP laminates anchorage solutions (e.g. FRP U-wrap or discrete steel restrain) to prevent composite end-debonding and increase the performance of the joint panel FRP strengthening.

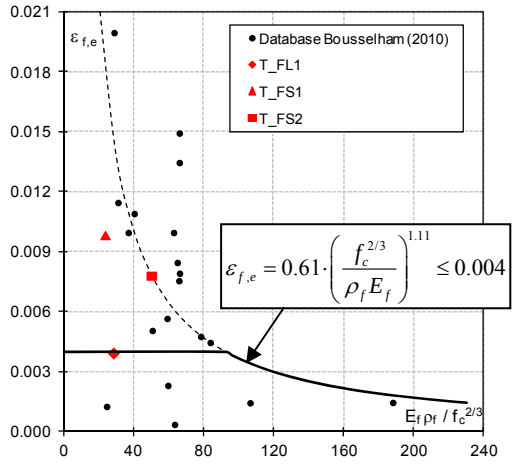

Figure 5.1 Effective FRP strains: comparison of the Bousselham's model (2010) with experimental data.

Furthermore, in a typical corner joint the presence of a beam orthogonal to the joint panel does not allow for both sides of the joint to be wrapped. In this case, the mechanical anchorage, with discrete restrains or wrapping the adjacent members, represent a suitable solution to improve the strengthening system performance. Another aspect that affects the performance of the FRP system is the presence of severe initial damage. In these conditions, experimental evidence (Antonopoulos and Triantafillou, 2003) pointed out that even if the cracks in the damaged concrete can be

repaired with advanced and innovative materials, the joint panel mechanical properties cannot be completely restored (see also Section 3). All these aspects, not directly accounted in the Bousselham's model, are typical of the FRP strengthening layouts widely adopted in field applications and recommended in recent guidelines for the use of externally bonded FRP laminates for shear strengthening (CNR-DT 200, 2013); thus they should be properly accounted for in the design formulations. In developing simple and reliable models for FRP strengthened beam–column joints, the nonlinearities associated with concrete core mechanical behavior and the high variability of the effective strains of the FRP strengthening system must be considered. The same aspects were identified as critical by Triantafillou (1998) and Khalifa et al. (1998) in the developing of design models for the shear strengthening of RC beams. They also pointed out that, due to concentration of stresses, the FRP systems may fail at stress levels far below their ultimate capacity. To account for this criticism, they proposed an experimental calibration of the effective FRP strains, back calculated from experimental tests. The data were then statistically fitted to obtain a theoretical formulation. A similar approach was adopted by Bousselham (2010) to estimate the strength increase of the FRP system in the retrofit of poorly detailed corner joints. However, to better correlate experimental results and predictions, it was then suggested that the effective FRP strain, $\varepsilon_{f,e}$, is limited to 0.4%, which is much lower than the effective strain experimentally recorded. This is especially true in cases where anchorage systems are used to prevent FRP end-debonding. This limit, also reported in (CNR-DT 200, 2013), is commonly adopted to preserve the concrete integrity in cases when the RC member is confined by externally bonded FRP systems. It does not seem to be appropriate for member that are governed by shear (e.g. experimental evidences are clearly showed in Akguzel and Pampanin (2010) and in Section 4). Furthermore, advanced mechanical formulations for RC members subjected to shear validated on extensive experimental programs (the Modified Compression Field Theory – MCFT,(Vecchio and Collins, 1986)) demonstrated that the high shear

stresses can be carried with large shear cracks if there is sufficient reinforcement to guarantee the equilibrium conditions.

5.2 PROPOSED ANALYTICAL MODEL

The perimetral frames have different types of joints, interior (X) joints or (T-shaped) corner joints. The different actions and boundary conditions make the mechanical behavior of these joints substantially different. Because of the lower confinement and the more complex stress field related to the longitudinal reinforcement end anchorage, the corner joints are commonly weaker than the interior ones. In this section, a strength capacity model to predict the shear capacity increase of corner beam–column joints strengthened by using FRP laminates is presented. The model is validated on a large database of experimental tests subjected to a plane load pattern consisting of reverse cyclic actions representative of severe earthquakes. Although Akguzel and Pampanin (2010) demonstrated the influence of the axial load variation and bidirectional cyclic loads on the performance of the FRP systems, further experimental tests are needed to quantify these effects. As a result of experimental evidence and theoretical concerns reported in the previous sections, several assumptions are made: (i) the principal tensile stress approach is adopted, Priestley (1997), summarized in Section 2.5.1; (ii) the FRP strengthening system, inclined at an angle β with respect to the beam axis, contributes to the principal tensile stress with the component inclined at 90°– θ (this hypothesis is in compliance with Bousselham (2010) and CNR DT-200 R1 (2013)); (iii) in analogy with the Modified Compression Field Theory (Vecchio and Collins, 1986), the FRP fibers are assumed to provide a similar contribution as the internal steel reinforcement, the inclination of principal stresses at the peak strength is assumed variable as a function of the stress field. Based on these assumptions, the total principal tensile stress, $p_{t,tot}$, in the FRP strengthened joint panel can be computed as the sum of the concrete contribution, $p_{t,c}$, and the FRP contribution, $p_{t,f}$ (Eq. (5.1) and Figure 5.2):

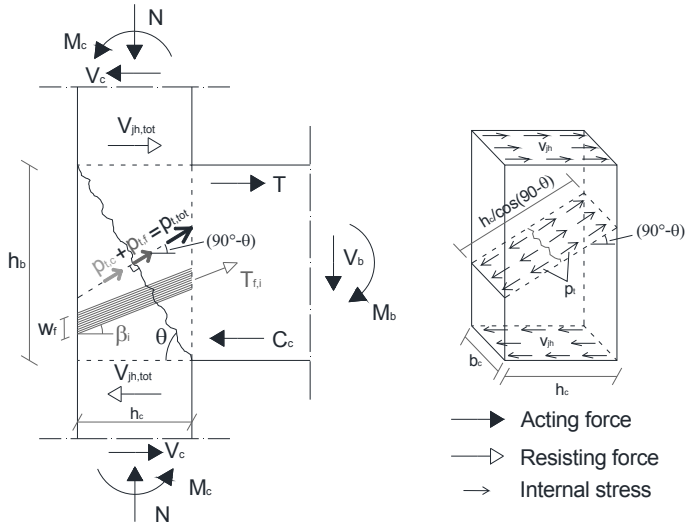

(a) (b)

Figure 5.2 Schematic illustration of the proposed model: actions on the joint panel (a) and internal stresses (b).

$$p_{t,tot} = p_{t,c} + p_{t,f} \tag{5.1}$$

The concrete contribution, $p_{t,c}$, can be accurately estimated by Eq. (2.26) with k equal to 0.29 for deformed longitudinal bars (0.20 for smooth bars). The FRP contribution, $p_{t,f}$, can be estimated as the sum of the contributions of the fibers in the different directions. In particular, the contribution in a generic direction can be derived from the tension force in the FRP system:

$$T_{f,i} = A_{f,i} \cdot f_{f,e} \tag{5.2}$$

where $A_{f,i}$ is the total FRP area in the generic direction β_i (Figure 5.2a) and $f_{f,e}$ the effective tensile stress in the FRP fibers given by the product of the FRP Young's Modulus, E_f, and the effective FRP strain, $\varepsilon_{f,e}$. The FRP strengthening area in the direction β_i should take into account for the presence of the beam orthogonal to the joint panel, and of the FRP strengthening layout (i.e. continuous laminates or strips). These parameters can be considered by computing the total FRP area as:

$$A_{f,i} = n_s \cdot n_l \cdot t_f \cdot b_f \tag{5.3}$$

In Eq. (5.3) n_s represents the number of joint panel sides strengthened in shear with FRP systems in the plane of the load (1 or 2 sides, see Figure 5.3), n_l is the number of FRP layers, t_f is the equivalent thickness of the FRP reinforcement (dry fibers only), and b_f is the width of the FRP sheet, which can be computed according to Eq. (5.4), depending on the fiber inclination, see Figure 5.4a and b):

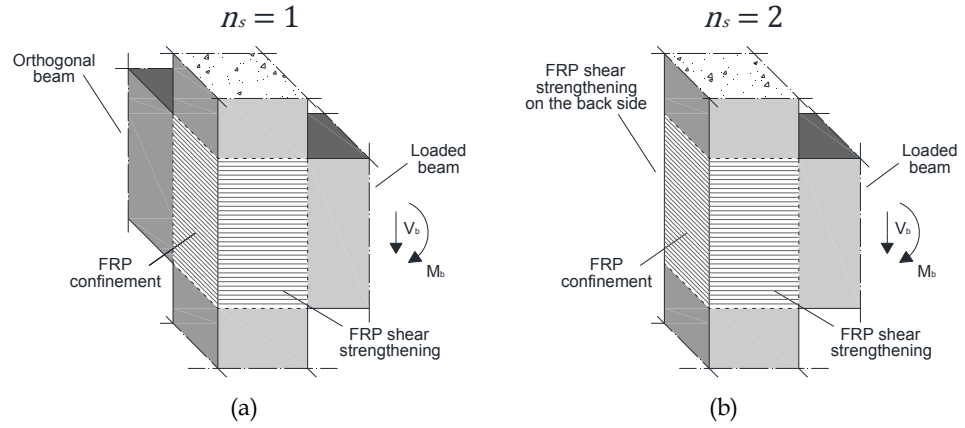

Figure 5.3 Joint panel sides strengthened in shear with FRP: one side (n_s =1) (a); and two sides (n_s =2) (b).

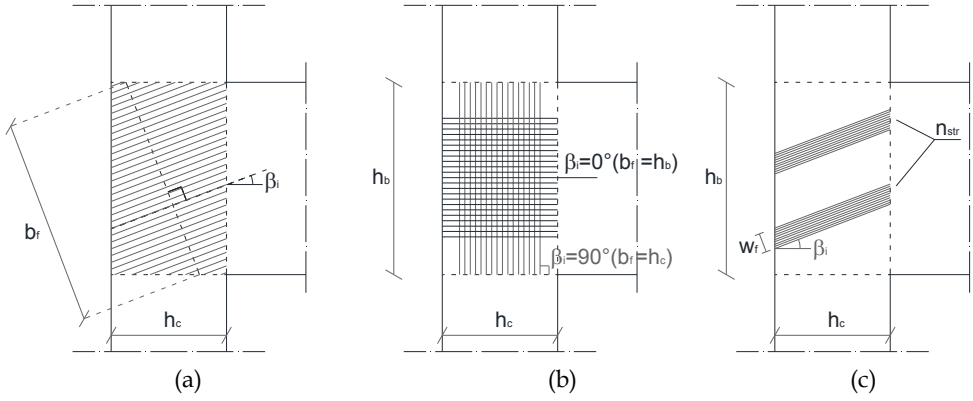

Figure 5.4 Joint panel FRP strengthening, definition of b_f : continuous fabric in a generic direction (a), continuous fabric in the direction of beam or column axis (b) FRP strips in a generic direction (c).

$$\begin{cases} b_f = h_b / \cos\beta & \text{for } \beta < \theta \\ b_f = h_c / \sin\beta & \text{for } \beta \geq \theta \end{cases} \tag{5.4}$$

In the case of discontinuous FRP reinforcements (i.e. strips), b_f can be computed by Eq. (5.5):

$$\begin{cases} b_f = \left(w_f \cdot n_{str}\right)^2 \cos\beta / h_b & \text{for } \beta < \theta \\ b_f = \left(w_f \cdot n_{str}\right)^2 \sin\beta / h_c & \text{for } \beta \geq \theta \end{cases} \tag{5.5}$$

where w_f is the strip width and n_{str} is the number of strips on the joint panel (see Figure 5.4c). Therefore, the maximum increase of the principal tensile stress, $p_{t,f,i}$, provided by the amount of fiber $A_{f,i}$, in a generic direction can be obtained dividing the component of tension force by the cross section of the concrete core inclined at 90°–θ (see Figure 5.2):

$$p_{t,f,i} = \frac{T_{f,i} \cdot \cos\left(90° - \theta - \beta_i\right)}{b_c \cdot \dfrac{h_c}{\cos\left(90° - \theta\right)}} = \frac{A_{f,i} \cdot f_{f,e} \cdot \sin\left(\theta + \beta_i\right)}{b_c \cdot \dfrac{h_c}{\sin\theta}} = \frac{A_{f,i} \cdot E_{f,i} \cdot \varepsilon_{f,e} \cdot \sin\left(\theta + \beta_i\right)}{b_c \cdot \dfrac{h_c}{\sin\theta}} \tag{5.6}$$

In the case of FRP strengthening systems with fibers in multiple directions, the proposed model can be applied considering the sum of the contributions $p_{t,f,i}$ of the fibers in the n-different inclinations β_i, as reported in Eq. (5.7).

$$p_{t,f} = \sum_{i=1}^{n} p_{t,f,i} \tag{5.7}$$

and defining the equivalent FRP area on the joint panel as:

$$A_{f,eq} = \sum_{i=1}^{n} A_{f,i} \cdot \sin\left(\theta + \beta_i\right) \tag{5.8}$$

Eq. (5.7) can be modified as following:

$$p_{t,f} = \frac{A_{f,eq} \cdot E_f \cdot \varepsilon_{f,e}}{b_c \cdot \frac{h_c}{sin\theta}} \tag{5.9}$$

A further simplification of the proposed model can be achieved assuming fixed inclinations of the FRP strengthening system. In field applications, the FRP fibers are generally applied in the horizontal and/or vertical direction or in multiple directions in the case of multi-axial fabrics (0°, 90°, ±45°). Thus, in order to simplify the calculation of the equivalent FRP area, $A_{f,eq}$, several equations have been developed for the most common applications. Uniaxial fabric with fibers in the direction of beam axis (0°) or column axis (90°):

$$\begin{cases} A_{f,eq} = n_l \cdot n_s \cdot t_f \cdot h_b \cdot sin\theta & \text{for } \beta = 0° \\ A_{f,eq} = n_l \cdot n_s \cdot t_f \cdot h_c \cdot cos\theta & \text{for } \beta = 90° \end{cases} \tag{5.10}$$

Bidirectional fabric with fibers in the direction of beam and column axes (0°, 90°):

$$A_{f,eq} = n_l \cdot n_s \cdot t_f \cdot h_c \cdot cos\theta \cdot \left(1 + tan^2\theta\right) \tag{5.11}$$

Quadriaxial fabric with any fibers in the direction of beam (0°) and column (90°) axes and ±45°:

$$A_{f,eq} = n_l \cdot n_s \cdot t_f \cdot h_c \cdot cos\theta \cdot \left(1 + tan\theta + 2tan^2\theta\right) \tag{5.12}$$

Once the total principal tensile stress has been calculated $p_{t,tot} = p_{t,c} + p_{t,f}$, the Mohr's circle approach can be used to derive the joint horizontal shear stress, as reported in Eq. (5.13).

$$v_{jh} = p_{t,tot} \cdot \sqrt{1 + \frac{f_a}{p_{t,tot}}} \tag{5.13}$$

Finally, the joint panel shear strength can be computed by Eq. (5.14):

$$V_{jh} = v_{jh} \cdot A_{col} = v_{jh} \cdot b_c \cdot h_c \tag{5.14}$$

with the column gross area, A_{col}, assumed equal to the joint area (Priestley, 1997). This simplified assumption obviously fails in cases of joints with thin beams. Further experimental tests are required in order to quantify the effectiveness of the FRP strengthening in these cases. In the described process the only unknown needed to compute the increase of the principal tensile stress is the effective FRP strain $\varepsilon_{f,e}$.

5.3 EFFECTIVE FRP STRAIN

The prediction of the effective strain of fibers represents a critical issue in the design of the FRP strengthening externally bonded to RC members. The debonding phenomena and the stress concentrations on the cracks may result in the failure of FRP reinforcement, even in cases when stress levels are much lower than the ultimate strength. Furthermore, the available analytical formulations for FRP debonding are, commonly, calibrated on experimental tests not representative of structural members with complex and variable stress fields found in beam–column joints. The calibration of a new expression suitable to compute the effective FRP strain is needed; to this end, a specific set of experimental data on beam–column joints have been analyzed. A similar approach has been adopted to calibrate the FRP effective strain for the shear strengthening of beams (Khalifa et al., 1998; Triantafillou, 1998) and beam–column joints (Bousselham, 2010). In this section a more refined calibration of the effective FRP strain based on a large database of corner beam–column joints externally bonded with different FRP systems is presented. The experimental data have been selected according to the following criteria: (i) tests on corner joints, with or without the transverse beam orthogonal to the load plane; (ii) static tests with cyclic actions applied at the beam or column tip along with a constant axial load on the column; (iii) tests on beam–column joints without internal transverse reinforcement; (iv) tests on specimens with column width equal to beam width; (v) tests on subassemblies with deformed bars only. At this

stage, these limitations are required in order to create a homogeneous database and have a reliable estimation of the effective FRP strain. However, due to its simple mechanical basis, this model can be properly modified for FRP strengthened interior beam–column joint or subassemblies with plain bars when enough test data becomes available. Only few tests have been selected in this study to assess the model accuracy for the different joint types. The experimental tests selected with these criteria have been classified according to the specimen failure mode (see Figure 5.5).

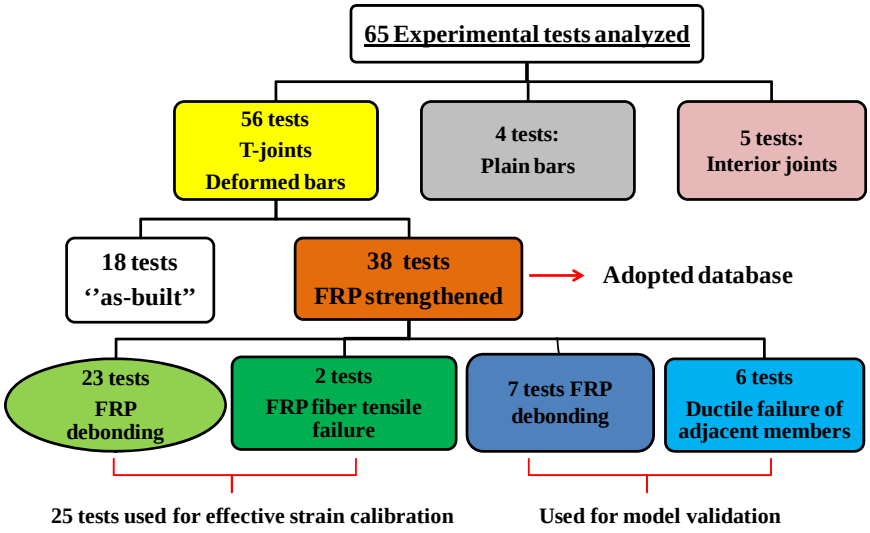

Figure 5.5 Details of the experimental tests selected for the database.

In addition to the typical FRP failure modes (debonding or fiber tensile failure), the tests in which the FRP strengthening allowed for a more favorable ductile failure (i.e. beam or column flexural yielding) have been also included. These tests can be useful to demonstrate the model effectiveness where the FRP strengthening allows the joint shear failure to be prevented. A database of 31 tests on corner joints strengthened with externally bonded FRP systems is presented in Table 5.1: 25 tests exhibited FRP failure (i.e. Fiber Debonding (FD) or Fiber tensile Failure (FF)); 7and for

Table 5.1. Database of experimental tests on corner joints retrofitted with FRP systems.

Subassembly characteristics				Member dimensions			FRP strengthening properties							Experimentally determined parameters			
Test ID [a]	Failure [b]	f_c (MPa)	N (kN)	b_c (mm)	h_c (mm)	h_b (mm)	Fibers	E_f (GPA)	β (°)	t_f (mm)	n_l	n_s	FRP charact.[c]	v_{jh}^{exp} (kN)	θ^{exp} (°)	$A_{f,eq}$ (mm²)	$\varepsilon_{f,e}^{exp}$
GHO (T1R)	FD	30.8	600	250	400	400	GFRP	72.4	0 (90)	0.312	1	2	M - C	6.17	58.0	344	0.0071
GHO (T2R)	BH	30.8	300	250	400	400	GFRP	72.4	0 (90)	0.312	2	2	M - C	4.69	53.9	698	-
GHO (T9)	BH	30.8	600	250	400	400	GFRP	72.4	±45	0.359	3	2	M - C	4.69	61.3	1169	-
EL-AM (TR1)	FD	43.5	600	250	400	400	GFRP	72.4	0 (90)	0.312	2	2	M - C	5.89	58.5	686	0.0027
EL-AM (TR2)	FD	39.5	600	250	400	400	GFRP	72.4	0 (90)	0.312	2	2	M - C	6.43	57.5	689	0.0036
ANT (S33)	FD	26.0	46	200	200	300	CFRP	150	0 (90)	1.05	1	2	3+(3) S	3.17	50.1	68	0.0060
ANT (S63)	FD	24.2	46	200	200	300	CFRP	150	0 (90)	1.05	1	2	6+(3) S	3.62	49.5	158	0.0037
ANT (S33L)	FD	26.3	46	200	200	300	CFRP	150	0 (90)	1.05	1	2	3+(3) S	4.01	49.1	68	0.0069
ANT (F11)	FD	22.8	46	200	200	300	CFRP	230	0 (90)	0.13	1	2	C	3.85	49.3	93	0.0048
ANT (F22)	FD	27.2	46	200	200	300	CFRP	230	0 (90)	0.13	2	2	C	4.50	48.6	186	0.0031
ANT (F21)	FD	27.0	46	200	200	300	CFRP	230	0 (90)	0.13	2 (1)	2	C	4.60	48.6	151	0.0039
ANT (F12)	FD	29.5	46	200	200	300	CFRP	230	0 (90)	0.13	1 (2)	2	C	4.00	49.1	127	0.0034
ANT (F22A)	FD	27.8	115	200	200	300	CFRP	230	0 (90)	0.13	2	2	C	5.16	52.8	187	0.0028
ANT (F22W)	FF	29.2	46	200	200	300	CFRP	230	0 (90)	0.13	2	2	M - C	5.02	48.3	186	0.0024
ANT (F22in)	FD	21.0	46	200	200	300	CFRP	230	0 (90)	0.13	2	2	I - C	3.77	49.3	186	0.0029
ANT (GL)	FD	19.5	46	200	200	300	GFRP	70	0 (90)	0.17	2.5	2	C	3.97	49.1	304	0.0054
ANT (S-F22)	FD	19.0	46	200	200	300	CFRP	230	0 (90)	0.13	2	2	C	3.97	49.1	186	0.0027
ANT (T-F33)	FD	26.0	46	200	200	300	CFRP	230	0 (90)	0.13	3	1	C	4.00	49.1	140	0.0033
ANT (T-F22S2)	FD	22.0	46	200	200	300	CFRP	230	0 (90)	0.13	2	1	2 S	3.60	49.5	93	0.0048
GHO2 (T-SB8)	BH	22.5	600	250	400	400	GFRP	72.4	0 (90)	0.312 (0.353)	3 (1)	2	M - C	4.51	61.8	793	-
GHO2 (T-SB7)	BH	22.5	600	250	400	400	GFRP	72.4	0 (90)	0.312 (0.353)	3 (1)	2	M - C	4.51	61.8	793	-
PAR (U.S.2-RC2U1)	FD	25.0	700	300	300	500	CFRP	240	0 (90)	0.176	1 (2)	2	M - C	7.00	59.5	259	0.0030
PAR (U.S.3-RC3U3)	FD	25.0	700	300	300	500	CFRP	240	0 (90)	0.176	3	2	M - C	7.06	59.4	616	0.0013
PAR (U.S.4-RC3U3)	FD	25.0	350	300	300	500	CFRP	240	0 (90)	0.176	3	2	M - C	7.29	52.5	612	0.0021
ALS (ECFRP)	FD	33.4	321	160	300	350	CFRP	230	0	0.37	1	2	M - C	6.74	58.2	220	0.0019
ALS (EGFRP)	FF	33.4	321	160	300	350	GFRP	72.4	0	0.359	2	2	M - C	6.67	58.3	428	0.0030
DEL (T_RFL1)	FD	16.38	295	300	300	500	CFRP	230	0 (±45) (90)	0.053	1	1	M – I - C	3.69	57.0	68	0.0056
DEL (T_FL1)	FD	13.5	243	300	300	500	CFRP	230	0 (±45) (90)	0.053	1	1	M - C	3.15	56.6	68	0.0047
DEL (T_FS1)	CH	17.7	319	300	300	500	CFRP	230	0 (±45) (90)	0.053	1	1	M - C	3.53	58.3	67	-
DEL (T_FS2)	CH	16.4	295	300	300	500	CFRP	230	0 (±45) (90)	0.053	2	1	M - C	3.63	57.1	135	-
REA (J-02)	FD	19.5	300	300	300	400	CFRP	390	0	0.22	2	2	C	3.73	57.0	295	0.0011

[a] GHO= (Ghobarah and Said, 2002), EL-AM= (El-Amoury and Ghobarah, 2002), ANT= (Antonopoulos and Triantafillou, 2003), GHO2= (Ghobarah and El-Amoury, 2005), PAR= (Parvin et al., 2010), ALS= (Al-Salloum et al., 2011), Del Vecchio (tests in Section 3); REA= (Realfonzo et al., 2014).

[b] FD= FRP debonding, FF= FRP tensile failure, BH= Beam plastic hinge, CH= Column plastic hinge.

[c] FRP strengthening: M = Mechanical anchorage, I = Initial damage, S = Strips, number = number of Strips, C = Continuous fabric

Note: the number in the brackets and are referred to FRP layouts with multiple inclinations and the related properties.

6 tests the peak strength was achieved with plastic hinge formed on the beam or column end (BH or CH, respectively).

The mean concrete compressive strength, f_c, of the selected beam–column joints is in the range 13.5–43.5 MPa. The subassemblies are characterized by various member dimensions, b_c, h_c, h_b, and subjected to cyclic tests with axial load ratios in the range $\nu = N/(A_{col} \cdot f_c) = 0.04–0.31$. The FRP strengthening schemes include: carbon (CFRP) or glass fibers (GFRP) with elastic modulus, E_f, in the range 72–390 MPa; continuous or discontinuous laminates (i.e. strips) with fibers oriented in one or multiple directions (0°, 90° or ±45°); dry thickness of FRP reinforcement, t_f, ranging between 0.053 and 1.05 mm; number of layers, n_l, between 1 and 3; FRP laminates applied on 1 or 2 sides, n_s, of the joint panel with or without mechanical anchorages (M.A.). In some cases the FRP strengthening has been applied to the specimens after damage by a previous test (Initial Damage, I.D.). A summary of the subassembly characteristics, member dimensions and FRP strengthening properties is reported in Table 5.1. The experimental data have been used to derive the joint shear stress at the peak strength, v_{jh}^{exp}, the inclination of the principal compressive stress, θ^{exp}, and the FRP equivalent area, $A_{f,eq}$. These data are required to back calculate the effective FRP strain, $\varepsilon_{f,e}^{exp}$ reported in the last column of Table 5.1. The experimental joint shear stress can be derived from the maximum recorded shear force on the beam V_b (see Figure 5.2) with Eq. (5.15).

$$v_{jh}^{exp} = \frac{T - V_c}{b_c \cdot h_c} = \frac{V_b \left[\frac{l_b}{d_b} - \frac{l_b}{l_c - h_b} \right]}{b_c \cdot h_c} \tag{5.15}$$

where l_b is the beam length measured from the column face to the actuator; l_c is the total column height and d_b is the beam internal lever arm (assumed for simplicity equal to $0.75h_b$). Note that in case of experiments with the horizontal load applied at column tip, the beam shear can be derived from the equilibrium relation $V_b = 2 \cdot M_c / l_b = V_c \cdot (l_c - h_b)/l_b$.

Once that the joint shear is known, the inclination of the principal compressive stress, θ^{exp}, and the principal tensile stress, $p_{t,f}^{exp}$, can be calculated from the effective stress field acting in the joint core with Eqs. (5.16) and (5.13) derived from the Mohr's circle.

$$\theta^{exp} = \frac{1}{2}\left[\pi - atan\left(\frac{v_{jh}^{exp}}{f_a/2}\right)\right] \tag{5.16}$$

This angle can be used to compute the equivalent FRP area, $A_{f,eq}$, on the joint panel by Eq. (5.8). Once that $A_{f,eq}$ has been determined, the effective FRP strain can be computed by equating the experimentally determined principal tensile stress, $p_{t,f}^{exp}$, to Eq. (5.9) and back calculating $\varepsilon_{f,e}$ with Eq. (5.17).

$$\varepsilon_{f,e}^{exp} = \frac{p_{t,f}^{exp} \cdot b_c \cdot h_c}{A_{f,eq} \cdot E_f \cdot sin\theta} \tag{5.17}$$

The effect of mechanical anchorage on the performance of the FRP system has been demonstrated through experimental tests (see also Section 4). The anchorage of the joint panel FRP strengthening, by wrapping the adjacent members or by discrete restrains, significantly increases the member performance preventing the fiber end-debonding. The fiber strains of the strengthening system can be significantly higher and a different failure mode, fiber tensile failure or intermediate debonding, may occur (Antonopoulos and Triantafillou, 2002). The influence of the mechanical anchorage has been considered with a numerical coefficient, $C_{M.A.}$, based on the experimental evidence and theoretical considerations. In particular, specimens ANT (F22) and ANT (F22W) differ only because of the mechanical anchorages and the experiments showed a significant increase of the shear strength. The effect of the mechanical anchorages on the fiber strain, has been set in order to match the $\varepsilon_{f,e}$ of the anchored specimen (F22) with the unanchored one (F22W). In this case, the effective FRP strain of the anchored specimen has been reduced from a factor of 1.5, that represents

the contribution of the mechanical anchorages to the effective strain. Further experimental observations confirmed the magnitude of this coefficient. The comparison between the test results reported in Section 4 showed that the improved end anchorage of the joint panel strengthening system can increase the effective FRP strain to 50%. The same increase in the magnitude of the fiber strain can be observed in the experimental tests by Khalifa and Nanni (1998) on the shear strengthening of beams with FRP systems with and without end anchorages. The assumption on the magnitude of this coefficient is also in compliance with guidelines provisions (CNR-DT 200, 2013) that suggest neglecting the end-debonding and consider the FRP system as fully wrapped. This results in an increase of the effective FRP strain by even more than 1.5. The same approach was adopted for the FRP systems applied to joint subassemblies that were subjected to an initial damage (I.D.). In this case a reduction coefficient $C_{I.D.}$ = 0.8 was set by comparing the experiments ANT (F22) with ANT (F22in). The adopted value is in compliance with the experimental tests on beam column joints recently tested with and without initial damage (see Section 3). In particular, the repair techniques considered in this study only involve a limited portion of the joint panel. The cracks filling and cover replacement is essentially aimed at restoring the joint panel initial capacity. These techniques can be identified as ''light repair'' because they aim at restoring the joint panel initial capacity. Other repair techniques consisting in a substantial replacement of the joint core with high performance materials are herein not considered and, thus, the proposed model cannot be extended to these applications. Once the effective FRP strain has been determined a specific study has been conducted to identify the independent variables. The selection of the parameters that relate to the effective strain was based on existing formulations for FRP debonding and experimental evidence on beam–column joints. In the case of the shear strengthening of beams with FRP systems, Triantafillou (1998) observed that the effective strain is a function of the axial rigidity of the FRP sheet ($\rho_f E_f$). Khalifa et al. (2000) adopted a bond based approach and, including the effects of the concrete strength, proposed to relate the effective strain to the ratio $f_c^{2/3}/(t_f \cdot$

E_f). A similar ratio was adopted in this study because of the high influence of the concrete substrate mechanical properties on the FRP strengthening performance (see Section 4). However, due to the high variability of the FRP strengthening layout and the use of fiber in multiple directions, a more representative parameter, such as the equivalent FRP area on the joint panel ($A_{f,eq}$), has been adopted in place of t_f. In order to evaluate the sensitivity of the effective FRP strain to the selected mechanical and geometrical parameters, a statistical study based on the analysis of the linear correlation coefficient have been carried out. The effective FRP strain depends on several variables, outlined in the previous sections. The correlation of these variables with the FRP effective strain has been investigated evaluating the linear correlation coefficient expressed by:

$$\rho_{xy} = \frac{1}{n}\sum_{i=1}^{n} z_{x_i} \cdot z_{y_i} \tag{5.18}$$

Where:

- n is the number of available experimental data;
- z_{xi} is the scatter between the selected independent variable and the mean value normalized by the Root Mean Square (RMS):

$$z_{x_i} = \frac{x_i - \overline{x}}{SQM} \tag{5.19}$$

- z_{yi} is the scatter between the reference variable ($\varepsilon_{f,e}^{exp}$) and the mean value normalized by the Root Mean Square (RMS):

$$z_{y_i} = \frac{y_i - \overline{y}}{SQM} \tag{5.20}$$

The linear correlation coefficients computed for the selected variables are reported in Table 5.2 and Figure 5.6.

Table 5.2. Statistical parameters adopted in the variable selection.

Variable	X_i	Mean	RMS	ρ_{xy}
Concrete compressive	f_c	0.00369	0.0015762	-0.17
Axial load	N	229.72	232.04371	-0.21
Fiber elastic modulus	E_f	196384	75312.722	-0.48
FRP area	$A_{f,eq}$	256.72	193.9867	-0.42
FRP axial stiffness	$A_{f,eq}E_f$	7452.85	7429.7794	-0.32
Proposed ratio	$A_{f,eq}E_f/f_c^{2/3}$	5245473	4483214.4	-0.68

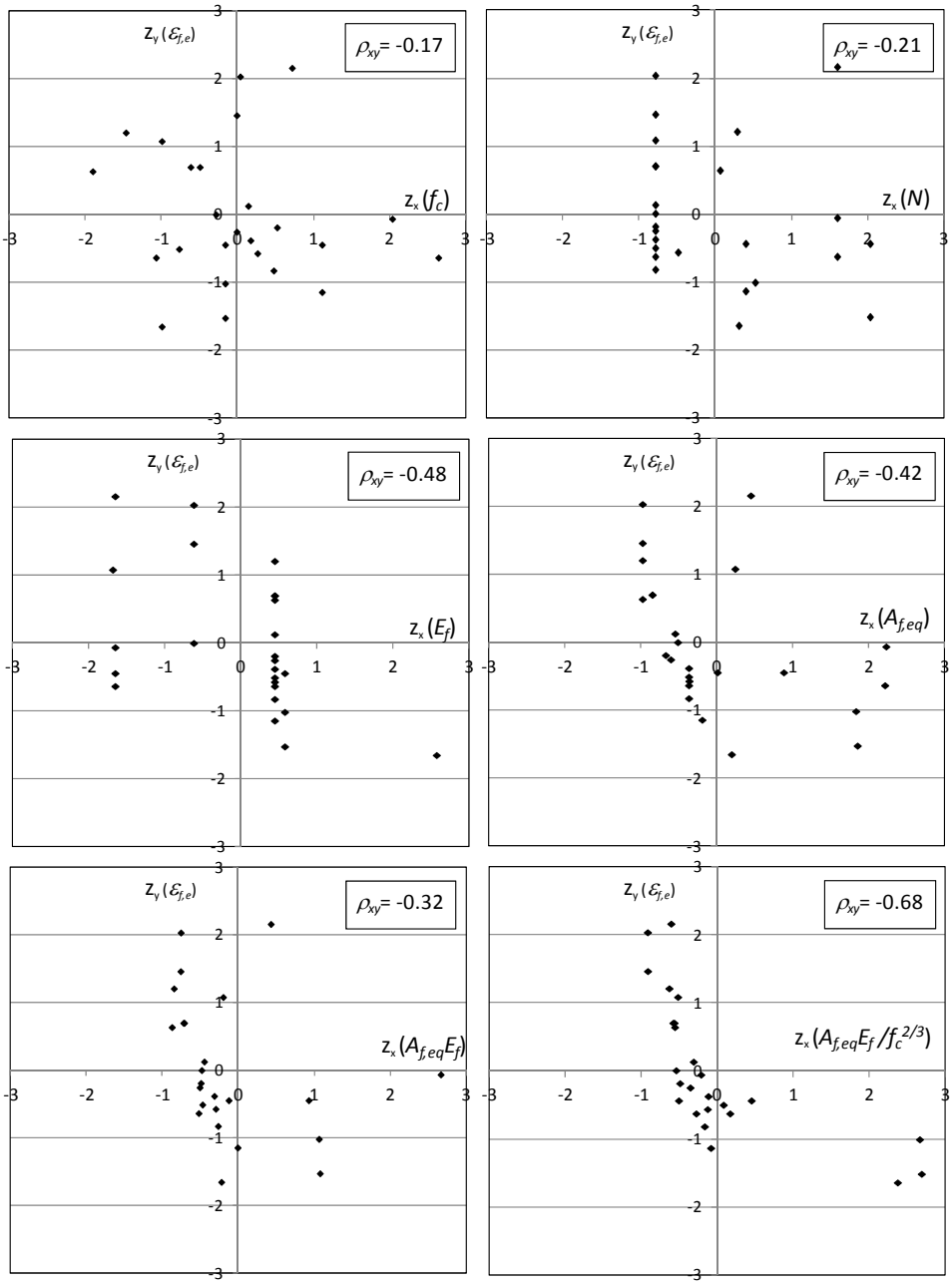

Figure 5.6 Dependency of the effective FRP strain and linear correlation coefficients.

The ratio $(A_{f,eq}E_f)/f_c^{2/3}$ has the strongest correlation with the FRP effective strain and it has been selected as independent variable for the fitting of experimental data. With this purpose, the effective FRP strain is plotted against the ratio $(A_{f,eq}E_f)/f_c^{2/3}$ in Figure 5.7 for the 25 specimens that exhibit a failure mode in the FRP strengthening system (FD or FF)

A power-type expression is used as a best fit to the data in Figure 5.7. Including the two numerical coefficients adopted to account for the influence of the mechanical anchorages and initial damage, the final expression for the FRP effective strain is showed in Eq. (5.20).

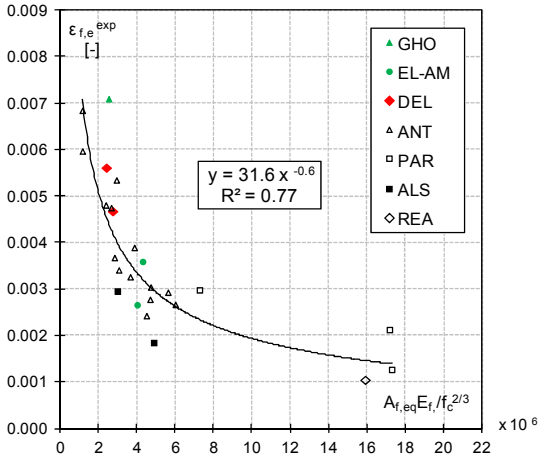

Figure 5.7 Effective FRP strains in terms of $A_{f,eq}E_f/f_c^{2/3}$.

$$\varepsilon_{f,e} = 31.6 \cdot C_{I.D.} \cdot C_{M.A.} \cdot \left(\frac{f_c^{2/3}}{A_{f,eq} \cdot E_f} \right)^{0.6} \tag{5.20}$$

with $C_{I.D.}$ = 1.0 in case of undamaged joint panel or 0.8 if the FRP strengthening system is applied on a cracked joint panel. The coefficient $C_{M.A.}$ = 1.0 in the case that the FRP fibers are extended on the adjacent beams or columns without mechanical anchorages or 1.5 if the joint panel FRP strengthening is mechanically anchored at the ends. The good statistical correlation (R^2 = 0.77) between the data and the variables selected for the regression illustrate that the $A_{f,eq}E_f/f_c^{2/3}$ relationship is effective.

An initial validation of the model predictions is proposed comparing the fiber effective FRP strain with the average FRP strain reported in section 4 and in available literature studies (Ghobarah and Said, 2002). The comparison, reported in Table 5.3, demonstrated the accuracy of the model in estimating the average FRP effective strain for specimens with different concrete strength and different amounts of fibers.

Table 5.3. Comparison of predicted and experimentally recorded FRP strains.

Test	fiber inclination	Exp. Record $\varepsilon_{f,e}^{exp}$	Average $\varepsilon_{f,e}^{exp}$	Pred. (Eq. 5.20) $\varepsilon_{f,e}^{pred}$	$\varepsilon_{f,e}^{exp}/\varepsilon_{f,e}^{pred}$
GHO (T9)	45°	0.0029	0.0029	0.0032	0.91
DEL (T_FL1)	0°	0.0049	0.0061	0.0065	0.94
	+45°	0.0062			
	-45°	0.0072			
DEL (T_FS1)	0°	0.0066	0.0075	0.0073	1.03
	+45°	0.0102			
	-45°	0.0057			
DEL (T_FS2)	0°	0.0050	0.0048	0.0046	1.05
	+45°	0.0066			
	-45°	0.0029			

The calibration of the proposed formulation has been performed with reference to means values of materials' mechanical properties. This formulation can be adopted to design the FRP strengthening of existing beam column joints; indeed, in the case of existing structures, the mean mechanical properties of materials are commonly adopted in the design process. In order to adopt the proposed formulation in code or guidelines design provisions, a reliability analysis is needed in order to convert the mean values of materials' mechanical properties to design values; this can be done according to the target level of structural safety established by the code. This process may be performed according to standard procedures as also recalled in EN1990 (2002) for the European area. This process, because of its specificity, is out of the scope of the present paper.

5.4 MODEL ACCURACY

To examine the accuracy of the proposed design approach, the test results selected for the model calibration are compared with the model predictions (see Table 5.4). The analytical predictions of the effective FRP strain, Eq. (5.20), have been used to compute the increase in the principal tensile stress due to the FRP strengthening, $p_{t,f}$. Summing the FRP and concrete contributions, the total principal tensile stress, $p_{t,tot}$, can be calculated and substituted in Eq. (5.13) to compute the resisting shear stress of the joint panel, v_{jh}. The analytical predictions computed with the experimentally determined inclination of the concrete compressive strut, θ_{var}, Eq. (5.16) are reported in Table 5.4; the comparison between predicted principal tensile stress, $p_{t,f}^{teor}$, or joint shear stress, v_{jh}^{teor}, and the experimental ones, $p_{t,f}^{exp}$ and v_{jh}^{exp}, are reported in (Figure 5.8a) and (Figure 5.8b), respectively.

Table 5.4. Joint shear stress predicted with the proposed model.

Test	v_{jh}^{exp} (kN)	Predictions with θvar (Eq. 5.16)					Predictions with θcost (Eq. 2.28)					
		$\varepsilon_{f,e}$	$p_{t,c}$ (MP	$p_{t,f}$ (MPa)	v_{jh} (kN)	v_{jh}/v_{jh}^{exp}	θ_{cost} (°)	$A_{f,eq}$ (mm²)	$\varepsilon_{f,e}$	$p_{t,f}$ (MPa)	v_{jh} (kN)	v_{jh}/v_{jh}^{exp}
GHO (T1R)	6.17	0.0068	1.61	1.44	5.25	0.85	45.0	353	0.0067	1.21	4.99	0.81
GHO (T2R)	4.69	0.0045	1.61	1.82	4.69	n.c.	45.0	706	0.0044	1.60	4.46	n.c.
GHO (T9)	4.69	0.0033	1.61	2.43	6.37	n.c.	45.0	1218	0.0032	1.99	5.88	n.c.
EL-AM (TR1)	5.89	0.0052	1.91	2.19	6.44	1.09	45.0	706	0.0051	1.84	6.05	1.03
EL-AM (TR2)	6.43	0.0050	1.82	2.09	6.23	0.97	45.0	706	0.0049	1.77	5.87	0.91
ANT (S33)	3.17	0.0072	1.48	1.42	3.43	1.08	56.3	66	0.0074	1.52	3.52	1.11
ANT (S63)	3.62	0.0042	1.43	1.92	3.87	1.07	56.3	164	0.0042	2.13	4.09	1.13
ANT (S33L)	4.01	0.0109	1.49	2.11	4.13	1.03	56.3	66	0.0112	2.28	4.31	1.07
ANT (F11)	3.85	0.0044	1.38	1.79	3.70	0.96	56.3	94	0.0044	1.97	3.89	1.01
ANT (F22)	4.50	0.0031	1.51	2.51	4.56	1.01	56.3	187	0.0031	2.79	4.84	1.08
ANT (F21)	4.60	0.0035	1.51	2.30	4.34	0.95	56.3	159	0.0034	2.60	4.65	1.01
ANT (F12)	4.00	0.0041	1.58	2.24	4.35	1.09	56.3	123	0.0041	2.43	4.54	1.14
ANT (F22A)	5.16	0.0031	1.53	2.69	5.47	1.06	56.3	187	0.0031	2.81	5.60	1.08
ANT (F22W)	5.02	0.0048	1.57	3.85	5.96	1.19	56.3	187	0.0048	4.30	6.42	1.28
ANT (F22in)	3.77	0.0023	1.33	1.83	3.69	0.98	56.3	187	0.0022	2.01	3.87	1.03
ANT (GL)	3.97	0.0042	1.28	1.67	3.48	0.88	56.3	306	0.0041	1.85	3.66	0.92
ANT (S-F22)	3.97	0.0027	1.26	2.19	3.99	1.01	56.3	187	0.0027	2.42	4.22	1.06
ANT (T-F33)	4.00	0.0036	1.48	2.21	4.23	1.06	56.3	141	0.0036	2.44	4.46	1.11
ANT (T-F22S2)	3.60	0.0047	1.36	1.68	3.57	0.99	56.3	94	0.0047	1.83	3.73	1.03
GHO2 (T-SB8)	4.51	0.0036	1.38	1.84	5.45	n.c.	45.0	729	0.0038	1.43	4.97	n.c.
GHO2 (T-SB7)	4.51	0.0036	1.38	1.84	5.45	n.c.	45.0	729	0.0038	1.43	4.97	n.c.
PAR (U.S.2-RC2U1)	7.00	0.0036	1.45	2.15	6.41	0.91	59.0	260	0.0036	2.15	6.40	0.91
PAR (U.S.3-RC3U3)	7.06	0.0022	1.45	3.04	7.43	1.05	59.0	616	0.0022	3.03	7.41	1.05
PAR (U.S.4-RC3U3)	7.29	0.0022	1.45	2.80	5.88	0.81	59.0	616	0.0022	3.03	6.13	0.84
ALS (ECFRP)	6.74	0.0046	1.68	4.12	8.51	1.26	49.4	197	0.0049	3.52	7.86	1.17
ALS (EGFRP)	6.67	0.0062	1.68	3.39	7.71	1.16	49.4	382	0.0066	2.89	7.17	1.07
DEL (T_RFL1)	3.69	0.0056	1.17	0.81	3.23	1.14	59.0	67	0.0056	0.83	3.25	1.11
DEL (T_FL1)	3.15	0.0065	1.07	0.94	3.07	0.88	59.0	67	0.0065	0.96	3.09	0.88
DEL (T_FS1)	3.53	0.0073	1.22	1.06	3.65	0.97	59.0	67	0.0073	1.07	3.65	0.98
DEL (T_FS2)	3.63	0.0046	1.17	1.34	3.82	n.c.	59.0	135	0.0046	1.37	3.85	n.c.
REA (J-02)	3.73	0.0015	1.28	1.62	4.25	n.c.	53.1	282	0.0016	1.52	4.14	n.c.
					Mean	**1.02**					**Mean**	**1.03**
					CoV	**0.11**					**CoV**	**0.10**

n.c. are the tests that exhibited a flexural failure of the adjacent members (BH or CH) and the ratio v_{jh}/v_{jh}^{exp} has not been computed.

The proposed design approach gives an acceptable estimation of the experimentally observed contribution of the FRP systems to the principal tensile stress (Figure 5.8a). Furthermore, comparing the results in terms of joint panel shear stress (Figure 5.8b), the proposed model is even better, with a mean value very close to the 1.0 and a reduced coefficient of variation. These comparisons demonstrate the reliability of the proposed model in predicting the shear strength of joint panel strengthened with a various FRP layouts. Furthermore the heterogeneous distribution of the available test data, in terms of joint panel shear stress, validates the model application for a wide range of cases.

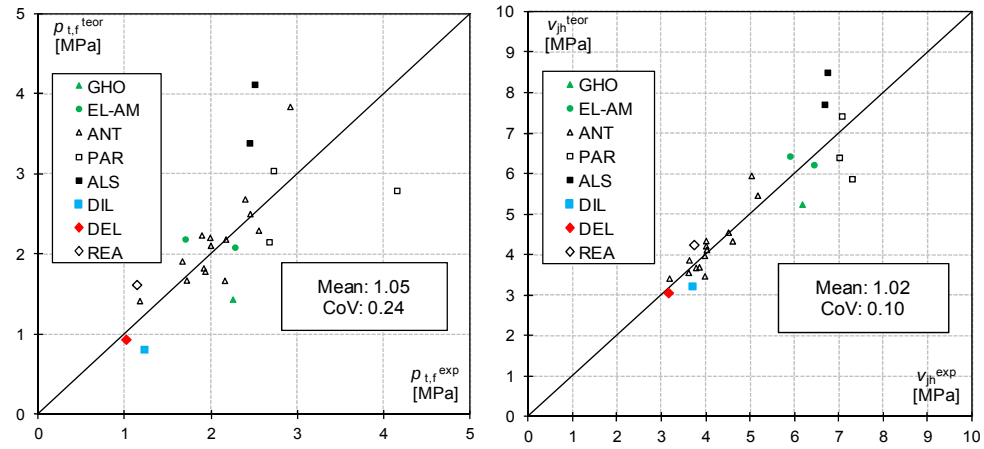

(a) (b)

Figure 5.8 Comparison of predictions and experimental results in terms of: FRP contribution to the principal tensile stress (a); joint panel shear stress (b).

5.5 MODEL SIMPLIFICATION

Even though the accuracy of the proposed analytical model has been demonstrated at different levels showing a good match with various database of experimental results, further considerations are required in order to make the model suitable for practical applications. In fact, the model formulation, the experimental calibration and the final comparison has been performed by calculating the inclinations of the cracks with the

rigorous Mohr's circle approach. However, this approach may not be suitable for practical purpose because it is necessary to iterate since both the crack inclination and the joint shear stress are not known. In the case of joint panels strengthened with FRP systems, the assumption that the direction of the cracks depends only on joint panel geometry (Eq. (2.28)) may not be accurate. This is because it was validated for joint panel without any kind of reinforcements. Although a corner to corner crack was observed on joint panels strengthened with FRP system in recent experimental tests (see Section 3), Eq. (2.28) should be widely validated for different FRP layouts representatives of real applications in order to quantify the level of accuracy related to this approximation. By comparing the analytical predictions and the experimental results for the tests in the database (see Table 5.4), it can be assumed that the use of Eq. (2.28) (i.e. a constant value of θ) for beam–column joints strengthened with various FRP layouts do not affect the accuracy of the proposed model. As reported in Table 5.4, both the increase in the principal tensile stress and in the joint shear stress are estimated with the same level of accuracy of the rigorous approach with variable inclination of the cracks.

5.6 CAPACITY DESIGN APPROACH

The main goal of the FRP strengthening of joint panels is to avoid the shear failure of the joint, commonly associated to a sudden strength and stiffness degradation, and to allow flexural yielding of adjacent members. In order to demonstrate the accuracy of the proposed model to assess changes in the failure sequence, several experimental tests on joint subassemblies strengthened with FRP systems that allow the joint shear failure to be prevented leading to a flexural failure mode, have been included in the database. These tests were not used for the model calibration but can be used to show the ability of the proposed procedure to predict the shear strength of the joint panel such that it is higher than that required for flexural yielding. This check can be performed by comparing the predicted

joint shear stress v_{jh} and the joint shear stress associated to the flexural yielding, $v_{jh}(M_y)$ (see Table 5.5).

Table 5.5. Comparison between shear and flexural capacity of beam-column joint subassemblies.

		θ_{var} (Eq. 5.16)	θ_{cost} (Eq. 2.28)	
Test	Failure	v_{jh} (kN)	v_{jh} (kN)	$v_{jh}(M_y)$[a] (kN)
GHO (T2R)	BH	4.69	4.74	4.69
GHO (T9)	BH	6.37	5.88	4.69
GHO2 (T-SB8)	BH	5.45	4.97	4.51
GHO2 (T-SB7)	BH	5.45	4.97	4.51
DEL (T_FS1)	CH	3.65	3.65	3.53
DEL (T_FS2)	CH	3.82	3.85	3.63

[a] $v_{jh}(M_y)$ is the joint panel shear stress at the flexural yielding of adjacent members.

In the case of joint subassemblies characterized by the flexural yielding of adjacent members (BH or CH), the predicted joint shear strength is always higher than that associated to the flexural yielding. Therefore, the proposed model can be employed to design the proper amount of FRP reinforcement necessary to prevent the joint panel shear failure and allows for flexural yielding of adjacent structural members. The design procedure for FRP strengthening of existing deficient corner beam–column joint is illustrated in the next paragraph.

5.7 MODEL VALIDATION

In this paragraph the accuracy of the proposed analytical model is assessed comparing the analytical predictions in terms of joint shear stress and effective FRP strain with available experimental results not adopted in the model calibration (see Figure 5.5).

Table 5.6. Database of experimental tests for model validation.

Subassembly characteristics					Member dimensions										Predictions with θ_{cost} (Eq. 2.28)							
Test ID[a]	Joint Type[b]	Failure[c]	f_c (MPa)	N (kN)	b_c (mm)	h_c (mm)	h_b (mm)	Fibers	E_f (GPa)	β (°)	t_f (mm)	n_l	n_s	FRP-charact.[d]	θ_{cost} (°)	$A_{f,eq}$ (mm²)	$\varepsilon_{f,e}$	$p_{t,f}$ (MPa)	v_{jh}	v_{jh}^{exp} (MPa)	$v_{jh,f}^{jh}/v_{jh}^{exp}$	$\varepsilon_{f,e}^{exp}$
GER (3)	Cor	FD	20	0	356	407	407	CFRP	64.7	45	1.32	1	1	M - C	0.79	760	0.0038	0.91	2.21	2.30	0.96	0.0033
GER (4)	Cor	FD	20	0	356	407	407	CFRP	64.7	±45	1.32	1	2	M - C	0.79	1520	0.0025	1.21	2.50	2.37	1.06	0.0033
GER (5)	Cor	FD	20	0	356	407	407	CFRP	64.7	45	1.32	1	1	M - C	0.79	760	0.0038	0.91	2.21	2.04	1.09	0.0033
GER (6)	Cor	FD	20	0	356	407	407	CFRP	64.7	45	1.32	1	1	M - C	0.79	760	0.0038	0.91	2.21	2.00	1.11	0.0033
GER (7)	Cor	FD	20	0	356	407	407	CFRP	64.7	45	1.32	1	1	M - C	0.79	760	0.0038	0.91	2.21	1.97	1.12	0.0033
GER (8)	Cor	FD	20	0	356	407	407	CFRP	64.7	±45	1.32	1	2	M - C	0.79	1520	0.0025	1.21	2.50	2.37	1.06	0.0033
GER (9)	Cor	FD	20	0	356	407	407	CFRP	64.7	±45	1.32	1	2	M - C	0.79	1520	0.0025	0.85	2.15	2.73	0.79	0.0033
PAN(R24-3)	Int	FD	43	709	406	406	610	CFRP	43	0 (±60)	1.35	2	2	M - C	0.98	5011	0.0021	2.32	7.07	9.96	0.71	n.a.
PAN(R24-4)	Int	FD	43	709	406	406	610	CFRP	106	0 (±60)	1.02	2	2	M - C	0.98	3786	0.0015	2.98	7.80	9.22	0.85	n.a.
PAN(R16-2)	Int	FD	43	709	406	406	406	CFRP	80	0 (±60)	0.76	2	2	M - C	0.79	2249	0.0024	1.84	6.50	9.01	0.72	n.a.
PAN(R16-3)	Int	FD	43	709	406	406	406	CFRP	43	0 (±60)	1.35	2	2	M - C	0.79	3996	0.0024	1.80	6.46	9.40	0.69	n.a.
PAN(R16-4)	Int	FD	43	709	406	406	406	CFRP	106	0 (±60)	1.02	2	2	M - C	0.79	3019	0.0017	2.31	7.06	9.79	0.72	n.a.
PAM (2DR2)	Cor - PB	BH	18.9	108	230	230	330	GFRP	76	0 (90)	0.36	1	2	M - C	0.96	231	0.0069	1.88	3.59	2.55	n.c.	0.0071
PAM (2DR3)	Cor - PB	BH-FD	18	230	230	230	330	GFRP	76	0 (90)	0.36	1	2	M - C	0.96	231	0.0068	1.84	4.30	2.87	n.c.	0.008
PAM (2DR4)	Cor - PB	BH	18.7	220	230	230	330	GFRP	76	0 (90)	0.36	1	2	M - C	0.96	425	0.0048	2.39	4.87	2.55	n.c.	0.0041
PAM (3DR2)	Cor - PB	FD	16.9	185	230	230	330	GFRP	76	0 (90)	0.36	1	1	M - C	0.96	213	0.0069	1.74	3.89	2.19	n.c.	0.0048

[a] GER= (Gergely et al., 2000), PAN = (Pantelides et al., 2008); PAM = (Akguzel and Pampanin, 2010);
[b] Cor = Corner joint; Int = interior joint; PB = joint with plain internal reinforcements;
[c] FD= FRP debonding, BH= Beam plastic hinge,.
[d] FRP strengthening: M = Mechanical anchorage, C = Continuous fabric
n.c. are the tests that exhibited a flexural failure of the adjacent members (BH) and the ratio v_{jh}/v_{jh}^{exp} has not been computed.
Note: the number in the brackets and are referred to FRP layouts with multiple inclinations and the related properties.

For this scope, seven corner beam-column joints tested by Gergely et al. (2000) have been selected in the database (see Figure 5.5). The subassembly characteristics, material properties and other details on the selected specimens are reported in Table 5.6. The comparison with the predictions of the proposed analytical model show a good match with the experimental results both in terms of joint panel shear strength and effective FRP strains. This validation confirms the model reliability predicting the contribution of the FRP on the shear strength of poorly detailed corner beam-column joints.

In order to extend the model applicability, joint subassemblies with plain round internal reinforcements and interior joints have been also included in Table 5.6.

In particular, three experimental tests carried out by Akguzel and Pampanin (2010) on corner joints with plain round bars have been selected. Furthermore, in order to assess the model accuracy also for joint subassembly subjected to biaxial shear, one reference specimen (3DR2) tested by the same authors have been selected. The direct comparison in terms of joint shear strength is not allowed in this case. This is because of the flexural failure mode exhibited in these tests. However, as already performed in the previous section, these tests can be used to show the ability of the proposed procedure to predict the shear strength of the joint panel such that it is higher than that required for flexural yielding. This check can be performed by comparing the predicted joint shear stress v_{jh} and the maximum joint shear stress (in this case governed by the flexural yielding) v_{jh}^{exp} (see Table 5.6). Also in the case of joint subassemblies with plain round internal reinforcements, the predicted joint shear strength is always higher than that associated to the flexural yielding. Therefore, the proposed model can be employed to design the proper amount of FRP reinforcement necessary to prevent the joint panel shear failure and allows for flexural yielding of adjacent structural members. The comparison in terms of effective FRP strains on the joint panel demonstrated the model reliability also in the case of subassemblies with plain internal reinforcements.

In conclusion, the proposed model is used to predict the joint shear strength of interior subassemblies (beams framing from both sided of the joint panel). For this scope the tests carried out by Pantelides et al. (2008) have been selected and compared with predicted joint shear strength. The results are reported in Table 5.6 along with the subassemblies characteristics. For interior joints the comparison between predicted and experimental shear strength points out the significant underestimation of the proposed model. The analysis of the predicted results, demonstrated that such underestimation is mainly related to the capacity model adopted to represent the capacity of the as-built joint. In fact, in compliance with the modeling strategy proposed for corner joints, the joint first cracking (in this case $0.48\sqrt{f_c}$, (Anderson et al., 2008)) has been adopted to consider the concrete contribution. However, exterior joint subassemblies, because of the confinement effects of transverse beams in both directions, may exhibit significant over-strength after the first cracking (i.e. until $1.0\sqrt{f_c}$, (Park, 1997)). In order to proper consider the concrete contribution and allow a more refined estimation of the shear strength, further studies are needed for interior joints.

5.8 SOLVED EXAMPLE

The specimen T_FS2 (see Section 3) is a corner beam–column joint with the geometry, reinforcement details and mechanical properties typical of existing structural systems of the Mediterranean area designed without seismic actions. The examined subassembly has a square column (h_c = b_c = 300 mm) reinforced with a total of 4ϕ16, one in each corner. The beam has a rectangular cross section with a base b_b = 300 mm and a height h_b = 500 mm. The internal steel reinforcements are 5ϕ16 and 3ϕ26 at the top and bottom side, respectively. The concrete cover both for the beam and the column is 24 mm. The mean concrete cylinder compressive strength is about 16.4 MPa and the steel longitudinal reinforcement has a yield stress of 470 MPa. The column is subjected to a constant axial load of 295 kN. The

lack of internal transverse reinforcement in the joint panel leads to its premature shear failure which is detrimental to the seismic performance of the structural system. The proposed procedure is applied to design the proper amount of joint panel FRP fibers to avoid the shear failure and to allow a more ductile flexural failure. The shear stress capacity of the as-built joint, v_{jh}, can be computed according to the principal stress approach by Eq. (5.13), assuming $p_{t,tot} = p_{t,c} = 0.29\sqrt{f_c} = 0.29\sqrt{16.4} = 1.175$ MPa .

$$v_{jh} = p_{t,tot} \cdot \sqrt{1 + \frac{f_a}{p_{t,tot}}} = p_{t,c} \cdot \sqrt{1 + \frac{N/(h_c \cdot b_c)}{p_{t,c}}} \Rightarrow$$

$$v_{jh} = 1.175 \cdot \sqrt{1 + \frac{295000/(300 \cdot 300)}{1.175}} = 2.29 \text{ MPa}$$

The design shear stress, v_{jh}^d, that represents the target value for the design of the FRP strengthening, is assumed as the joint shear stress associated with the flexural yielding of the weaker member between the beam and the column. This is in compliance with a capacity design approach. In this case, the first yielding of the subassembly is associated with the column yielding (M_y = 77.8 kNm) that corresponds to a joint shear stress v_{jh}^d = 3.63 MPa, computed with Eq. (5.15). Because the shear strength of the as-built joint is significantly lower than the design value, the FRP strengthening of the joint panel is required (i.e. the originally shear capacity should be increased of 58%). In this example, it is assumed to strength the joint panel with two layers (n_l = 2) of quadriaxial CFRP fabric with fibers inclined of 0°, ±45° and 90° at the beam axes. The elastic modulus, E_f, is about 230 GPa. The thickness of the dry fibers, t_f, is about 0.053 mm in each direction. Because of the presence of a beam, orthogonal to the load plane, only one side of the joint panel can be strengthened in shear (n_s =1). In order to estimate the equivalent area of the FRP system by Eq. (5.12), the inclination of the crack at the maximum strength capacity, θ, can be computed by Eq. (2.28).

$$\theta = atan\left(\frac{h_b}{h_c}\right) = atan\left(\frac{500}{300}\right) = 59°$$

$$A_{f,eq} = n_l \cdot n_s \cdot t_f \cdot h_c \cdot cos\theta \cdot \left(1 + tan\theta + 2tan^2\theta\right) \Rightarrow$$
$$A_{f,eq} = 2 \cdot 1 \cdot 0.053 \cdot 300 \cdot cos\left(59°\right) \cdot \left(1 + tan\left(59°\right) + 2tan^2\left(59°\right)\right) = 134.5\ mm^2$$

Once that the FRP equivalent area is known, the effective FRP strain can be computed by Eq. (5.20) by assuming no initial damage in the joint panel ($C_{I.D.}$ = 1). The bonding conditions will be improved by means of mechanical anchorage at the ends of the FRP system ($C_{M.A.}$ = 1.5).

$$\varepsilon_{f,e} = 31.6 \cdot C_{I.D.} \cdot C_{M.A.} \cdot \left(\frac{f_c^{2/3}}{A_{f,eq} \cdot E_f}\right)^{0.6} = 31.6 \cdot 1 \cdot 1.5 \cdot \left(\frac{16.4^{2/3}}{134.5 \cdot 230000}\right)^{0.6} = 0.00465$$

The contribution of the FRP system to the principal tensile stress can be calculated by Eq. (5.9)

$$p_{t,f} = \frac{A_{f,eq} \cdot E_f \cdot \varepsilon_{f,e}}{b_c \cdot \frac{h_c}{sin\theta}} = \frac{134.5 \cdot 230000 \cdot 0.00465}{300 \cdot \frac{300}{sin\left(59°\right)}} = 1.37\ \text{MPa}$$

The total resisting principal tensile stress can be computed by summing the concrete contribution, $p_{t,c}$, and the FRP contribution, $p_{t,f}$, Eq. (5.1).

$$p_{t,tot} = p_{t,c} + p_{t,f} = 1.175 + 1.370 = 2.545$$

and substituting again in Eq. (5.13), the shear strength of the joint panel strengthened with the proposed FRP system is:

$$v_{jh} = p_{t,tot} \cdot \sqrt{1 + \frac{f_a}{p_{t,tot}}} = p_{t,tot} \cdot \sqrt{1 + \frac{N/(h_c \cdot b_c)}{p_{t,tot}}} \Rightarrow$$

$$v_{jh} = 2.545 \cdot \sqrt{1 + \frac{295000/(300 \cdot 300)}{2.545}} = 3.85 \text{ MPa}$$

that is higher than the design target, v_{jh}^{d} = 3.63 MPa.

Finally, it must be checked that the joint capacity is not limited by the crushing of the concrete compressive strut. The joint panel capacity in compression can be calculated with Eq. (2.29) assuming $p_c = 0.5f_c$ and it is equal to v_{jh}^{c} = 6.35 MPa which is significant higher than v_{jh}. The proposed strengthening system with two plies of quadriaxial CFRP increases the joint panel shear capacity by about 70%. The designed FRP shear strengthening prevents the joint panel from shear failure which then allows for the development of a plastic hinge on the column changing the brittle failure mode to ductile one.

CHAPTER 6
NUMERICAL MODELING

Although the analytical modeling of joint behavior assumed significant relevance in the recent years, few capacity models, reliable for poorly detailed beam-column subassembly are nowadays available. The complex hysteretic behavior of these members, characterized by significant strength and stiffness degradation and pinching phenomena related to the shear cracks, makes it difficult to be reproduced. Among the proposed models, particular emphasis should be given to the principal stresses approach (Priestley, 1997). Its mechanical basis along with the use of empirical coefficients make the model simple and suitable for practical applications. This model have been adopted in several national standards limiting the joint panel strength to the first cracking (CEN, 2005; MI, 2008). Analytical studies pointed out that this limit is detrimental for the global seismic performances (Di Ludovico et al., 2008; Frascadore et al., 2014). Experimental tests demonstrated that further shear forces can be carried by

the joint panel after the first cracking (see Chapter 3). However, as already formulated by Priestley et al. (Priestley et al., 1996) large shear deformations are exhibited after the joint panel first cracking. Indeed, to accurately reproduce the joint behavior, the joint shear deformation cannot be neglected. This is also confirmed by several research studies (Calvi et al., 2002; Park and Mosalam, 2013) that quantified the effects of joint deformability on the overall seismic behavior.

6.1 JOINT HYSTERETIC BEHAVIOR

Although several capacity model have been proposed to predict the joint behavior and the effects on the structural system performances (Priestley et al., 1996; Lowes and Altoontash, 2003; ASCE/SEI, 2007; Lafave and Kim, 2011; Park and Mosalam, 2013), they are commonly based on empirical approaches or calibrated for specific joint types. Few models can accurately reproduce the joint hysteretic behavior. This because of the significant Strength and Stiffness Degradation (SSD) and pinching phenomena related to the shear cracking that strongly affect the cyclic response. Recent studies, pointed out the importance to accurately reproduce the member hysteretic behavior in the seismic assessment of shear critical structures (Del Vecchio et al., 2015; Huang and Kwon, 2015). However include the effects of SSD in the seismic response of structural member is nowadays a critical issue. Sophisticated numerical models have been proposed to predict the structural response of SSD members for large displacement demand (i.e., the modified compression field theory, MCFT (Vecchio and Collins, 1986) and disturbed stress field model, DSFM (Vecchio, 2000), but significant computational demand has limited their application to structures. In recent years, the development of advanced and efficient algorithms in computer programs suitable for practical applications (i.e., Membrane 2000 (Bentz, 2000), VecTor programs (Wong et al., 2013)) promoted their use to reliably simulate the cyclic behavior of SSD RC structural systems.

A new strategy to model the beam-column joint cyclic behavior, based on the recent developments in the analytical models and computer software dedicated to shear critical systems, is presented in this paper. Available finite element method (FEM)-based software, implementing rigorous theoretical approaches (i.e. the MCFT and the DSFM) have been adopted in the model development. The proposed FEM model is described in detail, with particular attention to the material mechanical models and the effects of reinforcement anchorages. The model has been validated with reference to experimental tests; in particular, comparisons between theoretical and experimental outcomes are presented and discussed in the paper in terms of global response, local stress-strain behavior and crack pattern prediction. Further considerations on the joint panel stress levels are also presented.

6.2 PROPOSED ANALYTICAL MODEL

The advanced numerical models proposed in the recent years improved accuracy in reproducing the behavior of RC structural systems. New mechanical models and solution algorithms have been developed and great effort has been made to combine them with the state-of-the-art knowledge in refined tools suitable for the use in the practical applications (e.g., OpenSees (2006), VecTor programs (Wong et al., 2013), among others).

The continuum element considered in this study is based on the Modified Compression Field Theory (MCFT) (Vecchio and Collins, 1986) and Disturbed Stress Field Model (DSFM)(Vecchio, 2000). Both these theories have been developed at University of Toronto and validated through large experimental programs on shear critical RC panel, structural members and entire structural systems. The MCFT is a two-dimensional analytical model in which compatibility, equilibrium, and constitutive relationships were derived based on average stress and strain of concrete. In the MCFT, it is assumed that the directions of averaged stress and strain are identical. The formulation of the model was simplified by assuming cracks

are smeared and fully rotating. Local stresses and strains at cracks are computed based on the stress-strain relationship developed for cracked concrete. Out-of-plane and in-plane transverse reinforcements are smeared over the entire concrete core. Such a theory has been later generalized by the DSFM, modifying some basic assumptions (i.e. alignment of shear stress and strain) and enlarging the applicability to more complex stress fields. The complexity of this approach and the number of information contained in the analysis strongly limited its application in the past year. Recently, it has been implemented in accurate computer tools suitable for practical applications. In this paper, the response of a reference beam-column joint will be reproduced by mean of two different computer software (Membrane 2000, M2k (Bentz, 2000), and VecTor2, VT2 (Wong et al., 2013)). They are characterized by increasing level of difficulty in the modeling and, in turn, higher accuracy in the response prediction.

The joint subassembly selected for the model validation is a poorly detailed corner beam-column joint typical of existing structures designed for gravity load only. The specimen (named T_C3 in the experimental program carried out at University of Naples and described in the Chapter 3) has no stirrups in the joint panel and geometry and internal reinforcement details typical of existing buildings. It has been tested with an imposed cyclic displacement applied at the beam tip and under constant axial load on the columns. To simulate gravity loads, a preload of 19.2 kN was applied to the beam along with a constant axial load ($\nu = P/A_g f_c = 0.21$) to the column. The specimen was constrained to the strong floor by two rigid steel frames, with a steel roller placed inside the lower column end to simulate a pin connection. The top column was constrained to a rigid frame by two steel rollers that grabbed the column end externally and allowed top column elongation. The beam and column length were designed to allow for the typical story height and the portion of the beam up to the zero point of the bending moment diagram, respectively. The cylindrical concrete compressive strength is about 16.4 MPa and the longitudinal steel reinforcement yielding stress about 470 MPa. The experimental test pointed

out a shear failure of the joint panel before the flexural yielding of longitudinal steel reinforcement of members framing into the joint.

6.2.1 Membrane 2000

Membrane 2000 (M2k) is a simple computer program implementing the MCFT. It allows analysis of reinforced concrete shells subjected to in-plane forces (axial force in X and Y directions and in-plane shear). Internal reinforcement may be placed in orthogonal directions X and Y with an arbitrary number of bar layers and spacing allowed. Membrane elements subjected to in-plane forces can be found in structural walls, the webs of beams, containment vessels, and cooling towers among many others. This is the type of experimental element tested to develop the modified compression field theory. The complex stress field and geometry of a joint subassembly can be reduced to a simple shell loaded in shear and axial force by using the assumptions reported in the previous paragraph. In particular, the actions transmitted by the member framing in the joint should be reduced to acting shear stress (assumed equal for all the faces of the joint) and axial compression stresses acting on the joint horizontal faces. It should be noted that this modeling approach can be extended only to joint subassemblies suffering the premature shear failure of the joint panel without relevant nonlinear phenomena in the adjacent members. According to these assumptions, the selected joint T_C3 has been modeled in M2k by using a shell element 300 mm thick subjected to a constant axial stress of 3.50 MPa (it is obtained spreading the axial load on the joint horizontal surface). The specimen shear strength has been evaluated under monotonic joint shear stresses and the results are plotted in Figure 6.1 against the joint shear strain, γ_{xy}. Comparison with available experimental results, points out a significant underestimation of the real joint performances in terms of joint panel peak strength (v_{jh}=2.56MPa). The analysis of the Mohr's circle of stress and the crack pattern at the peak strength (Figure 6.1) demonstrated that the ultimate joint capacity is reached along with joint panel first cracking, for a principal tensile stress about 1.38MPa. This is in compliance with the stress

limit proposed by Priestley (Priestley, 1997), $p_t = 0.29\sqrt{f_c}$. Such underestimation is related to the effects of the longitudinal reinforcement anchorages, neglected in the model. In fact, larger shear stress can be achieved in the joint panel if the longitudinal beam reinforcements are bent into the joint (Priestley, 1997) ($p_t = 0.42\sqrt{f_c}$).

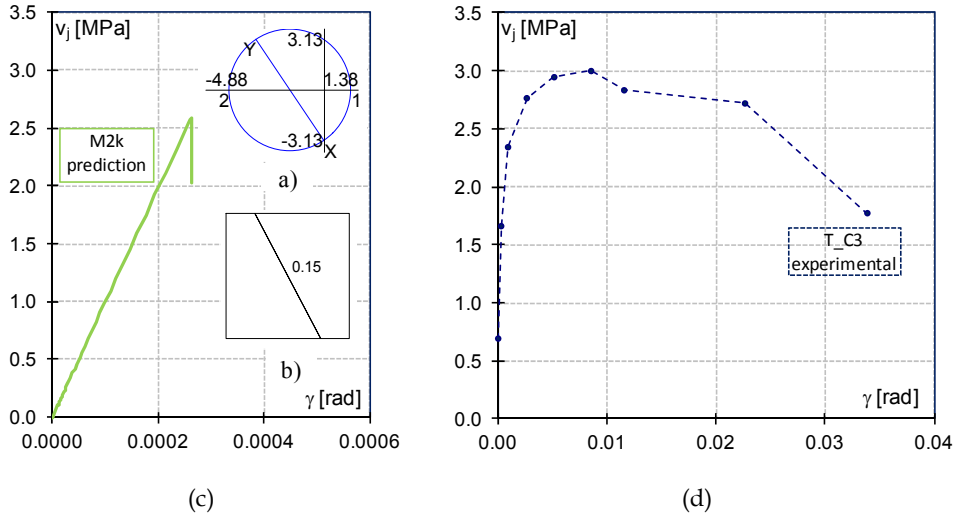

Figure 6.1 Membrane 2000 (M2k) monotonic response prediction without the anchorage effects: (a) Mohr's circle and (b) crack patter at the peak strength; (c) analytical shear stress-strain behavior; (d) experimental shear stress-strain behavior.

However there are no simple options to include the effects of beam bar anchorages in the M2k model. To overcome this issue, the maximum lateral pressure provided by the bar bents have been computed and an equivalent amount of transverse reinforcement providing the same lateral pressure has been inserted in the model. Details on the modeling procedure are reported in Figure 6.2.

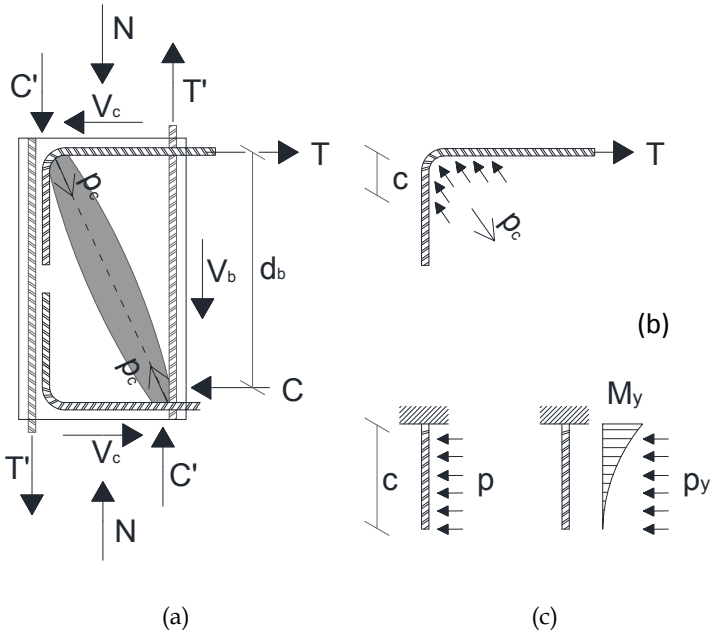

Figure 6.2 Mechanical model of the anchorage effects.

The lateral pressure of the beam bar anchorages represents is activated by the concrete compressive forces developing in the diagonal strut. The maximum pressure carried by the anchorage is assumed equal to the pressure needed to yield the longitudinal reinforcement in flexure. In the calculation it is assumed that the straight length of the anchorage is fixed in correspondence of the bent. This pressure can be computed with Eq. (6.1).

$$M_y = \frac{pl^2}{2} \Rightarrow p_y = \frac{2M_y}{c^2} = \frac{2f_{ym} \cdot \pi \cdot r^3}{c^2 \cdot 4} = \frac{2 \cdot 470 \cdot \pi \cdot 8^3}{85^2 \cdot 4} = 52.2 \frac{N}{mm} \tag{6.1}$$

where c is the straight length of the anchorage subjected to the lateral pressure of the concrete compressive strut. It can be assumed equal to the total height of the concrete compressive zone above the longitudinal reinforcement $0.25h\text{-}c_c\text{-}d_b$=125-25-16=85mm, where c_c is the concrete cove and d_b is the diameter of longitudinal reinforcements.

The total pressure acting on the external face of the joint panel can be computed multiplying the maximum pressure of the single anchorage for the number of anchorages and dividing by the joint width:

$$p_{t,tot} = \frac{p_y \cdot n_b}{b_j} = \frac{52.2 \cdot 5}{300} = 0.87 \frac{N}{mm^2} \tag{6.2}$$

where n_b is the number of beam bars bent into the joint panel, in this case 5, and b_j the joint width assumed equal to the column width, 300mm.

Once that the maximum lateral pressure has been identified, the equivalent amount of joint reinforcement (in terms of percentage of transverse reinforcements) can be derived dividing this pressure for the yield stress of steel:

$$p_{t,tot} = f_{ym} \cdot \rho_s \Rightarrow \rho_s = \frac{p_{t,tot}}{f_{ym}} = \frac{0.87}{470} = 0.186\% \tag{6.3}$$

In this case an equivalent amount of joint stirrup, representative of the confinement effects of the beam bar anchorages, will be placed into the joint. This solution has been preferred with respect to a constant value of the lateral pressure in order to be representative of the variability of the confinement pressure, that increases increasing the shear stress.

Comparison between the proposed analytical model and experimental results is reported in Figure 6.3 in terms of joint shear stress-strain behavior, joint panel stress field and crack pattern.

The comparison points out the good match of the proposed analytical model in terms of joint panel shear behavior at different levels. In particular, the joint panel first cracking (where hairline cracking was detected during the test) is well predicted by the proposed analytical model in terms of shear strength and crack pattern (see Figure 6.3, level II). Furthermore, the joint panel circle of stresses highlights the good match in terms of principle tensile stress with the limit proposed by Priestley (Priestley, 1997), p_t

$=0.29\sqrt{f_c}$ =1.2MPa. The analytical predictions match well the experimental results also at the peak strength (see Figure 6.3, level III) in terms of stress-strain behavior and crack pattern, where large shear cracks can be detected. The good match in terms of joint panel principal tensile stress with the stress limit proposed by Priestley, $p_t = 0.42\sqrt{f_c}$ =1.7MPa, shows the reliability of the proposed model to account for the effects of anchorages bent into the joint. The full strength degradation cannot be captured by this software and more refined calculations are needed.

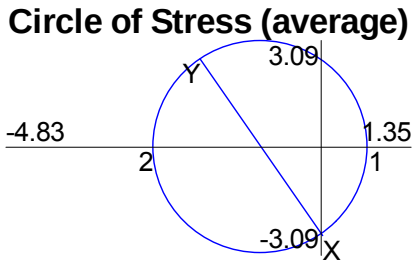

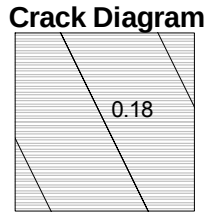

Level II: Joint panel first cracking

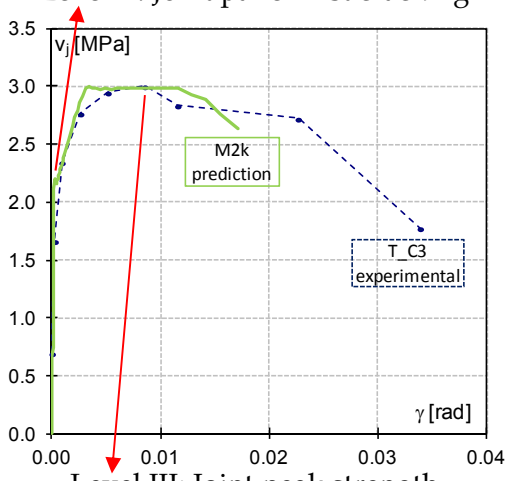

Level III: Joint peak strength

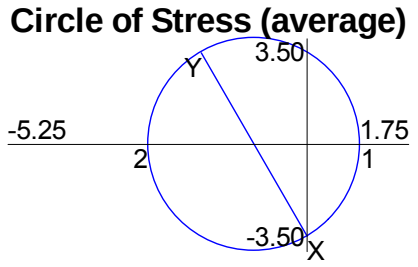

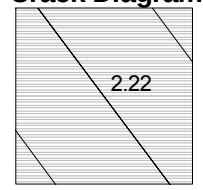

Figure 6.3 Experimental vs. M2k prediction in terms of shear stress-strain behavior and crack patterns (Crack widths in mm).

6.2.2 VecTor2

VecTor2 is a program based on the MCFT/DSFM for nonlinear finite element (FEM) analysis of reinforced concrete membrane 2D structures that permits accurate assessments of structural performance (strength, post-peak behavior, failure mode, deflections and cracking). The Vector2 bundle (Wong et al., 2013) includes: FormWorks, a graphics-based preprocessor program that simplifies the model building; Augustus, a complete VecTor2 post-processor that may provide all the global and local results in useful numeric or graphic formats. It is also able to display the specimen crack pattern at each stage of imposed displacement and this represents a very useful tool to detect numerical model failure mode. The FEM elements require a different and more complex modeling approach. The VecTor2 model was developed using a pre-processor unit FormWorks (Wong et al., 2013) that simplified the meshing and the input of the model parameters. Similar to other continuum elements, mesh size plays an important role in computational efficiency and accuracy. A mesh size in the range of about 25 mm, and approximately square elements have been adopted as suggested in the related studies (Palermo and Vecchio, 2003; Sagbas et al., 2011; Del Vecchio et al., 2013). The software can accommodate only 2D elements. A specific thicknesses equal to 300 mm has been set for all members. Longitudinal reinforcements are modeled with truss elements. Link elements were adopted to model the bond-slip behavior using the *Embedded deformed bar* option available in the software option (Wong et al., 2013). To account for the stress concentration at the anchorages of longitudinal beam bars, the *Hooked bar option* has been adopted for the link element in correspondence of reinforcements ends. Transverse reinforcements in the beam and columns were modeled as smeared reinforcements with appropriate in-plane (ρ_t) and out of- plane (ρ_z) average ratios. The same approach was used to account for the joint panel internal reinforcement representative of the anchorage effects as determined by Eq. (6.3).

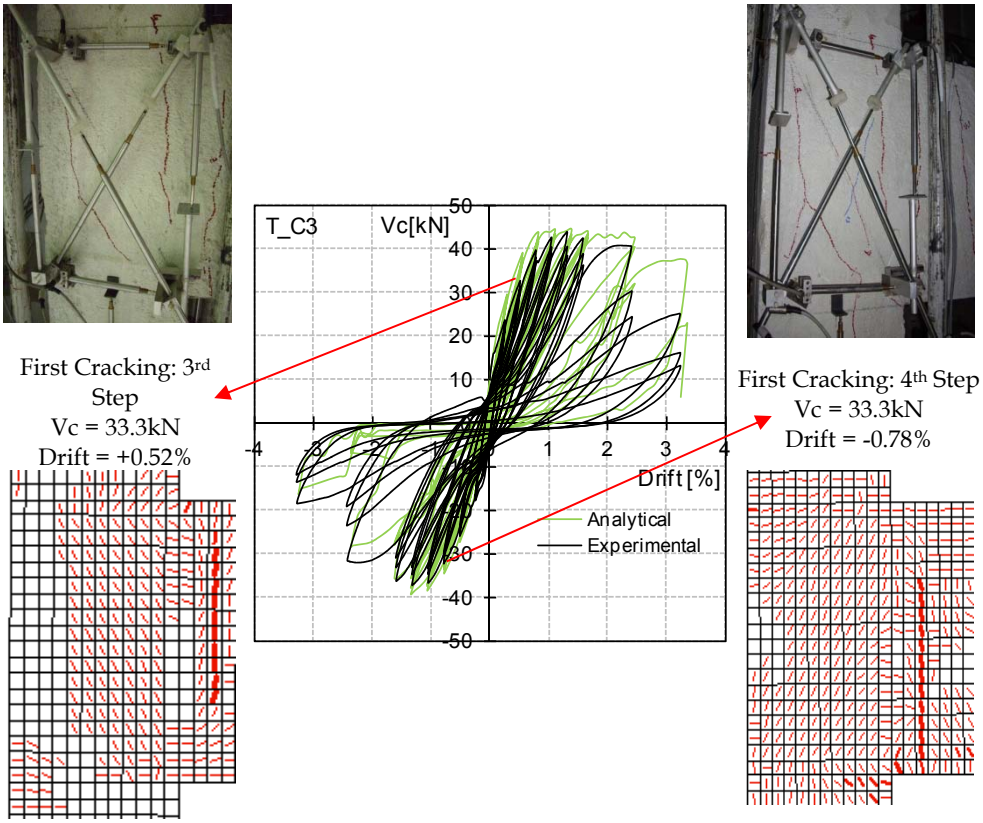

Figure 6.4 Experimental and analytical crack patterns at the joint panel first cracking (Crack widths: thin<0.5mm; thick>1mm).

The concrete cover was modeled as unconfined concrete. The material properties are defined in accordance with the material tests reported in the Chapter 3. All analyses are performed with the use of basic default material behavior models and analysis options. The concrete constitutive model by Popovic and Mander (Popovic, 1973; Mander et al., 1988) is adopted to reproduce concrete compressive behavior. A proper representation of the concrete cyclic behavior is critical in determining the strength and energy-dissipation capacity of the subassembly. Indeed, as suggested by Sagbas et

al. (Sagbas et al., 2011), the hysteretic model proposed by Palermo and Vecchio (Palermo and Vecchio, 2003) has been adopted in this study.

As in the experimental test, joint models are subjected to cyclic displacement and axial load applied at the beam tip and column, respectively. The comparisons between the analytical model and experimental results at the significant steps of the test are reported in Figure 6.4-Figure 6.6.

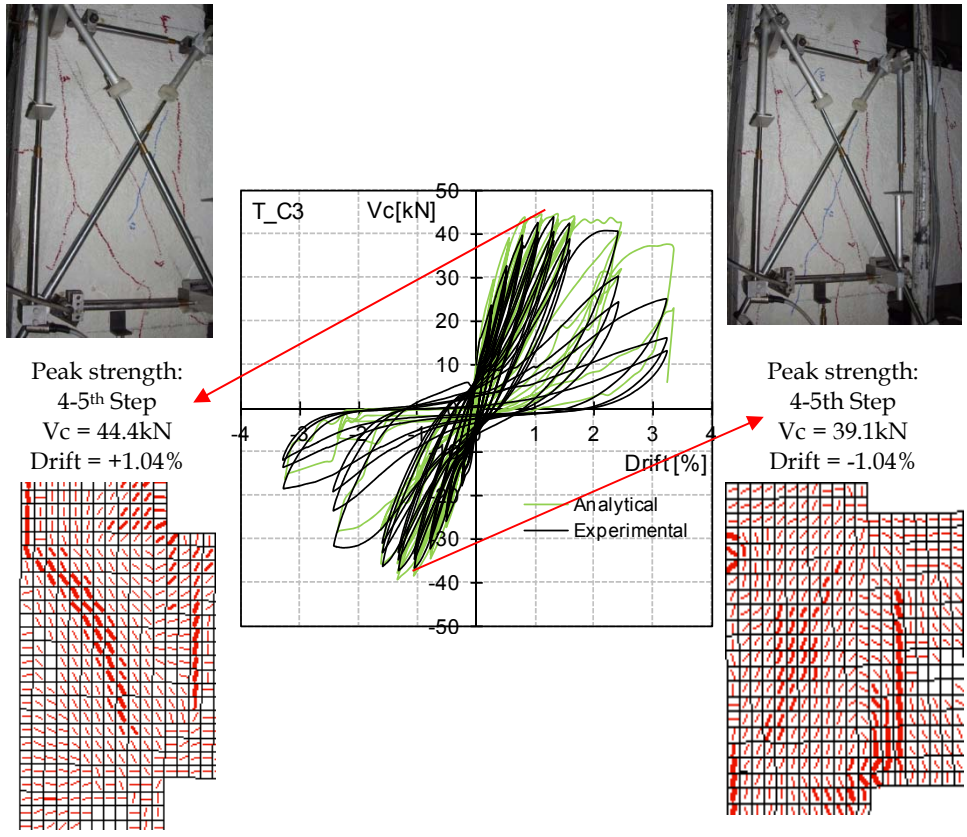

Figure 6.5 Experimental and analytical crack patterns at the subassembly peak strength (Crack widths: thin<1mm; thick>2mm).

The comparison between the proposed analytical model and experimental results demonstrated the accuracy in predicting the joint subassembly global behavior. The theoretical predictions show a good match with respect to the parameters significant in the seismic assessment, including initial stiffness, peak strength, strength and stiffness degradation, pinching effects and energy dissipation. Furthermore, a crack pattern very similar to the experimental one is predicted. In particular, the joint panel first cracking (depicted in Figure 6.4) occurs for a column shear of about 33kN, significantly lower than the maximum strength. At this step diffused hairline cracks appears in both directions. At the same step, a flexural crack appears on the beam in the section of the maximum bending moment. Because of the higher magnitude of the flexural crack, in the analytical model joint shear cracks are represented with a thin line.

The joint peak strength is characterized by deep and large diagonal cracks in the order of millimeters. As reported in Figure 6.5 a corner-to-corner diagonal crack appears in the joint panel for the positive loads. Reverse cyclic actions produces a change in the crack orientation; however, due to the strong nonlinear behavior of the cracked concrete, the opposite diagonal cracks are not completely closed.

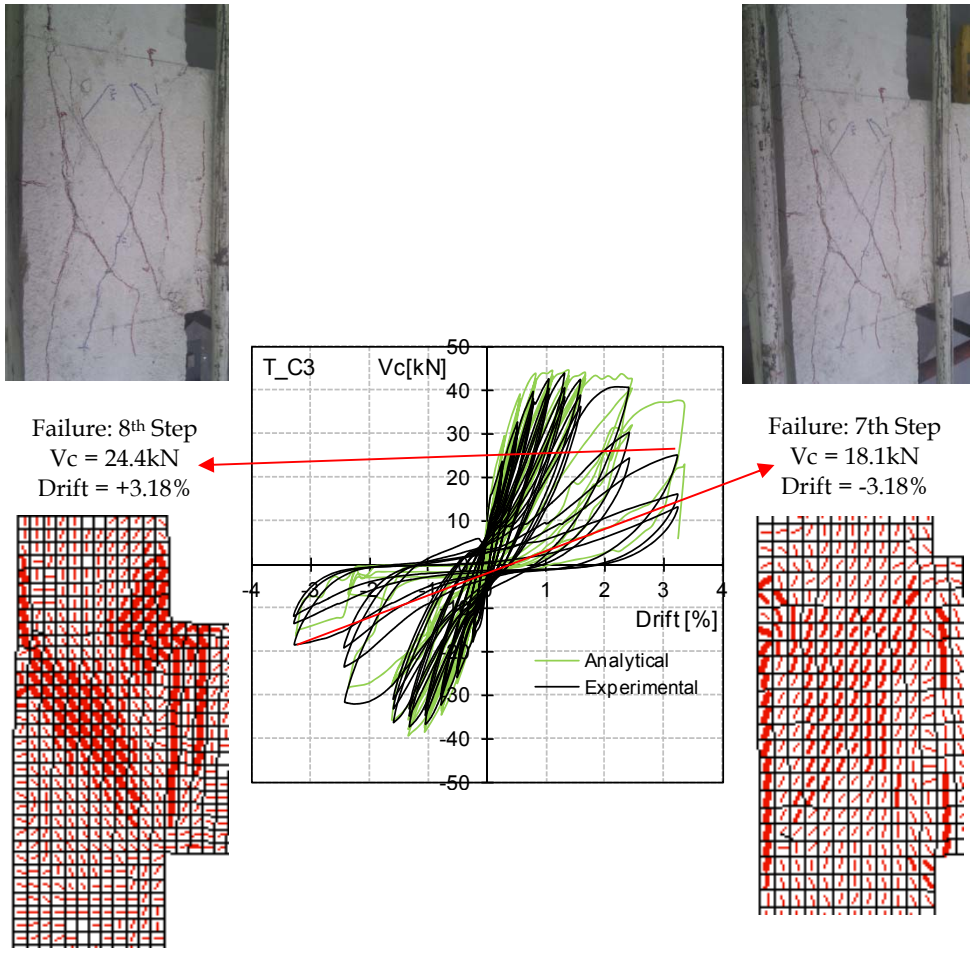

Figure 6.6 Experimental and analytical crack patterns at joint panel shear failure (Crack widths: thin<2mm; thick>4mm).

The crack pattern at the joint panel failure, after which a significant drop in the shear strength can be observed, shows marked cracks in both direction and the spalling of concrete cover (see Figure 6.6). Due to the severe damage of the joint panel, large shear cracks, in the order of centimeters, can be observed in both directions.

Further information on the joint panel failure mode are provided by analyzing the local behavior of members. No relevant damage is detected on columns and beam framing in the joint panel. Analytical prediction confirmed that the internal longitudinal reinforcements are far below the tensile yielding. On the other side the joint panel shear stress-strain behavior shows significant nonlinear phenomena (see Figure 6.7). In compliance with experimental results, the joint panel first cracking is followed by significant joint shear deformations. Once that the peak strength is achieved, the strength degradation is related to joint shear strains even double respect to the peak strength. The VecTor2 model is able to capture the shear stress-strain behavior with enough accuracy until a significant drop in the shear strength occurs.

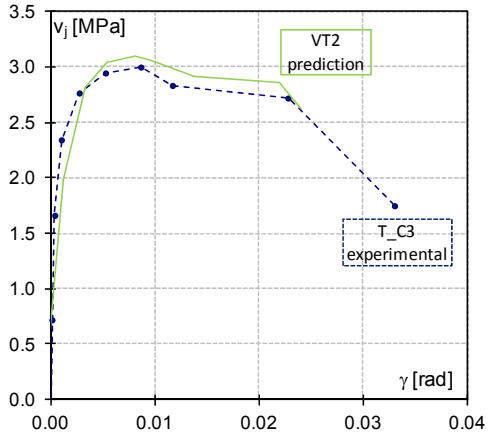

Figure 6.7 Joint panel shear stress-strain behavior.

CHAPTER 7
CONCLUSIONS

This thesis focuses on the seismic behavior of beam-column joints of existing RC buildings designed for gravity loads and on their seismic retrofit with Fiber Reinforce Polymer (FRP) systems. Recent seismic events and scientific studies pointed out that the seismic vulnerability of existing RC structural systems is often related to the brittle failure of these structural members. In fact, minor attention has been reserved to beam-column connections in the design code and construction practice of the past century. This led to have a large number of structural systems that are vulnerable to seismic events because of poorly detailed beam-column joints.

This background strongly promoted the development of seismic retrofit techniques for beam-column joints. The demonstrated effectiveness, along with the easy installation procedure, light weight and durability has spread the use of FRP systems in the aftermath of major recent earthquakes. Even though, the effectiveness of the FRP materials in strengthening poorly detailed beam column joints has been largely demonstrated, a simple and reliable design formulation to account for the FRP contribution to the shear strength was still missing. This is due to the complex mechanical behavior

of the beam-column joints and to the high variability of the FRP response characterized by debonding phenomena.

In this thesis, a wide literature review was carried out in order to clarify the mechanical behavior of RC beam-column joints. Furthermore, the main parameters that influence the mechanical behavior of the externally bonded FRP systems were pointed out. Relevance was also given to the recent developments in the capacity models for the FRP strengthening of beam-column joints. In spite of the model accuracy, they adopt rigorous mechanical approaches that make these models complex to be adopted in practical applications. In order to develop a simple design formulation, the main parameters need to be identified and several assumptions are needed.

To investigate the seismic response of poorly-detailed beam-column joints and to clearly identify the main parameters affecting the FRP response, a wide experimental program was performed. The experimental program involved seven full-scale beam-column joints typical of an existing RC frame designed for gravity load only. The subassemblies were partially confined corner joints without stirrups in the joint core and were designed to achieve the shear failure in the joint panel before the column yielding. The design of the experimental program, the details of the reference building, test setup, load protocol and instrumentation were widely described along with the main experimental results.

Experimental tests on as-built joints showed a failure mode similar to that commonly detected on unconfined joints in the post earthquake inspections; the joint panel failure occurred with wide and deep diagonal cracks and concrete "wedge" spalling off. The comparison with available capacity models and code prescription was widely discussed and the following conclusions were achieved:

- Comparison among several strength capacity models available in the literature and the experimental results showed an absolute maximum scatter of 10%. The minimum difference was obtained by using the principal tension stress approach suggested by Priestley (1997);

- Joint shear capacity computed at first cracking, as suggested by EN 1998-1 CEN (2004), provided very conservative predictions (i.e., 30% lower than experimental maximum strength capacity). The accuracy of joint strength capacity expressions provided by ASCE/SEI 41-06 ASCE/SEI (2007) and AIJ (1999) strongly depends on proper evaluation of the confinement benefits given by transverse beams on exterior joints;
- The analysis of the joint panel stress-strain behavior showed that if high joint shear stresses are considered (i.e. higher than joint first cracking), the joint shear deformations cannot be neglected;
- The analyses suggested that suitable capacity models of joint shear deformability should be specifically calibrated on poorly detailed beam-column joints. The existing prediction models may lead to significant underestimation of joint shear stress and strain.

Furthermore, the experimental tests on FRP-strengthened specimens showed the effectiveness of the proposed strengthening solutions for seismic retrofit of poorly detailed RC beam-column joints. In particular, they showed that:

- The use of 0.4% as design maximum strain for FRP retrofit of a beam-column joint seems to be too conservative according to the experimental results presented. The maximum strain recorded on FRP was in each case larger than 0.4%, with a maximum value of 1.0%;
- The amount of FRP joint panel reinforcement substantially affects joint panel deformations. To reduce joint deformations, it will likely be necessary to limit the effective FRP strain to values lower than 1.0% for design purposes. Further research is needed to define an upper bound limit;
- The use of a proper FRP joint panel anchorage solution (i.e., U-shaped uniaxial sheet wrapped also around the beam top side) was a sound solution to avoid FRP end full debonding. However, intermediate debonding occurred on the joint panel CFRP strengthening. Thus, the adoption of discrete restraint points in the joint region may be

necessary to prevent CFRP debonding. To confirm this result, further experimental tests are necessary;
- A suitable amount of joint panel FRP fibers combined with a stronger anchoring system reduced joint panel shear deformation leading to significant strength enhancement. This led to a subassembly seismic capacity improvement and to an energy dissipation increase associated with a more favorable ductile failure mode;
- FRP strengthening provided no changes in the subassembly initial stiffness whereas a more gradual stiffness degradation was observed after the first crack of the joint panel was attained.

Based on the observations pointed out by the experimental tests and by other available literature studies, a simple and reliable analytical model was developed and compared with a large database of experimental tests (47 tests on FRP strengthened joints). The model definition, calibration and final validations with available experimental results was widely discussed. In particular, the model is based on the principal tensile stress approach. Because of the complex stress field acting in the joint panel, a new formulation for the effective FRP strain, that accounts for the debonding phenomena, was calibrated on experimental tests. The proposed formulation matches well with the experimental evidence in terms of average effective strain. The proposed expression allows to overcome the limitation of the FRP strain to 0.4% as conventionally assumed in available guidelines. The proposed design procedure was calibrated with experimental tests on corner beam column joints with geometry and mechanical properties typical of existing structural systems subjected to severe seismic actions. It allows to predict the shear strength of corner beam–column joint strengthened with: different fiber types (CFRP and GFRP); different strengthening layouts in terms of: amount of fibers on the joint panel, number of layers, number of strengthened sides (to account for the presence of the orthogonal beam) and inclination of fibers (or multiple inclinations); continuous reinforcement or strips; strengthening system applied on a damaged and lightly repaired joint panel; adoption of mechanical anchorages to improve the fiber performance. Furthermore, the

model was validated against experimental tests not employed in the model calibration.

The proposed model allows practitioners involved in the seismic strengthening of existing structures to easily and reliably quantify the amount of FRP reinforcement needed to avoid the brittle shear failure of corner joints.

In conclusion, a numerical modeling procedure was proposed to reproduce the hysteretic behavior of poorly detailed beam-column joints. The proposed model was developed in a nonlinear FEM-based environment (VecTor2) which allows to proper consider the effects of shear failures in RC members. A new modeling strategy was proposed to account for the confinement effects of the longitudinal reinforcements bents on the joint core. The proposed model is able to accurately reproduce the subassembly hysteretic behavior and predict the crack pattern at each step of the analysis. A further validation was achieved comparing the predicted and experimental shear stress-strain behavior of the joint panel. A close match demonstrated the accuracy of the proposed model that enable to predict the joint panel failure mode and the large shear deformations associated to the joint panel shear cracks.

Further studies are needed to explore the possibility to extend the proposed strength capacity model to other joint types that suffer the premature shear failure and may need for the FRP strengthening. This is the case of the joint types neglected in this study (i.e. joints with plain round reinforcements and interior joints), but widespread in existing RC structures. Because of the significant differences with the mechanical behavior of interior beam–column joints and subassemblies dominated by significant slip of the internal reinforcements (i.e. subassemblies with plain bars), only corner joints with deformed longitudinal reinforcements were considered in this study. However, the model predictions in terms of joint shear strength and effective FRP strains were also evaluated for some reference joints with plain round internal reinforcements and interior joints. The comparison demonstrated the accuracy of the proposed model

predicting the shear strength increase due to the FRP strengthening for corner joints with plain round reinforcements. However, only few tests were considered in the validation.

On the other side, the comparison with interior beam-column connections demonstrated that further studies are need in order to proper quantify the confinements effects of framing beams. In fact, neglecting these effects, the proposed capacity model underestimates their shear strength. Thus, further refinements of the proposed model should be performed when enough test data becomes available.

Once that a generalized version of the proposed model (including interior joints and subassemblies with plain round internal reinforcements) becomes available, further studies are needed in order to in order to adopt the proposed formulation in code or guidelines design provisions. For this purpose a reliability analysis is needed in order to convert the mean values of materials' mechanical properties to design values; this can be done according to the target level of structural safety established by the code. This process may be performed according to standard procedures as also recalled in EN1990 (2002) for the European area.

Concerning the proposed numerical model reproducing the hysteretic behavior of RC beam-column joints, further development may achieved performing nonlinear-FEM analysis on entire structural systems (i.e. RC frames). This studies may aim at quantifying the effects of joint deformability and strength and stiffness degradation on the seismic performances of the structural systems.

References

ACI 318, 1995. Building Code Requirements for Structural Concrete. Farmington Hills, MI, U.S.A.

ACI 318-11, 2011. Building Code Requirements for Structural Concrete and Commentar. Farmington Hills, MI, U.S.A.

ACI 369R-11, 2011. Guide for Seismic Rehabilitation of Existing Concrete Frame Buildings. American Concrete Institute, Farmington Hills, MI, U.S.A.

ACI 440, 2012. Guide Test Methods for Fiber- Reinforced Polymer (FRP) Composites for Reinforcing or Strengthening Concrete and Masonry Structures.

ACI-ASCE 352, 1976. Recommendations for Design of Beam-Column Joints for Monolithic Concrete Structures. Detroit, Mi, U.S.A.

AIJ, 1999. Design guideline for earthquake resistant reinforced concrete buildings based on inelastic displacement concept. Architectural Institute of Japan, Tokio.

AIJ, 1989. Design guidelines for earthquake resistant RC buildings based on the ultimate strength concept. Architectural Institute of Japan, Tokyo, Japan.

Akguzel, U., Pampanin, S., 2012. Assessment and design procedure for the seismic retrofit of Reinforced Concrete beam-column joints using FRP composite materials. J. Compos. Constr. 16, 21–34. doi:10.1061/(ASCE)CC.1943-5614.0000242.

Akguzel, U., Pampanin, S., 2010. Effects of variation of axial load and bidirectional loading on seismic performance of GFRP retrofitted reinforced concrete exterior beam-column joints. J. Compos. Constr. 14, 94–104. doi:1090-0268/2010/1-104

Al-Salloum, Y.A., Siddiqui, N.A., Elsanadedy, H.M., Abadel, A.A., Aqel, M.A., 2011. Textile-Reinforced Mortar versus FRP as strengthening material for seismically deficient RC beam-column joints. ASCE J. Compos. Constr. 15, 920–933. doi:10.1061/(ASCE)CC.1943-5614.0000222.

Anderson, M., Lehman, D., Stanton, J., 2008. A cyclic shear stress-strain model for joints without transverse reinforcement. Eng. Struct. 30, 941–954. doi:10.1016/j.engstruct.2007.02.005

Antonopoulos, C.P., Triantafillou, T.C., 2003. Experimental investigation of FRP-strengthened RC beam-column joints. J. Compos. Constr. 7, 39–49. doi:10.1061/(ASCE)1090-0268(2003)7:1(39)

Antonopoulos, C.P., Triantafillou, T.C., 2002. Analysis of FRP-strengthened RC beam-column joints. J. Compos. Constr. 6, 41–51. doi:10.1061/(ASCE)1090-0268(2002)6:1(41)

ASCE/SEI, 2007. ASCE/SEI 41-06. Seismic rehabilitation of existing buildings. Reston, VA, USA.

Bakis, C.E., Bank, L.C., Brown, V.L., Cosenza, E., Davalos, J.F., Lesko, J.J., Machida, A., Rizkalla, S.H., Triantafillou, T.C., 2002. Fiber-Reinforced Polymer Composites for Construction — State-of-the-Art Review. ASCE J. Compos. Constr. Constr. 6, 73–87. doi:1090-0268/2002/2- 73–87

Balsamo, A., Di Ludovico, M., Lignola, G.P., Prota, A., Manfredi, G., Cosenza, E., 2012. Composites for structural strengthening, in: Nicolais, L., Borzacchiello, A. (Eds.), Wiley Encyclopedia of Composites, Second Edition. John Wiley & Sons, Inc. doi:10.1002/9781118097298

Bentz, E.C., 2000. Sectional Analysis of Reinforced Concrete Members. University of Toronto, ON, Canada.

Beres, A., Pessiki, S.P., White, R.N., Gergely, P., 1996. Implications of experiments on the seismic behavior of gravity load designed RC beam-to-column connections. Earthq. Spectra. doi:10.1193/1.1585876

Bousselham, A., 2010. State of research on seismic retrofit of RC beam-column joints with externally bonded FRP. ASCE J. Compos. Constr. Constr. 14, 49–61. doi:1090-0268/2010/1-49-61

Calvi, G.M., 2010. Engineers Understanding of Earthquakes Demand and Structures Response, in: Garevski, M., Ansal, A. (Eds.), Earthquake Engineering in Europe, Geotechnical, Geological, and Earthquake Engineering. Springer Netherlands, Dordrecht. doi:10.1007/978-90-481-9544-2

Calvi, G.M., Magenes, G., Pampanin, S., 2002. Relevance of beam-column joint damage and collapse in RC frame assessment. J. Earthq. Eng. 6, 75–100. doi:10.1080/13632460209350433

CEN, 2005. Eurocode 8: Design of structures for earthquake resistance - Part 3: Assessment and reofitting of buildings. European Committee for Standardization, Brussell.

CEN, 2004. "Design of structures for earthquake resistance, part 1: General rules, seismic actions and rules for buildings." EN 1998-1, Eurocode 8. European Committee for Standardization, Brussels.

CNR-DT 200, 2013. CNR-DT 200-R1: Guide for the design and construction of externally bonded FRP systems for strengthening existing structures, R1 ed. Rome.

CS LL PP, 2009. Circolare 617: Istruzioni per l'applicazione delle Norme Tecniche per le Costruzioni (in Italian), Gazzetta U. ed.

D.M. 03/10/1978, "Criteri generali per al verifica della sicurezza delle costruzioni e dei carichi e sovraccarichi" (in Italian).

Del Vecchio, C., Di Sarno, L., Kwon, O., Prota, A., 2013. Validation of Numerical Models for RC Columns Subjected to Cyclic Load, in: Papadrakakis, M., Papadopoulos, V., Plevris, V. (Eds.), COMPDYN 2013, 4th ECCOMAS Thematic Conference on Computational Methods in Structural Dynamics and Earthquake Engineeering. Institute of Structural Analysis and Antiseismic Research School of Civil Engineering National Technical University of Athens (NTUA) Greece, Kos Island, Greece, 12 - 14 June, pp. 1958–1974. doi:978-960-99994-2-7

Del Vecchio, C., Kwon, O., Di Sarno, L., Prota, A., 2015. Accuracy of nonlinear static procedures for the seismic assessment of shear critical structures. Earthq. Eng. Struct. Dyn. (published). doi:10.1002/eqe.2540

Di Ludovico, M., Lignola, G.P., Prota, A., Cosenza, E., 2010. Nonlinear Analysis of Cross Sections under Axial Load and Biaxial Bending. ACI Struct. J. 107, 390–399.

Di Ludovico, M., Manfredi, G., Mola, E., Negro, P., Prota, A., 2008. Seismic behavior of a full-scale RC structure retrofitted using GFRP laminates. J. Struct. Eng. 134, 810–821. doi:ASCE, ISSN 0733-9445/2008/5-810-821

Di Ludovico, M., Prota, A., Manfredi, G., Cosenza, E., 2010. FRP strengthening of full-scale PC girders. J. Compos. Constr. 14, 510–520. doi:ASCE, ISSN 1090-0268/2010/5-510-520

Di Ludovico, M., Verderame, G.M., Prota, A., Manfredi, G., Cosenza, E., 2014. Cyclic Behavior of Nonconforming Full-Scale RC Columns. J. Struct. Eng. doi:10.1061/(ASCE)ST.1943-541X.0000891.

Dolce, M., Goretti, A., 2015. Building damage assessment after the 2009 Abruzzi earthquake. Bull. Earthq. Eng. Published . doi:10.1007/s10518-015-9723-4

DPC-ReLUIS, 2011. Linee Guida Per Riparazione E Rafforzamento Di Elementi Strutturali, Tamponature E Partizioni (in Italian), Doppiavoce. ed.

El-Amoury, T., Ghobarah, A., 2002. Seismic rehabilitation of beam–column joint using GFRP sheets. Eng. Struct. 24, 1397–1407. doi:10.1016/S0141-0296(02)00081-0

Elwood, K.J., Wallace, J.W., Lehman, D.E., Heintz, J.A., Mitchell, A.D., Moore, M.A., Valley, M.T., Lowes, L.N., Comartin, C.D., Moehle, J.P., 2007. Update to ASCE / SEI 41 Concrete Provisions. Earthq. Spectra 23, 493–523. doi:10.1193/1.2757714

European Commitee for Standardization, 2002. EN1990:2002 Eurocode — Basis of structural design. Brussels.

Fardis, M.N., 2009. Seismic Design, Assessment and Retrofitting of Concrete Buildings (Based on EN-Eurocode8), Series: Ge. ed. Springer, Istanbul, Turkey.

Fib, 2003. Seismic assessment and retrofit of reinforced concrete buildings. Bulletin 24,. Lausanne, Switzerland.

Frascadore, R., Di Ludovico, M., Prota, A., Verderame, G.M., Manfredi, G., Dolce, M., Cosenza, E., 2014. Local strengthening of RC structures as a strategy for seismic risk mitigation at regional scale. Earthq. Spectra In Press. doi:http://dx.doi.org/10.1193/122912EQS361M

Gergely, B.J., Pantelides, C.P., Reaveley, L.D., 2000. Shear strengthening RCT-joints using CFRP composites. J. Compos. Constr. 4, 56–64. doi:ASCE, ISSN 1090-0268/00/0002-0056-0064

Ghobarah, A., El-Amoury, T., 2005. Seismic rehabilitation of deficient exterior concrete frame joints. ASCE J. Compos. Constr. 9, 408–416. doi:1090-0268/2005/5-408-416

Ghobarah, A., Said, a., 2002. Shear strengthening of beam-column joints. Eng. Struct. 24, 881–888. doi:10.1016/S0141-0296(02)00026-3

Guimaraer, G.N., Kreger, M.E., Jirsa, J.O., 1989. PMFSEL Report: Reinforced concrete frame connections constructed using high-strength materials.

Hakuto, S., Park, R., Tanaka, H., 1995. Retrofitting of reinforced concrete moment resisting frame. Research report 95-4.

Huang, X., Kwon, O.-S., 2015. Numerical Models of RC Elements and their Impacts on Seismic Performance Assessment. Earthq. Eng. Struct. Dyn. 44, 283–298. doi:10.1002/eqe.2471

Ilki, A., Bedirhanoglu, I., Kumbasar, N., 2011. Behavior of FRP-Retrofitted Joints Built with Plain Bars and Low-Strength Concrete. J. Compos. Constr. 15, 312–326. doi:10.1061/(ASCE)CC.1943-5614.0000156.

ISTAT, 2001. (Istituto centrale di Statistica). 14° Censimento Generale della Popolazione e delle Abitazioni. (in Italian). Rome, Italy.

Khalifa, A., Gold, W.J., Nanni, A., Aziz, A., 1998. Contribution of externally bonded FRP to shear capacity. J. Compos. Constr. 2, 195–202. doi:1090-0268/98/004-0195-0202

Khalifa, A., Nanni, A., 2000. Improving shear capacity of existing RC T-section beams using CFRP composites. Cem. Concr. Compos. 22, 165–174. doi:0958-9465/00

Kurose, Y., 1987. PMFSEL report n°87-8: Recent Studies on Reinforced Concrete Beam-Column Joints in Japan.

Kwon, O.-S., Kim, E., 2010. Case study: Analytical investigation on the failure of a two-story RC building damaged during the 2007 Pisco-Chincha earthquake. Eng. Struct. 32, 1876–1887. doi:10.1016/j.engstruct.2009.12.022

Lafave, J.M., Kim, J., 2011. Joint Shear Behavior Prediction for RC Beam-Column Connections. Int. J. Concr. Struct. Mater. 5, 57–64. doi:10.4334/IJCSM.2011.5.1.057

Leon, R.T., Yuen Kam, W., Pampanin, S., 2014. Performance of beam-column joints in the 2010-2012 Christchurch earthquakes. ACI Spec. Pubblication SP-296-3.

Lowes, L.N., Altoontash, A., 2003. Modeling Reinforced-Concrete Beam-Column Joints Subjected to Cyclic Loading. J. Struct. Eng. 129, 1686–1697. doi:10.1061/(ASCE)0733-9445(2003)129:12(1686)

Maeda, T., Asano, Y., Sato, Y., Veda, T., Kakuta, Y., 1997. A study on bond mechanism of carbon fiber sheet, in: Non-Metallic (FRP) Reinforcement for Concrete Struct., Proc. 3rd Symp. Japan, pp. 279–286.

Mander, J.B., Priestley, M.J.N., Park, R., 1988. Theoretical Stress-Strain Model for Confined Concrete. ASCE J. Struct. Eng. 114, 1804. doi:10.1061/(ASCE)0733-9445(1988)114:8(1804)

Manfredi, G., Masi, A., Pinho, R., Verderame, G.M., Vona, M., 2007. Valutazione degli edifici esistenti in Cemento Armato. IUSS Press, Fondazione EUCENTRE, Pavia, Italy.

Masi, A, Vona, M., 2004. Vulnerabilità sismica di edifici in c . a . realizzati negli anni ' 70, in: XI Italian National Conference on Seismic Engineering - ANIDIS (in Italian). Genova, Italy.

MI, 2008. D.M. 14 Gennaio 2008 (D.M. 2008). Technical codes for structures (in Italian), GU n°29, F. ed. Rome, Italy.

MMLLPP, 1997. Circ. MM.LL.PP. n°65: "Istruzioni per l'applicazione delle Norme tecniche per le costruzioni in zone sismiche di cui al decreto ministeriale 16.01.1996". (In Italian). Italy.

MMLLPP, 1996. D.M.LL.PP. 09/01/1996: "Norme tecniche per il calcolo, l'esecuzione ed il collaudo delle strutture in cemento armato, normale e precompresso e per le strutture metalliche." (in Italian). Italy.

Moratti, M., 2000. Risposta sismica di nodi trave – colonna progettati per i soli carichi di gravità : studi analitici e sperimentali. University of Pavia.

NZS 3101, 2006. Concrete Structures Standard. New Zeland. doi:ISBN 1-86975-043-8

NZS 3101, 1995. Concrete Structures Standard. New Zeland.

NZS 3101, 1982. Concrete Structures Standard. New Zeland.

OpenSees: Open system for earthquake engineering simulation, 2006. doi:http://opensees.berkeley.edu

Palermo, D., Vecchio, F.J., 2003. Compression Field Modeling of Reinforced Concrete Subjected to Reverse Loading: Formulation. ACI Struct. J. 100. doi:10.14359/12803

Pampanin, S., Bolognini, D., Pavese, A., 2007. Performance-Based Seismic Retrofit Strategy for Existing Reinforced Concrete Frame Systems Using Fiber-Reinforced Polymer Composites. J. Compos. Constr. 11, 211–226. doi:10.1061/(ASCE)1090-0268(2007)11:2(211)

Pantelides, C.P., Clyde, C., Reaveley, L.D., 2002. Performance-based evaluation of reinforced concrete building exterior joints for seismic excitation. Earthq. Spectra 18, 449–480. doi:10.1193/1.1510447

Pantelides, C.P., Okahashi, Y., Reaveley, L.D., 2008. Seismic Rehabilitation of Reinforced Concrete Frame Interior Beam-Column Joints with FRP Composites. J. Compos. Constr. 12, 435–445. doi:10.1061/(ASCE)1090-0268(2008)12:4(435)

Park, R., 1997. A static force-based procedure for the seismic assessment of existing reinforced concrete moment resisting frames. Bull. New Zeal. Natl. Soc. Earthq. Eng. 30, 213–226.

Park, R., 1994. Simulated seismic load tests on reinforced concrete elements and structures, in: Tenth World Conference on Earthquake Engineering. Balkema, Rotterdam. doi:ISBN: 9054100605

Park, S., Mosalam, K.M., 2013. Simulation of Reinforced Concrete Frames with Nonductile Beam-Column Joints. Earthq. Spectra 29, 233–257. doi:10.1193/1.4000100

Park, S., Mosalam, K.M., 2012a. Analytical Model for Predicting Shear Strength of Unreinforced Exterior Beam-Column Joints. ACI Struct. J. 109, 149–160. doi:10.14359/51683626

Park, S., Mosalam, K.M., 2012b. Parameters for shear strength prediction of exterior beam – column joints without transverse reinforcement. Eng. Struct. 36, 198–209. doi:10.1016/j.engstruct.2011.11.017

Parvin, A., Altay, S., Yalcin, C., Kaya, O., 2010. CFRP rehabilitation of concrete frame joints with inadequate shear and anchorage details. ASCE J. Compos. Constr. 14, 72–82. doi:1090-0268/2010/1-72-82

Paulay, T., Priestley, M.J.N., 1992. Seismic design of Reinforced Concrete and masonry buildings. John Wiley & Sons, Inc., U.S.A.

Popovic, S., 1973. A numerical approach to the complete stress-strain curve of concrete. Cem. Concr. Res. 3, 583–599.

Priestley, M.J.N., 1997. Displacement-based seismic assessment of Reinforced Concrete buildings. J. Earthq. Eng. 1, 157–192. doi:10.1080/13632469708962365

Priestley, M.J.N., Seible, F., Calvi, G.M., 1996. Seismic design and retrofit of bridges. John Wiley & Sons, Inc., New York.

Prota, A., Di Ludovico, M., Balsamo, A., Moroni, C., Dolce, M., Manfredi, G., 2014. FRP local retrofit of non-conforming RC beam-column joints. Seismic evaluation and rehabilitation of structures, in: Ilki, A., Fardis, M.N. (Eds.), Geotechnical, Geological and Earthquake Engineering. Springer International Publishing, Switzerland.

Prota, A., Nanni, A., Manfredi, G., Cosenza, E., 2004. Selective upgrade of underdesigned Reinforced Concrete beam-column joints using carbon Fiber-Reinforced Polymers. ACI Struct. J. 5, 699–707.

Realfonzo, R., Napoli, A., Pinilla, J.G.R., 2014. Cyclic behavior of RC beam-column joints strengthened with FRP systems. Constr. Build. Mater. 54, 282–297. doi:10.1016/j.conbuildmat.2013.12.043

Regio Decreto Legge (R.D.L.) 2229-1939, 1939. Norme per l'esecuzione delle opere in conglomerate cementizio semplice o armato. [Guidelines for the execution of concrete structures] (in Italian). Italy.

Reluis, 2009. Report on the damages on buildings following the seismic event of 6th of april 2009, V1.20. by Verderame, GM; Iervolino, I; Ricci, P.

Ricci, P., De Luca, F., Verderame, G.M., 2011. 6th April 2009 L'Aquila earthquake, Italy: reinforced concrete building performance. Bull. Earthq. Eng. 9, 285–305. doi:10.1007/s10518-010-9204-8

Sagbas, G., Vecchio, F.J., Christopoulos, C., 2011. Computational Modeling of the Seismic Performance of Beam-Column Subassemblies. J. Earthq. Eng. 15, 640–663. doi:10.1080/13632469.2010.508963

Sharma, A., Eligehausen, R., Reddy, G.R., 2011. A new model to simulate joint shear behavior of poorly detailed beam–column connections in RC structures under seismic loads, Part I: Exterior joints. Eng. Struct. 33, 1034–1051. doi:10.1016/j.engstruct.2010.12.026

Triantafillou, T.C., 1998. Shear strengthening of Reinforced Concrete beams using epoxy-bonded FRP composites. ACI Struct. J. 95, 107–115.

Tsonos, A.G., 2008. Effectiveness of CFRP-jackets and RC-jackets in post-earthquake and pre-earthquake retrofitting of beam–column subassemblages. Eng. Struct. 30, 777–793. doi:10.1016/j.engstruct.2007.05.008

UNI EN 1504-3:, 2005. Prodotti e sistemi per la protezione e la riparazione delle strutture di calcestruzzo - Definizioni, requisiti, controllo di qualità e valutazione della conformità"- Parte 3: Riparazione strutturale e non strutturale. (in Italian).

Vecchio, F.J., 2000. Disturbed Stress Field Model for Reinforced Concrete: Formulation. ASCE J. Struct. Eng. 126, 1070–1077. doi:0733-9445/00/0009-1070-1077

Vecchio, F.J., Collins, M.P., 1986. The Modified Compression-Field Theory for Reinforced Concrete elements subjected to shear. ACI J. March-Apri, 219–231.

Verderame, G., Fabbrocino, G., Manfredi, G., 2008. Seismic response of r . c . columns with smooth reinforcement . Part II : Cyclic tests. Eng. Struct. 30, 2289–2300. doi:10.1016/j.engstruct.2008.01.024

Vona, M., Masi, A., 2004. Resistenza sismica di telai in c. a. progettati con il R.D. 2229/39 (in Italian), in: XI Italian National Conference on Seismic Engineering - ANIDIS (in Italian). Genova, Italy.

Wong, P.S., Vecchio, F.J., Trommels, H., 2013. VecTor2 & FormWorks User's Manual. Second Edition. Toronto, ON, Canada.

Yao, J., Teng, J.G., Chen, J.F., 2005. Experimental study on FRP-to-concrete bonded joints. Compos. Part B Eng. 36, 99–113. doi:10.1016/j.compositesb.2004.06.001

Yuan, H., Teng, J.G., Seracino, R., Wu, Z.S., Yao, J., 2004. Full-range behavior of FRP-to-concrete bonded joints. Eng. Struct. 26, 553–565. doi:10.1016/j.engstruct.2003.11.006

Notes